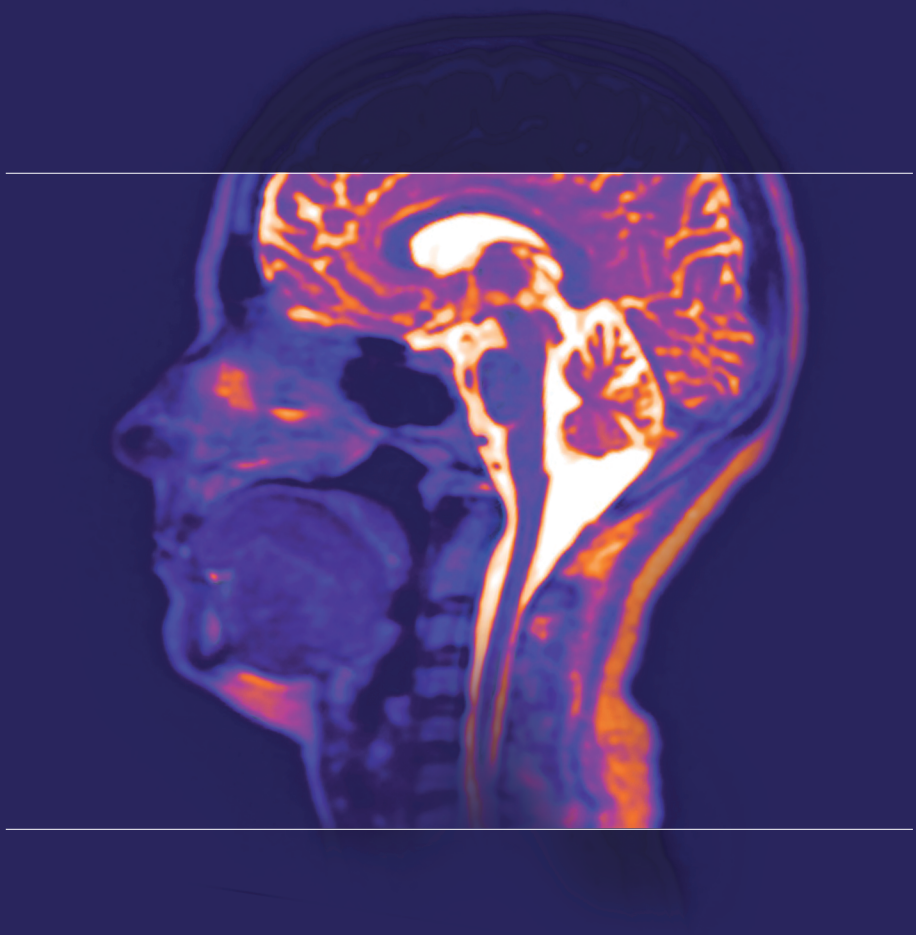

MR Thermometry for Hyperthermia in the Head and Neck

Theresa V. Feddersen

MR Thermometry for Hyperthermia in the Head and Neck

Theresa Viktoria Feddersen

ISBN 978-94-6361-949-3

MR Thermometry for Hyperthermia in the Head and Neck

MR thermometrie voor hyperthermie in de hoofd hals regio

Thesis

to obtain the degree of Doctor from the
Erasmus University Rotterdam
by command of the
rector magnificus

Prof. dr. A.L. Bredenoord

and in accordance with the decision of the Doctorate Board.

The public defence shall be held on

Tuesday the 23rd of January 2024 at 13.00 hrs

by

Theresa Viktoria Feddersen
born in Georgsmarienhütte, Germany.

Erasmus University Rotterdam

Doctoral Committee

Promotors:	prof. dr. G.C. van Rhoon
	prof. dr. J.A. Hernandez Tamames
	prof. dr. ir. M.M. Paulides
Other members:	prof. dr. H. Grüll
	dr. ir. S.F. Petit
	dr. S. Zinger
Copromotor:	dr. ir. D.H.J. Poot

Rüm Hart, klaar Kiming

CONTENTS

Chapter 1

Introduction

1.1 CANCER

Cancer is diagnosed in almost 20 million people worldwide each year [1], and this global burden is expected to grow in the future [2]. Over the last 50 years however, survival of cancer patients has become the norm rather than the exception [3]. The improvement in life expectancy can largely be attributed to the continuous development of the classical pillars of cancer therapy, see Figure 1.1. The benefits are from high to low: surgery, radiotherapy, chemotherapy, and more recently, immunotherapy [4] (see Figure 1.1). These treatments are also frequently used in combination with one another [5-7].

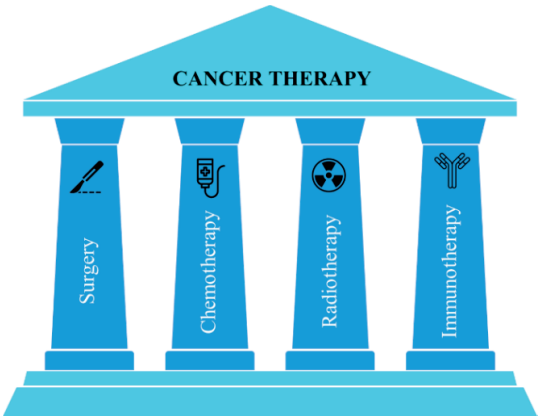

Figure 1.1: The four pillars of cancer therapy.

1.1.1 Head and neck cancer

Head and neck cancer is the seventh most common cancer worldwide with an increasing incidence of the disease [8]. The five-year survival for patients with locally advanced disease lies at 50% of cases [9] with little improvement in mortality over recent decades for this type of cancer [10]. The treatment of head and neck cancer depends on a number of factors, such as the stage of the disease and tumour location, and can potentially cause severe side effects [9, 11-13]. Recurrence of the disease occurs in 30-50% of patients [14-18], usually at the primary site or in the lymph nodes of the neck, leading to treatment failure.

Treatment of patients with a local recurrence is especially challenging, due to inoperable tumours, toxicity and the proximity of many important structures [11, 19]. The median survival of patients with recurrent, metastatic disease is 5.0-8.7 months [20-24]. There is thus a great need for a sensitizer for (repeated) treatment that can improve patient outcome without an increase in side effects.

Mild thermal therapy, also called hyperthermia, can provide such a sensitization. Beyond the potential benefit of adding hyperthermia for re-irradiation, it also has a strong potential to replace chemotherapy and part of the radiotherapy in primary treatment. The heat-related enhancement of radio- and chemotherapy can be used to improve outcome, while inducing minimal additional acute and late morbidities. It has been shown that giving hyperthermia along with radiotherapy increases the likelihood of complete response in head and neck cancers by 25% compared to radiotherapy alone [25].

1.2 HYPERTHERMIA THERAPY

1.2.1 Definition & biology

Hyperthermia is defined as the localised heating of a tumour and surrounding tissue to 39-43°C [12] for at least 60 minutes. It is given as adjuvant therapy to chemo-, radiation-, and immunotherapy [26]. Adding hyperthermia to other cancer treatments is effective due to its six hallmarks defined by Issels *et al.* [12]: 1) blocking cell survival, 2) inducing cellular stress response, 3) modulating immune response, 4) evading DNA repair, 5) changing tumour microenvironment, and 6) sensitisation to radiation and chemotherapy - where of course many of these are dependent on one another. The plethora of biological effects (each associated with their own specific temperature range) are comprehensively discussed in van den Tempel *et al.* [27] and summarised in Figure 1.2.

1.2.2 Clinical evidence

Hyperthermia is always given as an adjuvant therapy to chemo-, radio- and immunotherapy, as it effectively sensitizes the tumour tissue [28]. The benefits regarding local control and overall survival of adding hyperthermia have been demonstrated extensively in different tumour sites [13-17]. An example of the effectiveness of adding hyperthermia to radiotherapy is presented in Figure 1.3.

The majority of randomized clinical studies report no or minor increased late-toxicity in the hyperthermia treatment arm - this is an important benefit of hyperthermia [30].

1.2.3 Hyperthermia technology

The advantages and limitation of current existing, academic and commercial heating systems, as well as their technological working principles is provided by Kok *et al.* [31]. At present, the most commonly used hyperthermia systems are based on electromagnetic energy transfer to induce localized and tumour specific heating.

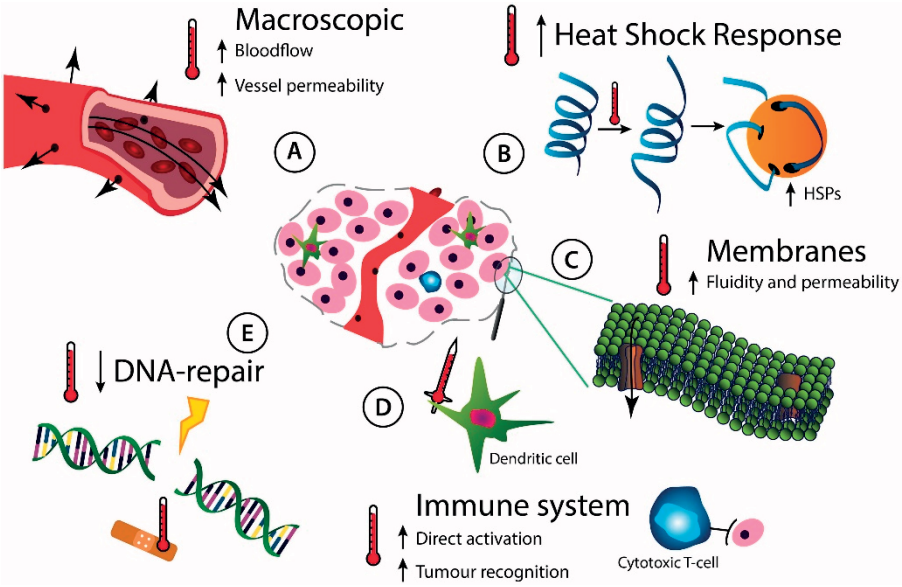

Figure 1.2: Biological effects of hyperthermia in the tumour. The tumour is depicted in the centre and the physiological and molecular effects of local hyperthermia are indicated. (A) Hyperthermia alters tumour vasculature: heat increases the blood flow and vessel permeability. (B) Heat causes proteins to unfold and increases the intracellular amount of protein-chaperoning heat-shock proteins. (C) Temperatures exceeding 37 °C result in increased cell membrane fluidity, thereby influencing their permeability. Specific biological effects of heat on membranes may be further affected by altering properties of membrane-bound-proteins. (D) Local heat helps to activate the immune system and causes it to attack the tumour directly, but might also cause a systemic effect by which immune cells attack tumour cells distant from the heated tumour. (E) Hyperthermia affects DNA damage repair pathways by deactivating specific repair proteins. Figure and caption (shortened) taken from [27].

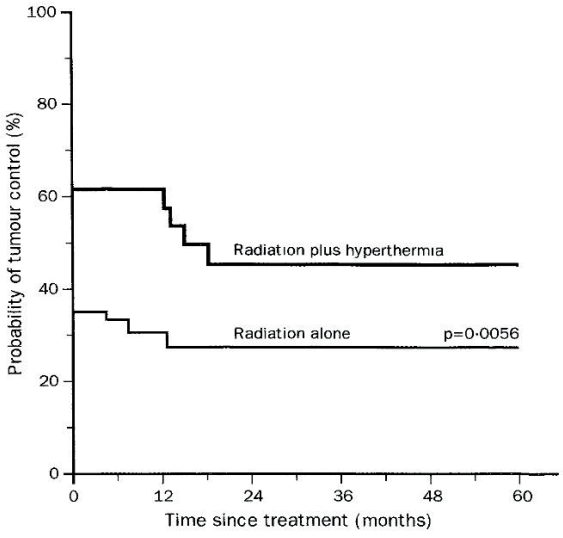

Figure 1.3: Example for the effectiveness of adding hyperthermia to, in this case, radiotherapy: the probability of malignant melanoma tumour control after treatment with radiation alone or radiation plus hyperthermia. Figure taken from Overgaard et al. [29].

1.2.4 Validation of temperature

In order for all the effects of hyperthermia to work to their full potential, it is important that the correct temperature range is reached in the tumour [32]. If the temperature in the tumour is too low, the desired effects are not observed; if the temperature is too high, permanent tissue damage in healthy surrounding tissues may be induced. It is therefore crucial to have real-time validation of the temperature during the treatment in order to optimally deliver the dose. Additionally, an accurate measurement allows the correlation of treatment outcome to the temperature reached retrospectively, an important factor to broaden the understanding and the effectiveness of hyperthermia.

Temperature monitoring is traditionally achieved by inserting probes invasively or intraluminally, close to the tumour [33]. However, the placement is not always feasible, such as in areas like the head and neck, and can involve complications [34, 35]. Even when successfully placed, the probes only supply point-like temperature readings that can easily overlook heating outside the desired range away from the measurement.

Several techniques for non-invasive temperature measurements during hyperthermia treatments are under investigation, for example magnetic resonance thermometry (MRT), active and passive microwave imaging, as well as ultrasound imaging. The only clinically applied method to obtain temperature data during hyperthermia is based on MR-techniques [36, 37]. The work by Charité University Medical Center, however, showed the feasibility to integrate Pyrexar's Sigma-Eye applicator into a 1.5 Tesla MR scanner (Symphony; Siemens AG, Munich, Germany) for treatment of tumours in the pelvis. They showed that quantitative MR measurements during heating are feasible for the pelvic region. However, they note that susceptibility artifacts and the distortions by the applicator must be carefully taken into account for accurate MR measurements [37, 38]. This device currently provides the only clinical option for MR guided radiofrequency hyperthermia [39], and in time became also available for GE and Philips MR scanners.

1.3 HYPERTHERMIA IN THE HEAD AND NECK

Commercial devices for phased array application for hyperthermia in the head and neck do not exist. Therefore, our group has in the past developed the HYPERcollar, a dedicated phased-array system [40] (see Figure 1.4), and first results have shown the system to be suitable and safe [41]. Subsequently, the HYPERcollar was redesigned

to improve the heating quality, heating reproducibility and patient comfort: the HYPERcollar3D [42]. Kroesen *et al.* [43] conducted a retrospective study investigating the feasibility and clinical outcome of recurrent or second primary head and neck cancer patients treated with the HYPERcollar3D. This study highlighted the relevance of better technology, as well as the need of better temperature measurements during the treatment.

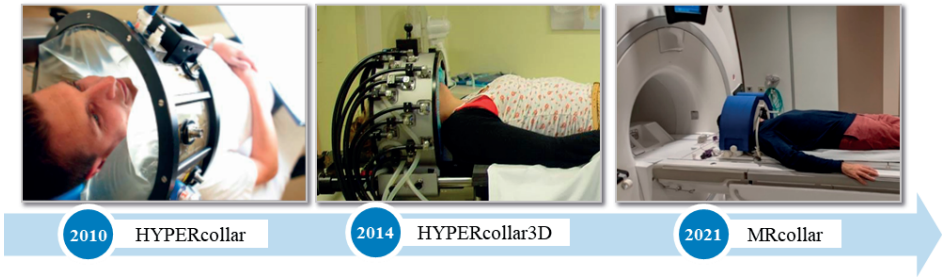

Figure 1.4: The evolution of head and neck hyperthermia applicators at Erasmus MC, as well as the year of introduction. From left to right: the HYPERcollar, the HYPERcollar3D and the MRcollar.

1.3.1 MRcollar

The need for improved temperature measurement during head and neck hyperthermia treatments led to the development of the MRcollar [44] in parallel to this thesis. The MRcollar (see Figure 1.4) is a fully integrated MR-compatible multi MR receive coil hyperthermia applicator, and an important enabler for the research in this thesis. Because the MRcollar is MR-compatible, the temperature can be measured using MRI. How this can be done is discussed in detail in Section 1.4.

The integration of multiple MRI coils inside the MRcollar provides a fivefold increase in SNR [45] when compared to imaging with the body coil, potentially improving the accuracy and precision of the temperature measurement. The multi-coil design opens the door for investigating acceleration approaches (see **Chapter 5**), and defines the needs for the MRI temperature post processing pipeline.

1.4 MAGNETIC RESONANCE THERMOMETRY (MRT)

An attractive solution for temperature validation during hyperthermia treatments is measuring the temperature change with MRI. This technique is called magnetic resonance thermometry (MRT). MRI is routinely used in the clinic and is very popular due to its excellent soft tissue contrast, without the downside of ionizing radiation that other modalities have (for instance CT). MRT can offer non-invasive

temperature maps in 3D, by acquiring appropriate images at time intervals during the hyperthermia treatment.

To be able to do this, the hyperthermia device needs to be able to operate inside the MRI and should not disturb the imaging, such as the MRcollar and the Pyrexar applicators. But the availability of the suitable hardware is only part of the solution to have reliable MRT. Another important part is the software development, which includes a MRI sequence that is able to provide images with sufficient quality in MRT. The demands on such a sequence are discussed in Section 1.4.2. The other important part is a robust post-processing method, which is introduced in **Chapter 3** and further developed in **Chapter 5**.

Figure 1.5 shows an example of the temperature change maps that can be generated by MRT during a hyperthermia treatment for a pelvic patient, supporting the scientific assumption that current MRT processes can be improved to effectively compensate for air, tissue movement etc. However, there are still many challenges that remain to be solved. These are discussed in Section 1.4.3.

In order to visualise temperature with an MRI, different tissue properties measured by a number of MR contrasts can be exploited. These are comprehensively discussed by Rieke *et al.* [47], but also in Ludemann *et al.* [48] and in Winter *et al.* [49]. In this thesis we have only focused on one of the methods available: the proton resonance frequency shift (PRFS).

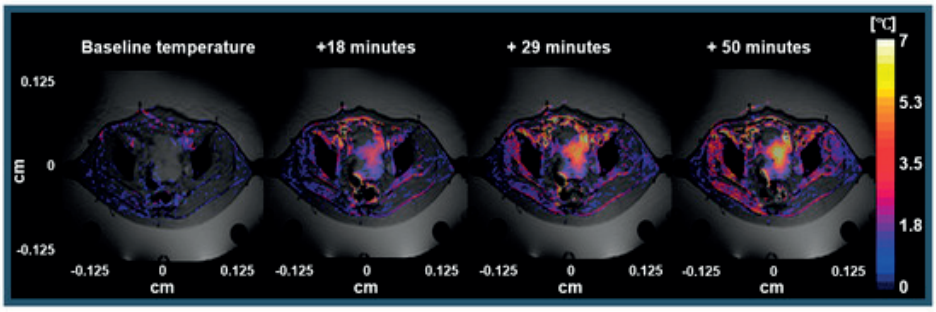

Figure 1.5: MRT maps showing the temperature changes from baseline in a pelvic patient during a hyperthermia treatment by the Sigma Eye applicator. Figure taken from [46], distributed under the terms and conditions of the Creative Commons Attribution (CC BY) license (https://creativecommons.org/licenses/by/4.0/).

1.4.1 Proton Resonance frequency shift (PRFS)

PRFS is the technique most widely used for MRT [50]. It is popular because of three reasons: it is insensitive of the tissue type (with the exception of fat), it changes

linearly with an increase in temperature, and it has been shown to have superior accuracy [51, 52] compared to other MRT methods.

PRFS works as follows: with an increase in temperature, the hydrogen bonds in water molecules become weaker and eventually break, releasing electrons. These free electrons shield the hydrogen nuclei, which results in a shift of the resonance frequency $\Delta\omega$ that is picked up by the MRI.

$$\Delta\omega = \frac{\varphi_t - \varphi_{ref}}{TE} \tag{1.1}$$

where φ_t is the phase at a time t, φ_{ref} is the phase at a reference time (usually before heating is commenced), and TE is the echo time of the acquisition.

The temperature change ΔT can be obtained from $\Delta\omega$ using the following relationship [47]:

$$\Delta T = \frac{\Delta\omega}{\gamma\alpha B_0} \tag{1.2}$$

where γ is the gyromagnetic ratio of protons (267.513*10^6 rad/s/T), α is the PRF temperature coefficient (−0.01 ppm/°C), and B_0 is the magnetic field strength of the MR scanner (usually 1.5 or 3T).

As the PRFS change coefficient α is only -0.01 ppm/°C in muscle tissue (see Equation 1.2), the temperature measurement is highly susceptible to other effects influencing the resonance frequency. These challenges are discussed in detail in Section 1.4.3.

1.4.2 Gradient recalled echo (GRE): sequence of choice

Temperature maps with PRFS are constructed by obtaining the change in phase from gradient-recalled echo (GRE) imaging sequences [53]. There are two main reasons why GRE sequences are usually used for PRFS temperature change measurements.

Firstly, the GRE echo can be read shorter after the first RF pulse than in spin echo (SE), as only one RF pulse needs to be applied [54]. This can lead to shorter total acquisition times, which is not only more pleasant for patients, but also gives less opportunity for motion to arise during scanning (for more detail on motion see Section 1.4.3.1). Besides speed, shorter echo times are also beneficial for fat-water separation, where the times between the echoes, called the echo spacing, needs to be sufficiently short to get in in- and out-of-phase behaviour (~2.1ms at 1.5T [55], described in more detail below).

Secondly, in GRE sequences more information about the dephasing can be obtained, as the gradient reversal only refocuses the spins that have been dephased by the gradient itself. Image contrast is therefore not ruled by T2-relaxation, but by T2*-relaxation, and hence contains an array of other factors including B0 inhomogeneities, chemical shift and temperature change [54]. This means that any phase shift due to these other factors are not cancelled, as they are for instance in SE sequences [56]. This sensitivity to inhomogeneities is crucial, otherwise we cannot detect the temperature changes with PRFS.

There are a few considerations to be made, both theoretical and practical, to optimise the settings of a GRE sequence for MRT. Firstly, the maximum phase contrast-to-noise is achieved when the echo time TE=T2*, which is about 30ms in muscle tissue [57]. However, with an increase in echo time the magnitude signal decreases (signal decay), hence the best feasible echo time may be smaller than T2*. This is because the information collected later on in the echo train will have a worsened signal to noise ratio (SNR), supplying little signal with the same amount of noise. Secondly, the magnitude signal is at its maximum when the flip angle is equal to the Ernst Angle $\theta_E = \cos^{-1}(e^{-TR/T1})$. Not all sequences may allow for the flip angle to be sufficiently large, which will come at the cost of signal to noise ratio (SNR).

Lastly, as already touched on above, water and fat can be separated when using multiple echoes, as they have different resonance frequencies which makes the two go in- and out-of-phase with one another [58]. For a 1.5T system water and fat will be out of phase at 2.1ms, 6.3ms, 10.5ms and so forth [55]. This phase cancellation effect can be used to identify (and quantify) fat content, an important feature for MRT (see section 1.4.3.3).

1.4.3 Challenges & considerations of MRT in the head and neck

1.4.3.1 Motion

Motion during imaging is a problem and causes artifacts in the images. It can be divided into intra-scan and inter-scan motion.

Intra-scan motion is caused by movement during a MRI acquisition and presents a problem for MRI in general. The resulting artifacts can be reduced by imaging the subjects faster, or immobilizing the subject where possible (considering the acquisition time and comfort of measures taken). An example of the artefacts that will arise from intra-scan motion are demonstrated in [59].

Inter-scan motion describes the motion occurring between two subsequent images taken. Since PRFS is a subtraction-based method, the temperature change is measured from a (usually unheated) baseline. If the subject moves between the baseline scan and a subsequent scan at some later time and this motion is not corrected for, the images are misaligned and wrong temperature changes appear in the MRT maps [60]. Hence, the PRFS method is vulnerable to tissue susceptibility changes and movement [61] of the subject. This motion can be dealt with by eliminating images that are too corrupt, by immobilizing the subject, or by correcting for motion retrospectively.

The head and neck is thus a fairly challenging area for MRT, because of the presence of 1. cyclic (breathing) and 2. non-cyclic (swallowing) motion (see **Chapter 5**). With so many confounders present it can be hard to make an unbiased initial investigation and hence it was decided to use the brain instead for our initial in-vivo investigations in **Chapter 3** and **Chapter 4**. The brain is (for MRT purposes) quite a homogenous area and relatively unaffected by motion and other internal disturbances. Additionally, safety control in the brain is very important as it is highly thermo-sensitive [62], but temperature measurements using current invasive approaches is not clinically acceptable.

1.4.3.2 Scanner drift

A further consideration when using PRFS MRT during hyperthermia treatments is the substantial scanner drift over the >60 minutes of treatment time. B0 drift is always present and can originate from gradient heating or subject motion, such as respiration. The scanner drift can cause considerable errors in the temperature estimation that, if left uncorrected, will worsen over the time of the treatment. The B0 drift can be corrected using fat as a reference, as the resonance frequency of fat is largely independent of a change in temperature, but still picks up other disturbances.

1.4.3.3 Fat

In order to perform a B0 drift correction, usually external fat references are attached either to the hyperthermia applicator or the subject [63]; although internal body fat has also been used in the past [49, 64]. Fat can be used to correct for scanner B0 drift because fat has no hydrogen bonds, and its resonance frequency is therefore effectively constant with an increase in temperature. This of course also means that PRFS based MRT cannot measure temperature changes in fat. Thus, when using the PRFS method, one needs to be aware that the fattier the tissue, the more unaffected the resonance frequency change will be. In voxels with a fat/water mixture, this will thus introduce faulty temperature measurements. If temperature measurement in

fat is desired, T1-based MRT [65, 66] can be a valuable method. There are also hybrid techniques available that combine T1- and PRFS-based MRT [67, 68].

1.4.3.4 Summary and aim of this thesis

In summary, measuring the temperature during hyperthermia treatments is important. Firstly, to ensure the optimal treatment for the patients by heating the tumour to the correct temperature and detecting potential hot spots before they cause patient discomfort. Secondly to correlate the treatment outcome to the quality of treatment given, therefore strengthening the understanding of what constitutes an optimal hyperthermia treatment. Developing accurate and reliable 3D MRT for hyperthermia treatments in the head and neck region has great potential to improve patient outcome by acting as a sensitizer for harmful therapies, without additional side effect. This is especially interesting in the head and neck, as the anatomy includes many important organs can limit the classical therapies. However, this area can present a challenge for MRT, as it is directly and indirectly affected by motion.

Solving MRT in the head and neck has always been a two-path research approach, i.e. development of the hardware (MRcollar) and software (MR sequences and post processing corrections). The MRcollar prototype has been developed in parallel to this thesis, and first experiments show an improvement in MR signal compared to the body coil. This thesis is part of this two-path approach and focuses on the software aspects. Hence, the aim is to develop motion-robust, 3D, MRT-guidance for hyperthermia treatments in the head and neck. The means to achieve that is via investigating new and improved sequencing approaches, developing a post-processing pipeline, and optimizing and validating the proposed approaches in phantoms and volunteers.

1.5 OUTLINE OF THIS THESIS

The efforts to achieve MRT for hyperthermia in the head and neck were subdivided in the following:

Chapter 2 presents a systematic review of the clinical performance and future potential of MRT in hyperthermia. Common ground, concerns, and novel developments are identified. In addition, considering the knowledge gained paired with considerable practical knowledge at the Erasmus MC on hyperthermia treatments, minimum MRT performance criteria are defined that ensure a successful temperature monitoring during hyperthermia treatments.

Chapter 3 presents a new method pipeline, including multi-echo fitting tool and a semi-automatic internal body fat selection. It uses this to compare the MRT performances of different multi-echo gradient sequences against the clinical standard DE-GRE sequence in phantom and the brains of unheated volunteers. The best performing sequence is identified providing a direction to rapidly improve MRT.

Chapter 4 explores the possibility of performing PRFS MR thermometry using a novel 3D radial GRE sequence called Looping Star. MRT performances and acoustic noise levels were measured in phantom and the brains of unheated volunteers, and compared to the clinical standard DE-GRE sequence.

Chapter 5 presents a first approach for MRT in the head and neck. Acquisitions were made in phantom and the oropharynx region of unheated volunteers. Different strategies were directly compared (such as breath-hold scanning or increasing the number of averaging) to see how much each is affected by motion, trying to identify the most robust acquisition method for this region.

Finally, **Chapter 6** provides a comprehensive discussion on this thesis, as well as recommendations for further research.

Chapter 2

Clinical performance and future potential of magnetic resonance thermometry in hyperthermia

Based on:

Clinical performance and future potential of magnetic resonance thermometry in hyperthermia

Theresa V. Feddersen[1,2], Juan A. Hernandez-Tamames[1], Martine Franckena[2], Gerard C. van Rhoon[2,4], Margarethus M. Paulides[2,3]

[1] Department of Radiology and Nuclear Medicine, Erasmus MC Cancer Institute, 3015 GD Rotterdam, The Netherlands;
[2] Department of Radiation Oncology, Erasmus MC Cancer Institute, 3015 GD Rotterdam, The Netherlands;
[3] Electromagnetics for Care & Cure research lab, Center for Care and Cure Technologies Eindhoven (C3Te), Department of Electrical Engineering, Eindhoven University of Technology, 5600 MB Eindhoven, The Netherlands
[4] Department of Applied Radiation and Isotopes, Reactor Institute Delft, Delft University of Technology, 2629JB Delft, The Netherlands

Published in:

Cancers (Basel) 2020 Vol. 13 Issue 1

2.1 ABSTRACT

Hyperthermia treatments in the clinic rely on accurate temperature measurements to guide treatments and evaluate clinical outcome. Currently, magnetic resonance thermometry (MRT) is the only clinically proven way to non-invasively measure 3D temperature distributions. In this review, we evaluate the status quo and emerging approaches in this evolving technology for replacing conventional dosimetry based on invasively placed probes.

First, we define standardized MRT performance thresholds, aiming at facilitating transparency in this field when comparing MR temperature mapping performance for the various scenarios that hyperthermia is currently applied in the clinic. This is based upon our clinical experience of treating nearly 4000 patients with superficial and deep hyperthermia. Second, we perform a systematic literature review, assessing MRT performance in (I) clinical and (II) pre-clinical papers. From (I) we identify the current clinical status of MRT, including the problems faced and from (II) we extract promising new techniques with the potential to accelerate progress.

From (I) we found that the basic requirements for MRT during hyperthermia in the clinic are largely met for regions without motion, for example extremities. In more challenging regions (abdomen and thorax), progress has been stagnating after the clinical introduction of MRT guided hyperthermia over 20 years ago. One clear difficulty for advancement is that performance is not or not uniformly reported, but also that studies often omit important details regarding their approach. Motion was found to be the common main issue hindering accurate MRT. Based on (II), we reported and highlighted promising developments to tackle the issues resulting from motion (directly or indirectly), including new developments as well as optimization of already existing strategies. Combined, these may have the potential to facilitate improvement in MRT in the form of more stable and reliable measurements via better stability and accuracy.

2.2 INTRODUCTION

Hyperthermia (39-43°C) has been successful as a cancer treatment due to several beneficial effects on tissue, such as enhancing the efficacy of radiotherapy and chemotherapy [27, 69]. The hallmarks of hyperthermia have been identified and are comprehensively presented by Issels *et al.* [70]. Due to these benefits paired with no major side effects, hyperthermia has established itself in the clinic for many tumour sites [71-74]. Dose-effect studies show a positive association between thermal dose parameters and clinical outcome, which implies that real-time temperature dosimetry is essential [32, 75-80]. Temperature during treatment is traditionally monitored by probes inside catheters that are placed inside lumina or pierced into tissue. These provide information at a limited number of points and may be difficult or unfeasible to place, or associated with toxicity [34, 35]. Magnetic resonance thermometry (MRT) can provide a real-time 3D temperature map in a non-invasive way (Figure 2.1) and hence has the potential to make hyperthermia more comfortable and safer for the patient. Visualizing what is heated and to what extent is not only useful to control hot-spots in normal tissue and adapt to cold-spots in tumour tissue, but also provides the means to perform a repeatable measurement as well as to investigate the true optimum temperature for maximizing clinical outcome. MRT has been shown to correlate with pathological response in soft tissue sarcomas of prospectively registered patients [81]. Despite this potential, MRT thus far has failed to establish itself as the standard temperature measurement method in hyperthermia treatments. Given the continued reported progress in the pre-clinical setting, we hypothesize that a major cause of this stagnation is the unclear validation status, as well as the non-standardized way of reporting pre-clinical performance. There is currently no overview of the clinical status quo of MRT in hyperthermia, and promising technologies are difficult to spot in the jungle of performance indicators. Also the substantial financial investment will be overcome, once the full contribution of MRT to hyperthermia quality is convincingly shown.

There have been many successful attempts to review the field. Rieke *et al.* [47] gives an overview of the different magnetic properties that can be exploited to obtain MRT. The importance of accuracy and stability of thermometry measurement are stressed, and acquisition and reconstruction methods that reduce motion artefacts are highlighted. Winter *et al.* [49] is expanding on those challenges faced, also supplying possible solutions. In addition to the hurdles, the implicit nature of the requirements for adequate MR temperature mapping during hyperthermia treatments complicate this quest. Different MRT techniques have different drawbacks and are thus suitable for different purposes of application. One example

is the proton resonance frequency shift (PRFS), which is most frequently used to measure temperature due to its linear variability with temperature and, with the exception of fat, tissue independence. As the investigated shifts are very small, they are not easily able to deal with physiological changes, hence accurate temperature measurements are hampered by changes in the microenvironment of the tissue, for example in flow, oxygen levels, perfusion and magnetic properties of the blood. Lüdemann *et al.* [48] compared MRT techniques and their achievable accuracies. Despite these excellent reviews in the field, there has not been a comprehensive analysis of the validation status and a ranking of the preclinical work based on a clear set of performance indicators.

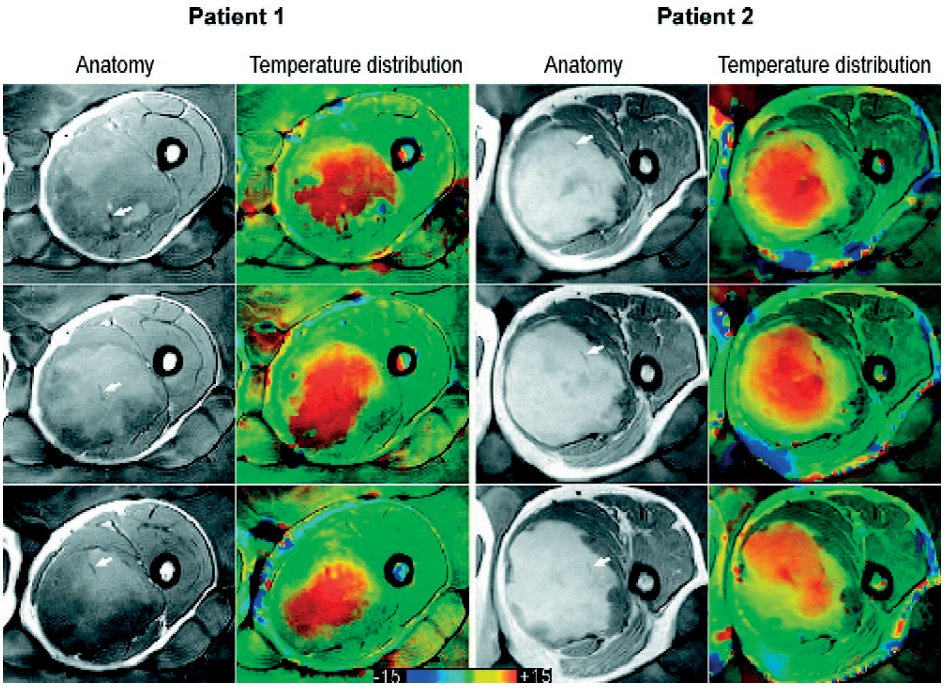

Figure 2.1: Example of anatomy with thermal mapping catheters (arrows) for 2 patients with MR temperature distributions. Figure is taken from Gellermann et al. [64].

For patients to benefit from MRT in hyperthermia treatments, it needs to become reliable so that the invasive probes are no longer needed. Our objective is to identify how MRT can be improved to a point where the added value is appreciated in the clinic, leading to a more widespread use. In order to aid this development, we will firstly define minimum requirements for a successful treatment, creating a benchmark for more uniform reporting and clear comparisons across studies. Secondly, after a systematic literature search, clinical data will be used to assess

to what extend the MRT performance metrics obtained satisfy these requirements. This will be used to identify areas of insufficiency, but also areas of overlap and common concerns. Finally, we will use pre-clinical data from the literature search to identify new techniques, which address those common concerns. By highlighting these 'most promising to advance the field' publications, we hope to emphasize the direction for future research and thus accelerate progress further.

2.3 MINIMUM RECOMMENDED CLINICAL MRT PERFORMANCE

There are a lot of performance measures that can be evaluated and reported on, which in turn depend on many different acquisition settings. To clarify the situation, we introduce the most important acquisition parameters and state which MRT performance measures are vital to report on and define what minimum values we consider acceptable, based on the group's expertise in nearly 4000 clinical (superficial and deep) hyperthermia treatments [73, 76, 82]. Our aim is to create a clear list of requirements of what is needed from a clinical MR guided hyperthermia treatment perspective. The focus is on MRT for mild and moderate hyperthermia (39-43°C) only, hence excluding ablative temperatures. The latter has been the aim for most techniques, since MR guided thermal ablation has a much wider use. Compared to ablation, temperature changes in mild and moderate hyperthermia are slow (about 10-30 minutes to reach the target temperature), target regions are generally large, and the temperature changes from baseline are low (2-8°C). Consequently, the desired temperature mapping performances are also different: although spatial resolution may be lower, measurement accuracy and stability (temporal precision) must be high and robustness against confounders much better.

The minimum acquisition parameters we recommend for successful MRT are reported in Table 2.1 and the minimum MRT performances are shown in Table 2.2.

Table 2.1: Minimum acquisition parameters, such that successful MRT in hyperthermia can be achieved.

Parameter	Definition	Minimum
Spatial resolution	In-plane resolution times slice width (2D) or through-plane resolution (3D)	125mm^3
Temporal resolution	Time needed to acquire one MRT slice	20s

Table 2.2: Minimum performance metrics for successful MRT in hyperthermia treatments.

Measure	Metric	Definition	Minimum
Bias	Mean error (ME)	$ME = \frac{1}{n}\sum_{j=1}^{n}(E_j - A)$	≤|0.5°C|
Spatial precision	Spatial standard deviation (SD)	$SD^2 = \frac{1}{n}\sum_{j=1}^{n}(E_j - \bar{E})^2$	≤0.5°C
Temporal precision	Temporal standard deviation (SD)	Variability at different time points over 90min	≤0.5°C
Accuracy	Mean absolute error (MAE)	$MAE = \frac{1}{n}\sum_{j=1}^{n}\left\|E_j - A\right\|$	≤1°C

Considering the large areas of heating in hyperthermia and consequently low thermal gradients, we consider a reasonable minimum spatial and temporal resolution to be 125mm^3 (for instance 5x5x5mm^3). A higher spatial resolution may be required to achieve acceptable accuracy, by avoiding partial volume effects in regions with many small and contrasting tissue.

For this recommendation we also considered the current spatial resolution that is achieved with invasive thermometry. In general, the distance between measuring points along a thermometry catheter track is 1-2cm. The distance between thermometry catheters is much larger still with 5-10cm. Additionally the MRT resolution should be considered with respect to the resolution or our ability to steer the energy distribution. At this moment the focus of the 100 MHz RF-deep heating has a diameter of 7-14cm. For the Hypercollar3D operating at 434 MHz this is 3cm. Finally, when utilizing hyperthermia treatment planning for deep as well as head and neck treatments, the CT images used for planning are acquired with a slice width of 5mm and resolution of 0.98mm in both x and y [83]. It is also worth considering that a higher resolution in hyperthermia treatment planning comes at the cost of increased intricacy and treatment time [84].

For deep heating, the clinical objective is to achieve a temperature increase between 0.5-2°C per 5 minutes. If it is lower (<0.5°C) the power is increased in order to speed it up; if it is higher (>2°C) the power is reduced to slow it down. Because of these relatively slow heating times and the resulting high time constant of thermal washout, the minimum temporal resolution should be 20s. This recommended minimum of the temporal resolution concerns the minimum acceptable time from a clinical perspective, faster scanning may be required in regions of motion to achieve acceptable accuracy. Another reason to speed up the acquisition may be

to when averaging of temperature data is required to achieve the minimum MRT performance as stated in Table 2.2.

Regarding the important performance measures, the first mentioned in Table 2.2 is bias, measured as the mean error (ME), which is defined by Walther *et al.* [85] as:

$$ME = \frac{1}{n}\sum_{j=1}^{n}(E_j - A) \tag{2.1}$$

This is the difference between the MRT measurement (E_j) and another temperature measurement that is considered true (A) over all measured time points (n). This reference A, i.e. the golden standard, can be a set of invasive temperature probes, or another MRT map originating from a well-established sequence. It is important to have a reliable and repeatable MRT readout, without a systematic over- or underestimation of temperature, translating to a low bias in measurements. Curto *et al.* made a comparison of the currently worldwide installed five RF-MR hybrid systems in anthropomorphic phantoms, showing with a mean error as low as 0.13°C what can be achieved with current systems in 'ideal condition' preclinical settings [86]. Indicating the best resolution feasible, we consider a ME of ≤|0.5°C| to be appropriate.

The following two measures, defined in Table 2.2, are spatial and temporal precision. The spatial standard deviation (SD) reflects the variability in the region of temperature evaluation, consisting of a ROI. Spatial SD of the ROI evaluated should be ≤0.5°C in order to guarantee that the noise present is not too large and there are no large temperature gradients within the heated region; in other words the heated region is sufficiently uniform. Temporal SD assesses the variability of the spatial mean temperature in a ROI across all time points and indicates the repeatability and stability of the measurement. Considering treatment times are long, but keeping in mind the importance of staying in the target temperature zone, the temporal precision should not exceed 0.5°C (after drift correction) for a 90 minutes thermometry measurement. Both the spatial and temporal SD are influenced by the size and location of the ROI chosen. This, in turn, is highly dependent on the MRT region imaged, as areas with poor uniformity (for example near tissue/air boundaries) need to be avoided for sufficient accuracy of the measurement. Due to this needed flexibility, no recommendation on size and location of the ROI will be stated. In order to fulfil the minimum requirement of the precision defined above, the ROI should be chosen with care in a region as uniform as possible. The measures of precision are only valuable when the ROI is kept constant throughout the measured time points.

The final performance measure that is vital to report on is the accuracy of the MRT measurement. Accuracy, as stated by Walther *et al.* [85], can either be presented as the mean squared error (MSE), the root mean squared error (RMSE) or the mean absolute error (MAE). We consider the MAE the best one for our application since it is less sensitive for outliers and easy to interpret:

$$MAE = \frac{1}{n}\sum_{j=1}^{n}\left|E_j - A\right| \tag{2.2}$$

Where E_j is the MRT measurement, A is another temperature measurement that is considered true and n is the number of all measured time points. Given the importance of keeping to the right heating range for the desired physiological changes in the tumour tissue, we think it should be ≤1°C.

2.4 METHODS

2.4.1 Literature search

In order to ensure that all papers published using MRT in hyperthermia treatments will be included, a logical search string was defined including a hyperthermia term, a magnetic resonance thermometry term, and excluding ablation in a major term. We searched the databases for papers published from inception of the databases until 24/11/2020.

Using the method from Wichor *et al.* [87] all papers were screened by title and abstracts for relevancy to our topic. At this stage, papers were excluded if they were not published in English, if they were not research articles or if the topic was not related to MRT in hyperthermia. Our definition of the combination of mild and moderate hyperthermia includes treatments with the heating goal between 39-45°C. We acknowledge that in some cases tumour temperatures can be higher than the target temperature, thus papers up to 47°C were considered relevant.

The resulting 206 relevant papers were then assessed for eligibility, using the following exclusion criteria: (#1) ex-vivo results, (#2) no original data, (#3) small animals. Ex-vivo results excluded those studies on simulation or phantoms, which we considered too far from the final intended use of the clinic to be included in this review. Not original data excluded reviews and studies using already published data as reference. Small animals were considered to be anything smaller than a dog. These studies were excluded since we deem these data not predictive for humans due to the different motion profile (e.g. faster heart rate) and their smaller size.

Additionally, the equipment used is especially made and non-clinical, lowering the ease of translation into the clinic. Large animal studies without heating were not included. After this eligibility assessment, 42 papers remain to be included in the systematic analysis. A PRISMA flow chart of the exclusion process is shown in Figure 2.2.

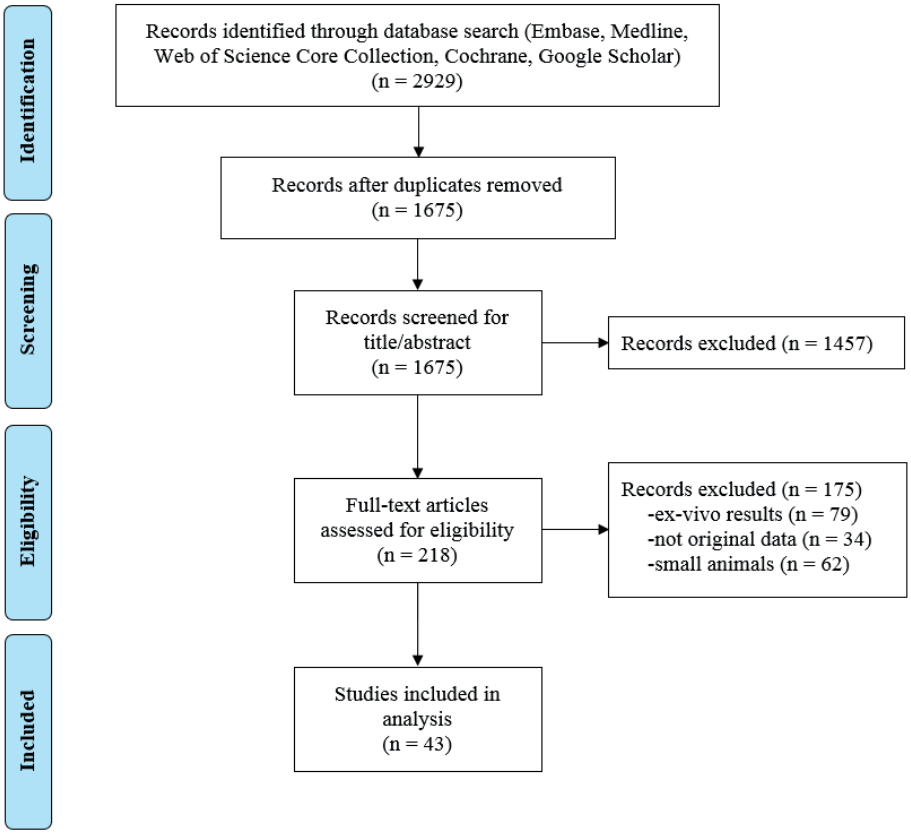

Figure 2.2: PRISMA flow chart

2.4.2 Categories and classification

The studies included were then categorised into patients with treatment intent and pre-clinical groups (with no hyperthermia treatment intent). Peller *et al.*[88] included treated and not treated patients and thus was allocated to both groups. Clinical studies included 10 studies. Pre-clinical studies consisted of 35 studies: 26 papers with human subjects and 12 studies including large animals. In early volunteer studies, heating and cooling were sometimes applied to the volunteers without therapeutic intend. These studies were also considered pre-clinical.

The relevant papers were read in detail and relevant data was extracted into Microsoft Excel tables. The information, such as first author and year of publication, is the one obtained from the EndNote library. Other study data considered relevant were: hyperthermia treatment approach, imaging set-up, MRT performance and the exclusion of data. Pre-clinical papers were also grouped and ranked based on their main aim and achieved improvement to identify promising techniques. Large animals, volunteers and non-heated patients are easier to image than treated patients, making it more likely for their MRT data to be artefact free. Large animals are typically sedated and mechanically ventilated during treatment, which reduces their breathing and makes it more predictable, and also lowers their blood perfusion. Muscle relaxant and bowel movement suppressants are also administered, minimizing any other avoidable motion. Volunteers have the advantage of no initial stress from illness and, when there is no heat applied, no additional stress during the treatment. Non-treated patients also lack the additional stress of treatment. Except for these differences, both large animals and volunteers have similar confounders such as size, motion profile and they generally use the same equipment for heating as well as imaging. Thus we consider these pre-clinical studies predictive for the reproducibility in patients during treatment.

2.5 MRT PERFORMANCE IN CLINICAL STUDIES

2.5.1 Status

MRT in hyperthermia is predominantly used for extremities (67%) and some studies investigated it in the pelvis (33%). This trend can be explained by the absence of motion and resulting artefacts in extremities. Data of ongoing research in our group shows that achieving successful MRT in the pelvic area is much harder than in more static regions of the body. The average maximum temperature achieved during the hyperthermia treatments was 43.8°C, which is well within the target treatment temperature range, and the treatment time varied from 30-90 minutes. All studies applied hyperthermia using radiofrequency (RF) electromagnetic waves. The most popular system is the BSD2000/3D/MR, which incorporates the twelve channel Sigma Eye applicator.

The imaging set up for the 10 clinical studies is presented in Table 2.3. The published MRT in hyperthermia clinical experience is limited to very few centres (Duke, Tubingen, Berlin, Munich). Hence there is a challenge on translating their high degree of specific experience to other centres. Additionally it is difficult to define a benchmark due to the limited amount of data published.

*Table 2.3: Imaging set-up for clinical papers. Body part imaged: E=extremities, P=pelvis. Metrics that are within our recommended minimum are shaded in green, (spatial and temporal resolutions of 125 mm^3 and 20s respectively). † supplied a 95% confidence interval of the MR temperature, * used T1 instead of PRFS for calculating MR temperature maps, ^ used a 0.2T instead of a 1.5T MRI, ~ standard error instead of SD.*

Author (year)	Body part	Sequence	Spatial res [mm^3]	Temporal res [s]	ME [°C]	Spatial precision [°C]	Temporal precision [°C]	MAE [°C]
Carter (1998) [94]	E	GRE	8.8	-	-	0.50	-	-
Craciunescu (2009) [63]	E	GRE	27.4	10	-	0.52	-	0.74
Craciunescu (2001) [92] †	E	GRE	11.9	-	-	0.49~	-	-
	E	GRE	13.7	-	-	0.56~	-	-
		EPI	156.0	1				
Dadakova (2015) [91]	E,P	EPI	67.6	1.08	-0.04	0.55	-	0.40
		GRE	152.1	3.12				
Gellermann (2005) [95]	P	GRE	146.8	3.12	-	2.10	-	1.50
Gellermann (2006) [64]	E,P	GRE	146.8	3.12	1.10	0.70	-	-
Peller (2002) [88] *^	E,P	GRE	96.1	64	-	0.10	-	-
Stauffer (2009) [90]	E	GRE	21.1	15	0.85	-	-	-
Unsoeld (2020) [81]	E	not stated	-	-	-	0.21	-	-
Wu (2020) [93]	P	GRE	152.1	3.32	-	-	-	-

The imaging coil used by most was the body coil, so when this information was absent the body coil was assumed. MRT was based on the proton resonance frequency shift (PRFS), except in Peller *et al.*[88], who used T1. This is not surprising, as PRFS varies linearly with temperature over an adequate range and is near independent of tissue type [89]. Gradient Recalled Echo (GRE) sequences were generally used (Table 2.3), and all sequences acquired 2D MRT maps. Peller *et al.*[88] was the only study which used a 0.2 Tesla MRI instead of 1.5T. The frequency of MRT acquisition varied from continuous to every 20 minutes. Studies that reported values for spatial and temporal resolutions within our recommended minimum of 125 mm^3 and 20s are shaded in green in Table 2.3. Most studies manage to satisfy the minimum requirements, as defined in Tables 1 and 2.

Methods used to improve the thermometry quality were:

- Increasing the number of excitations (NEX) > 1 (number of times each k-space line is read) [63, 90]
- Applying flow compensation [91]
- Including modelling of blood perfusion [92]
- Using background field removal algorithms to correct for motion-induced susceptibility artifacts [93]

- Only selecting evaluable volumes or treatments – all but one study (discussed in "Exclusion" section below)

Table 2.3 also shows the MRT performance reported in clinical papers. Values that meet our minimum requirements are shaded in green. Of the metrics that are reported, 6/9 of studies (67%) satisfy one or more of our minimum requirements.

Unsoeld *et al.* [81] shows the correlation of measured temperature with clinical outcome. Whilst this study investigates the true goal of the treatment, this study could have contributed more to the field if it had also reported bias, SD and accuracy. This would have helped to understand the required treatment quality and the relationship between thermal dose and treatment outcome. A similar line of thought applies to the study of Wu *et al.* [93], which gives accounts of TNR improvement from their investigated correction method, but neglects to quantify these. Table 2.3 demonstrates that few performance metrics are reported, which makes it difficult to compare the status of MRT between different studies. Additionally, definitions of parameters are often lacking, leading to the need for educated guesses.

2.5.2 Exclusion of data

Comparing these indicative performance metrics listed above comes with limitations. Often even the ROIs considered within the same study at different time points are not constant. Additionally, certain numbers of time points were often excluded from the evaluation – usually due to image artefacts that produce noisy thermometry maps. This decrease in the number of thermometry maps adds selection bias to the performances reported. In Table 2.4, we present what data was excluded post acquisition and which reason was mentioned by the authors. If exclusion was not explicitly mentioned, we assumed that all MRT data acquired was also included in the analysis.

As is shown in Table 2.4, only one study included all of the acquired MRT data. This apparent need to exclude data underlines the need for MRT to become more reliable in regions of motion before it can replace invasive temperature probes. Information on the total study sizes also provides objective information on the practicality of using MRT. The limited number of publications on clinical use of MRT is highlighted and confirms that experience is very local (and presumably the conclusion on the feasibility of MRT is biased by the positive attitude of the researchers). All of the above clearly demonstrates that MRT is still in a developing phase and there exist substantial need to make major improvements to expand to broader use of the technology.

Table 2.4: Exclusions of data from clinical studies post acquisition

Author	All data included?	Size of study	What was excluded?	Why?
Carter (1998) [94]	No	4 patients 5 treatments	Not stated	Artefacts
Craciunescu (2001) [92]	Yes	2 patients	-	-
Craciunescu (2009) [63]	No	10 patients 40 treatments	4 patients 12 treatments	Lack of MR information in HT treatments performed outside the MR scanner, image/motion artefacts, uncorrectable drift, impossibility to localize the fiber optic probes, missing/ corrupted data files
Dadakova (2015) [91]	No	3 patients 20 treatments	1 patient 1 treatment	Susceptibility artefact in the ROI from air in rectum
Gellermann (2005) [95]	No	15 patients	Everything but 1 best session per patient	MR data sets incomplete and/or disturbed by technical reasons
Gellermann (2006) [64]	No	9 patients 30 treatments	15 treatments	Breakdown or malfunction of applicator, restlessness of the patient
Peller (2002) [88]	No	1 patient	“Data sets”	Artefacts
Stauffer (2009) [90]	No	10 patients	3 patients All except 12 treatments	Uncorrected field drift or inability to locate or correlate sensor positions or significant patient position shift early in treatment
Unsoeld (2020) [81]	No	24 patients	13 patients: 11 patients with abdominal and pelvic tumours; 1 patient with different time course of therapy; 1 patient without surgery	Breathing and intestinal motion artefacts in MRT data; pathological response is not comparable; lack of information on pathological response
Wu (2020) [93]	No	4 patients	2 patients	Bulk motion due to discomfort during treatment, ROI contained too much gas

2.5.3 Preclinical status – how does it compare?

Comparing their imaging set-up, preclinical studies are very similar to clinical ones. The sequences and MRT methods used were more varied, but just like the patient studies investigated, the spatial resolution was met in all studies and temporal resolution requirement was met in 29/35 studies. Regarding MRT performance

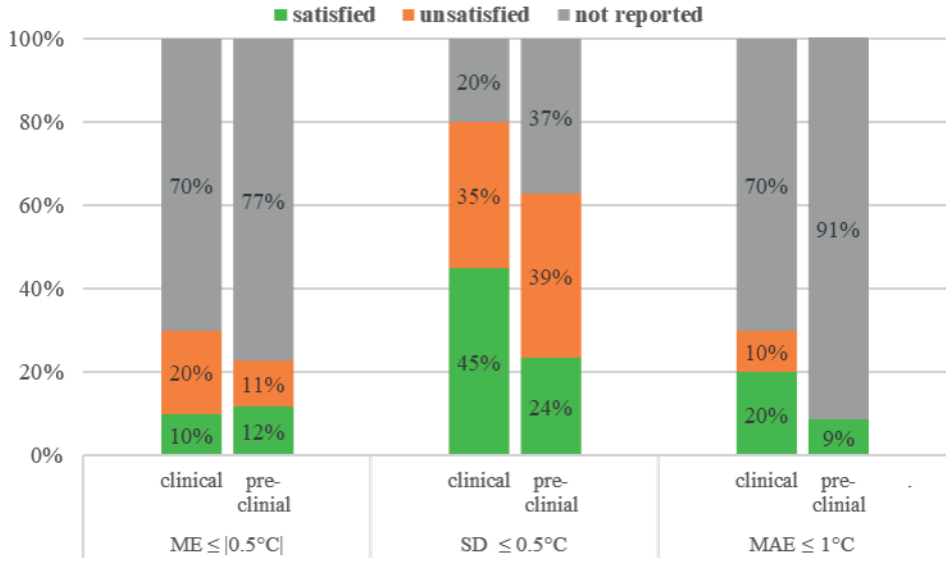

Figure 2.3: Performance values reported and how many of those satisfied our requirements for clinical and pre-clinical studies.

Table 2.5: Pre-clinical studies by the year of publication; including technique/method investigated, improvement found (where applicable) and main aim of the study. Studies satisfying our performance criterion are highlighted in green.

Author	Year	Technique/method investigated	Improvement	Main aim
Wu [93]	2020	Correction of motion-induced susceptibility artifacts	TNR improvement	B0 changes and image gaps due to motion, B0 drift
Ferrer [96]	2020	Different B0 drift corrections	IQR improved from 9.31 to 0.80°C. ME improved from -4.30 to 0.33°C	B0 drift
Bing [97]	2019	Forced breath-hold MR-HIFU	Accuracy and stability from 1.2 to 0.6°C and from 1.4 to 0.8°C	B0 changes and image gaps due to motion
Odeen [98]	2019	Different protocols for PRFS MRT for LITT	Factor 2 improvement in the SD	Comparison
Tan [99]	2019	Motion compensation using principal component analysis and projection onto dipole fields	Reduces SD from 3.02 to 0.86°C	B0 changes and image gaps due to motion
Wu [100]	2019	Novel fast spin echo method	TNR efficiency improved by 25%	Feasibility
Zhu [101]	2019	Feasibility/safety of MRgHIFU	N/A	Feasibility

Table 2.5: Pre-clinical studies by the year of publication; including technique/method investigated, improvement found (where applicable) and main aim of the study. Studies satisfying our performance criterion are highlighted in green. (continued)

Author	Year	Technique/method investigated	Improvement	Main aim
Jonathan [102]	2018	Proposed and validated a hybrid radial-EPI temperature mapping pulse sequence	Provides whole brain coverage, SD was 48% higher than standard	Feasibility
Kothapalli [103]	2018	MRT performance at different anatomical sites	N/A	Comparison
Chu [104]	2016	Feasibility (safety + performance) MRgHIFU for rectal cancer	Precision and stability improved from 7.8 and 2.3°C to 0.3 and 0.6°C	Feasibility
Svedin [105]	2016	Correction of respiration artifact in 3D MRT using phase navigators	Temperature measurement improved by a factor of 2.1	B0 changes and image gaps due to motion
Tillander [106]	2016	Hyperthermia for deep-seated heating volumes using HIFU	N/A	Feasibility
Boulant [107]	2015	FID navigator to correct for B0 field and variations induced by breathing	Reduces the SD of the data over first 8 minutes from 0.2 to 0.05°C	B0 drift and B0 changes due to motion
Senneville [108]	2015	Approach for motion estimation of abdominal organs	SD improvement of 0.4°C and reduction of artefacts by up to 3°C	B0 changes and image gaps due to motion
Gaur [109]	2015	Reconstruction method to accelerate MRT	Achieves same temperature error at up to 32x acceleration factors	Acceleration
Marx [110]	2015	MASTER sequence	SD improvement from 1.21 to 0.82°C	Feasibility
Mei [111]	2015	Different methods for B0 inhomogeneity correction	None	B0 drift
Pichardo [112]	2014	Multi-baseline MR-based thermometry	Reduced SD from 25.2 to 2.4°C	B0 changes due to motion
Shi [113]	2014	partial separability (PS) model and referenceless thermometry introduced	N/A	Feasibility
Minalga [114]	2013	Integrated multi-channel RF receive coil with MR-HIFU	163% SNR improvement averaged over all positions investigated	Feasibility
Ramsay [115]	2013	Segmented GRE-EPI technique	N/A	Feasibility

Table 2.5: Pre-clinical studies by the year of publication; including technique/method investigated, improvement found (where applicable) and main aim of the study. Studies satisfying our performance criterion are highlighted in green. (continued)

Author	Year	Technique/method investigated	Improvement	Main aim
Kickhefel [116]	2010	Comparison of fast sequences	Stability improvement from 1.07 to 0.21°C	Comparison
Wyatt [117]	2010	Correction of breathing-induced errors using multi-echo fitting methods	SD from 2.18 to 0.61°C and bias from 3.17 to -1.26°C	B0 changes and image gaps due to motion
Roujol [118]	2009	Reconstruction pipeline for adaptive TSENSE	Image latencies below 90ms at frame rates up to 40 images/s	Acceleration
Wyatt [119]	2009	Different stabilisation strategies	Improved error by up to 0.5°C	B0 drift
Silcox [120]	2005	Ultrasonic heating to control transgene expression spatially using a minimally invasive approach	N/A	Feasibility
Sun [121]	2005	Adaptive controllers with MRT	N/A	Feasibility
Peller [88]	2002	Characterize T1 for thermometry	N/A	Feasibility
Il'yasov [122]	1998	RARE sequence for diffusion MRT	N/A	Feasibility
Corbett [123]	1997	1H MR spectroscopy to measure absolute brain temperature	N/A	Feasibility
MacFall [124]	1996	Chemical shift of water for MRT	N/A	Feasibility
De Poorter [125]	1995	PRF thermometry in vivo	N/A	Feasibility
MacFall [126]	1995	Rapid diffusion weighted EPI, being less sensitive to motion	SD from 1.5 to 0.9°C	B0 changes due to motion
Young [127]	1994	Initial investigation of T1 dependence, D and perfusion	N/A	Feasibility
Hall [128]	1990	Investigation which MR parameter would be best for MRT in vivo	N/A	Comparison

metrics about half of the pre-clinical studies achieved our minimum requirements. This is illustrated and contrasted to the clinical performance in Figure 2.3.

Considering exclusion of data post acquisition, five preclinical studies (two with large animal and three with human subjects) excluded some, which is significantly less than the clinical studies investigated. This most likely can be linked back to the subjects making measurement conditions less challenging as mentioned above.

2.5.4 New techniques and their improvement

Table 2.5 presents the main techniques and methods investigated in the pre-clinical studies and their found improvement over standard methods. From this information, we have identified common main aims (last column).

When looking at the improvements mentioned over the benchmark methods (column 4 of Table 2.5), there was only one study that didn't find an improvement in their investigated techniques (Mei *et al.* [111]). This demonstrates the importance and success of pre-clinical work.

The most promising techniques from Table 2.5 are the 13 studies satisfying our MRT performance criterion, these are highlighted in green. It can be seen that in recent years more studies have satisfied these minimum requirements. 8 out of those 13 studies are feasibility or comparison studies, which can be grouped into having investigated:

1. Hardware: MR-HIFU for different treatment location applications [104, 106]
2. Thermometry method: MR spectroscopy to measure absolute temperature [123]
3. Sequences and parameters for MRT [102, 115, 116, 129]
4. Performance of MRT at different anatomical sites [130]

The remaining 5/13 pre-clinical studies satisfying our MRT performance criteria and not involving feasibility or comparisons, can be grouped by common main aims or problems to solve:

1. B0 drift: correction and stabilisations strategies [96, 119], navigator echoes [107]
2. B0 changes due to motion: breath hold [97], navigator echoes [107]
3. Image gaps due to motion: breath hold [97]
4. Acceleration: reconstruction method [109]

It needs to be highlighted that with the exception of Bing *et al.* [97] these studies have investigated only one subject, so their potential needs to be validated on a larger scale. Despite great potential, the possible limitations of the techniques above, when

transferred to patients in a clinical environment, must be mentioned. Breath-hold may not always be a viable option for the clinic. Some patients (for example young children) may not be able to hold their breath effectively, or may be sedated during the treatment. Additionally, the total treatment time will lengthen, as the patient needs periods of normal breathing to recover. Navigators to correct for B0 changes induced by breathing may only be valuable in areas with no motion in the treated area, as well as very regular breathing patterns. Similarly, B0 drift corrections may only be valuable in areas with no motion or motion induced changes present.

It can be seen from the investigated studies that groups working on MRT advances are generally different groups than those working on patients with a treatment objective. The consequence is that solutions are presented with very limited ability to be transferred to clinical practice in RF-hyperthermia MRT. This is highlighted by the face that no progress has been made in MRT for pelvic RF-hyperthermia in the past two decades: the body coil is still used for imaging and PRFS is used with no real solution for correction of external and internal movement, for instance by passing air.

However, the technological advances in recent years are promising in many ways. Multi-coil integrated hyperthermia systems are becoming available and provide much better SNR than the commonly used body coil [114, 131]. At the same time, multi-coil acquisition also offers acceleration of MRT by techniques such as, for example, parallel imaging or compressed sensing [132]. Additionally the computational power available now is much bigger and cheaper compared to only a few years ago, which makes more complicated reconstruction method and correction strategies feasible [93]. Last but not least, new sequences and approaches are being developed to increase MRT performance and explore the possibility to perform MRT in more difficult regions such as with motion, in fatty regions [68] or in bone. Considering all these innovations, the present conditions are favourable to push MRT to the next level and hopefully, in the near future, have the powers to elevate it from a research modality to clinical practice.

2.6 CONCLUSION

Standardised reporting of parameters used and performances obtained in MRT is important. Hence we defined a minimum benchmark of important performance metrics including bias, spatial and temporal precision as well as accuracy; these should be within $\leq|0.5°C|$, $\leq 0.5°C$, $\leq 0.5°C$ and $\leq 1°C$ respectively.

When systematically assessing the literature, we can conclude that MRT performance in hyperthermia is already achieving most of these requirements for extremities; but not yet in regions with more motion present. Motion as well as the B0 changes as a direct or indirect consequence emerged as the main problem of accurate and reliable MR temperature measurement.

Various techniques satisfying our performance requirements are already available at the preclinical stage addressing these problems. Most promising common solution proposals can be divided into either new approaches or optimisations. New approaches include hardware or software being developed; propitious optimisations include: correction and stabilisations strategies, navigator echoes, breath hold and reconstruction methods. We anticipate that highlighting these promising pre-clinical advancements will accelerate the progress of MRT.

Chapter 3

Multi-echo gradient echo pulse sequences: which is best for PRFS MR thermometry guided hyperthermia?

Based on:

Multi-echo gradient echo pulse sequences: which is best for PRFS MR thermometry guided hyperthermia?

Theresa V. Feddersen[1,2], Dirk H.J. Poot[2], Margarethus M. Paulides[1,3], Ghassan Salim[2], Gerard C. van Rhoon[1,4], Juan A. Hernandez-Tamames[2,5]

[1] Department of Radiotherapy, Erasmus MC Cancer Institute, University Medical Center Rotterdam, 3015GD Rotterdam, The Netherlands
[2] Department of Radiology and Nuclear Medicine, Erasmus MC Cancer Institute, University Medical Center Rotterdam, 3015GD Rotterdam, The Netherlands
[3] Electromagnetics for Care & Cure Research Lab, Center for Care and Cure Technologies Eindhoven (C3Te), Department of Electrical Engineering, Eindhoven University of Technology, 5600MB Eindhoven, The Netherlands
[4] Department of Applied Radiation and Isotopes, Reactor Institute Delft, Delft University of Technology, 2629JB Delft, The Netherlands
[5] Department of Imaging Physics, Applied Physics Faculty, Delft University of Technology, 2629JB Delft, The Netherlands

Published in:

International Journal of Hyperthermia 2023 Vol. 40 Issue 1 Pages 2184399

3.1 ABSTRACT

MR thermometry (MRT) enables non-invasive temperature monitoring during hyperthermia treatments. MRT is already clinically applied for hyperthermia treatments in the abdomen and extremities, and devices for the head are under development. In order to optimally exploit MRT in all anatomical regions, the best sequence setup and post-processing must be selected, and the accuracy needs to be demonstrated.

MRT performance of the traditionally used double-echo gradient-echo sequence (DE-GRE, 2 echoes, 2D) was compared to multi-echo sequences: a 2D fast gradient-echo (ME-FGRE, 11 echoes) and a 3D fast gradient-echo sequence (3D-ME-FGRE, 11 echoes). The different methods were assessed on a 1.5T MR scanner (GE Healthcare) using a phantom cooling down from 59°C to 34°C and unheated brains of 10 volunteers. In-plane motion of volunteers was compensated by rigid body image registration. For the ME sequences, the off-resonance frequency was calculated using a multi-peak fitting tool. To correct for B0 drift, the internal body fat was selected automatically using water/fat density maps.

The accuracy of the best performing 3D-ME-FGRE sequence was 0.20°C in phantom (in the clinical temperature range) and 0.75°C in volunteers, compared to DE-GRE values of 0.37°C and 1.96°C respectively.

For hyperthermia applications, where accuracy is more important than resolution or scan-time, the 3D-ME-FGRE sequence is deemed the most promising candidate. Beyond its convincing MRT performance, the ME nature enables automatic selection of internal body fat for B0 drift correction, an important feature for clinical application.

3.2 INTRODUCTION

In hyperthermia (HT) treatments, tumour tissue temperature is increased to sensitize it for other forms of cancer treatment such as radio-, chemo- and immunotherapy. Real-time temperature feedback during HT treatments is essential, as clinical outcome depends heavily on the temperature reached [32]. The target treatment temperature usually lies between 39-43°C. The temperature achieved in the region of interest (ROI) is commonly measured using temperature probes that are placed intraluminally or punctured into tissue in, or close to, the target volume. These probes provide temperature information for a limited region, and may sometimes be difficult or even unfeasible to place [33]. MR thermometry (MRT) promises to enable 3D non-invasive, real-time temperature measurement during HT treatments. These temperature maps could visualize the temperature in the target volume and identify hot- and cold-spots during treatments, hence enabling the optimization of treatment quality. Ultimately, good quality thermal dosimetry will facilitate enhanced understanding of the relationship between target temperature and treatment outcome. Hence, MRT carries the potential to make HT treatments more repeatable, safer and more effective for the patient.

In MR imaging, many temperature sensitive magnetic properties can be exploited for temperature measurement. Proton resonance frequency shift (PRFS) is the most frequently used, and considered the most accurate method [52], as it varies linearly over a large temperature range and is independent of tissue type (with the exception of fat) [53]. Measuring the temperature induced changes in the local resonance frequency by phase mapping may be confounded by other changes in the magnetic field occurring simultaneously, such as magnetic field drift [133]. Hence, even though MRT is relatively straight forward and regularly used when performing HT in patients with static tumours such as sarcoma [81], it's much more challenging in body sites where more movement can be expected e.g. abdomen, thorax and head&neck [46].

The scientific and clinical communities agree on the importance of having accurate and reliable MRT measurements [47]. The desired performances have been clearly defined, but as explained above, successful MRT is largely dependent on the treatment location [103, 134]. One way to improve MRT is by increasing the SNR, leading to better precision of the phase maps. This is largely made possible by novel MR HT devices that position multiple receiver coils close to the body [39]. Other strategies to improve MRT include various motion correction techniques and faster imaging; these are comprehensively discussed in Yuan et al. [89].

For the brain, motion is not a primary concern. Hence, in preparation of developing motion confounder corrections for other body sites, this location is ideal for testing which sequence will provide accurate temperature mapping. Consequently, the results can be of general value also when performing MRT in other (more challenging) anatomies, because the effect of the sequences are not being intermixed with motion effects. As such, any difference in error that will be encountered in other anatomies can be seen as advantages and drawbacks that can be expected in that particular anatomy, rather than a general trend of the sequence. High precision MRT in the brain has been demonstrated in the past [135, 136], using the help of field monitoring to correct for non-temperature induced frequency shift. While this method gives good results, it is expensive and thus not an option for most institutions. Also, the MRT approaches presented don't have sufficient spatiotemporal resolution to monitor temperature during thermal therapies [136].

The only clinical standard pulse sequence available for MRT is the DE-GRE sequence [64, 95], which hence is the baseline for comparison in this paper. DE-GRE has been compared to other pulse sequences before [91, 100], but never on a broader scale. Also multi-echo sequences have been used to calculate MRT, but often rely on creating a library of images as a baseline [137]. This takes additional time for imaging at the start of the experiment. Cheng et al. [138] developed a dual-step iterative temperature estimation algorithm, that improved both accuracy and precision. However, this only applies to areas where fat fractions are between about 10% and 90%. In areas with homogeneous water and fat distributions, fat-referenced thermometry has been shown to work well [139].

In this work, we compare the performance of different clinically available ME-GRE sequences for MRT. PRFS MRT performance, especially accuracy, is investigated in phantom and unheated volunteers. By investigating MRT in the brain, we aim to demonstrate the possible improvements also for more challenging treatment areas, whilst keeping the door open for further developments that could build on these results. The sequence used for clinical MRT monitoring during HT at most institutions (including ours) is double-echo gradient-echo, DE-GRE (2 echoes, 2D). We hypothesize that alternative multi-echo gradient-echo sequences might allow better monitoring of HT treatments than DE-GRE, and therefore compare it to two other multi-echo sequences: ME-FGRE (11 echoes, 2D) and 3D-ME-FGRE (11 echoes, 3D) [140]. MRT of the sequences having more than two echoes are being evaluated with a multi-peak and multi-echo fitting method developed previously: MMT-PRFS [42].

3.3 MATERIALS AND METHODS

3.3.1 Phantom design

A phantom was created with different fat percentages, containing T1 and T2 ranges similar to what is found in human tissue [141], following the recipe by Bush et al. [142] (see Figure 3.1). The water mixture (0% fat), positioned in the centre, is the only one being evaluated in this study. It consists of a mixture of distilled water, gadolinium-diethylenetriaminepentacetate (DTPA) contrast agent, water-soluble surfactant, agar, and sodium benzoate, and thus solidifies. The mixtures were filled in 50mL Polypropylene conical vials (30x115 mm) and placed in a PVC pipe with a lid Figure 3.1. The space between tube and pipe was filled with distilled water. Preliminary experiments of the different mixtures excluded susceptibility artefacts and evaluated SNR, and T1 and T2 values. Subsequently, catheters were added to facilitate easy insertion of temperature probes. The temperature probes are part of our PYREXAR BSD2000-3D-MRI deep HT system, and they serve as the ground truth temperature measurements. According to the vendor specification, the thermistor type sensors are non-perturbing and electromagnetically insensitive with an accuracy of ±0.2˚C over a range of 25 to 52˚C [143].

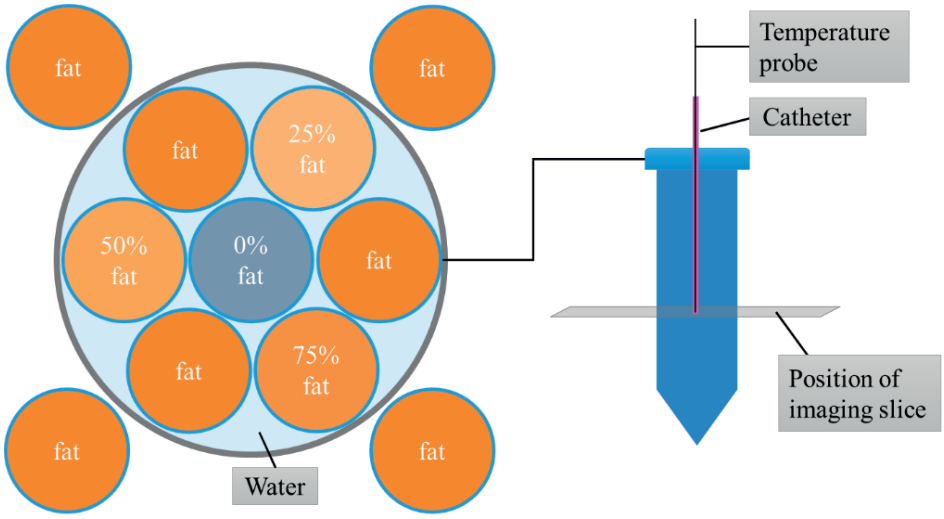

Figure 3.1: Schematic of the home-made phantom. In this study, only the MRT of the vial in the centre, containing the water mixture, is analysed. The outer four fat vials are used for correcting for the B0 drift.

3.3.2 Theory / method

Post-processing was conducted offline in MATLAB and SPSS. Figure 3.2 gives an overview of the post-processing pipeline that we developed, and the steps are

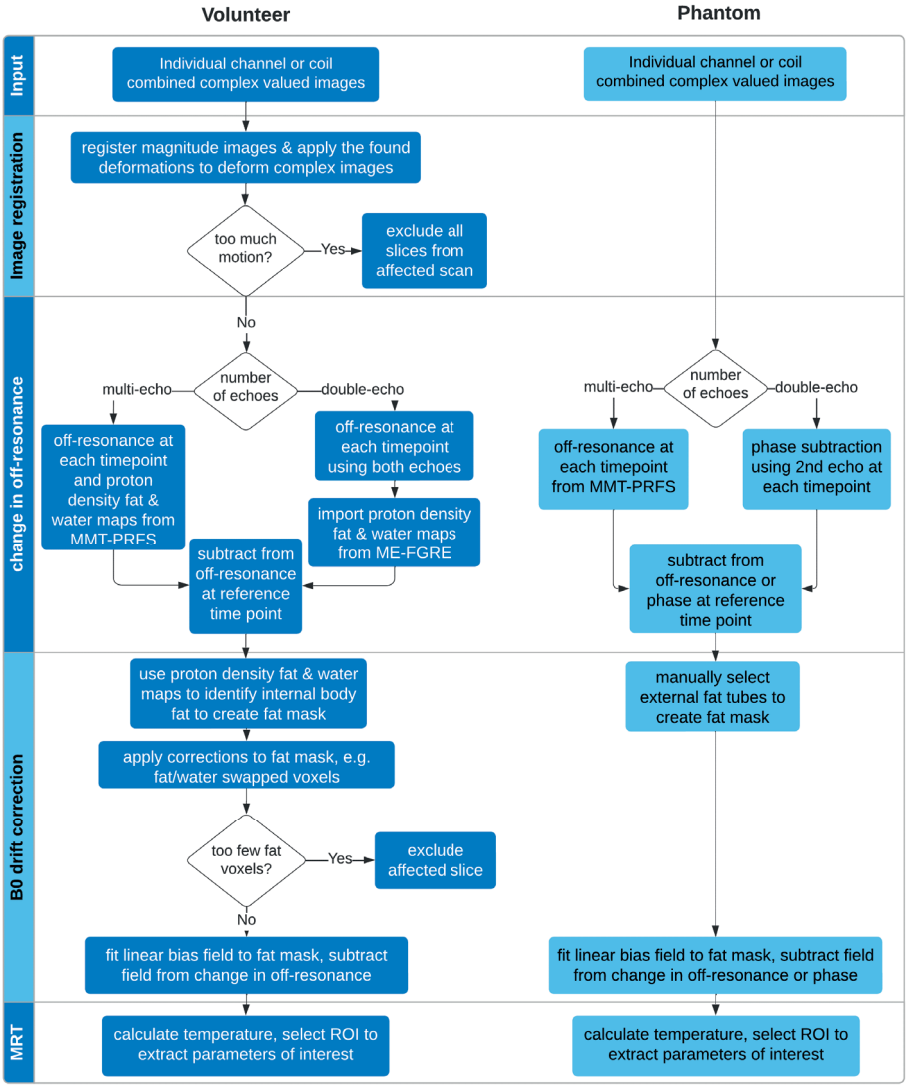

Figure 3.2: Flow chart of post-processing of experimental data. More detailed information on the methods in general can be found in the text..

described below in more detail. The code is publicly available on GitLab: https://gitlab.com/radiology/quantitative-mri/mr-thermometry.

3.3.2.1 Inputs

The acquisition of sequences was repeated at multiple time points and the input into the pipeline differed between the sequences. The ME acquisitions were automatically reconstructed by the scanner into DICOM images of the real and

imaginary components. For the DE-GRE acquisition the raw multi-channel k-space data was imported into MATLAB. In order to combine the k-space data for the individual coils, for each time point, one set of coil sensitivity maps is obtained by applying the ESPIRiT method [144]. The method was applied to each slice, with a calibration area spanning the centre 40% of k-space in both in-plane dimensions and using all echoes in the calibration matrix.

3.3.2.2 Image registration

For volunteers it was in hindsight deemed necessary to register the coil-combined complex valued data, to correct for subject motion along the time points. This was deemed especially important for performing the B0 drift correction (Section 3.3.2.4) using the thin fat layer see the supplementary information for support of this. For our experiments subject motion was not restricted, however patients motion will be severely constrained by the water bolus of the HT device. To compensate motion, we performed a rigid pair-wise image registration of the magnitude images using Elastix [145][1]. Subsequently the found deformation was applied to the complex valued images. Since the 2D acquisitions had a slice gap, and phase consistency across slices was not ensured, image registration could only be reliably applied in in-plane directions. However, 3D registration was used to quantify the z-motion for all data; scans for which the motion in the z-direction exceeded 20% of the slice thickness were excluded.

3.3.2.3 Change in off-resonance

For the DE-GRE acquisitions in volunteers both echoes were used, to correct for other not-temperature-related changes such as the conductivity [146]. The change in off-resonance $\Delta\omega$ of water only voxels, varies lineally with temperature and can be described by Equation 3.1:

$$\Delta\omega = \frac{\varphi - \varphi^r}{TE} \tag{3.1}$$

Where φ is the phase at the time point in question, φ^r is the phase at the reference time point r (here, r=1 is used) and TE is the echo time of the acquisition.

For the ME-FGRE and 3D-ME-FGRE sequence MMT-PRFS was used to calculate the change in off-resonance frequency, previously introduced by Salim et al. [42].

1 2D parameter file 'parameters_rigid.txt' and 3D parameter file 'parameters_rigid_3D.txt' at https://github.com/tfeddersen/ElastixModelZoo

3.3.2.4 B0 drift correction

In order to ensure that the MR temperature reading is not influenced by the B0 field drift of the scanner, a drift correction needs to be applied to all acquired images. Fat experiences a much smaller temperature related off-resonance frequency shift than water and tissues [50]; in the order of α=-1.8*10^{-10} /°C [147], compared to α= 1.0*10^{-8} /°C of water [94]. Therefore, as fat still experiences all other disturbances of the magnetic field, it can be used for field drift correction. Firstly, fat voxels need to be identified. For the phantom experiments, ROIs were drawn in the external fat tubes; for the volunteer data, we developed an automatic fat selection similarly to [67], selecting the internal body fat based on the water- and fat- density maps at zero echo time obtained from MMT-PRFS, see Figure 3.3. For DE-GRE, the fat mask could not be calculated with the same method and was hence imported from the ME-FGRE acquisition.

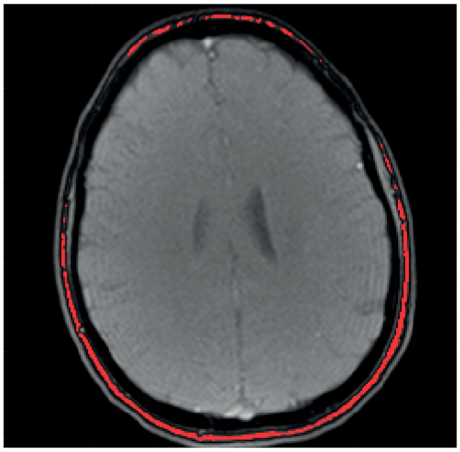

Figure 3.3: Example fat mask (of bone marrow) with volunteer 1, slice 1. The red fat mask is overlaid on the magnitude image of echo 1 at time point 2.

3.3.2.5 MRT

Once $\Delta\omega_{corr}$ is calculated, the change in temperature can be found by Equation 3.2:

$$\Delta T = \frac{\Delta\omega_{corr}}{\gamma * \alpha * B_0} \tag{3.2}$$

Where γ is the gyromagnetic ratio, α is the change coefficient for PRFS, and B_0 is the magnetic field strength of the MRI scanner. The constants used were γ=267.513*10^6 rad/s/T, α=-0.01ppm/°C and B_0=1.5T.

To mitigate a possible bias at higher temperatures, the phantom results are also calculated for the clinical temperature range of 37-43°C, referencing to the time point in each sequence that was closest to and above 37°C.

Since our method relies on the changes in the resonance frequency in the hydrogen of water molecules, we exclude voxels containing more than 20% fat as in these voxels the offresonance frequency estimate might be biased. This selection was made using the fat and water density maps, which contain the signal at zero echo time: $\rho_f > 0.2\ \rho_w$.

Additionally, voxels with low SNR were excluded; we defined those voxels with $\rho_w \leq 10\%$ of the mean ρ_w of the three voxels with the highest ρ_w in that time point and slice.

3.3.2.6 MRT performance quantities

To give a complete comparison of MRT performance for different sequences, we followed the standard suggested in [134] in order to calculate performance measures for the phantom experiments, i.e. reporting on bias (ME), spatial temperature standard deviation (spatial SD), temporal temperature standard deviation (temporal SD) and accuracy (MAE). The definitions with their respective formulas are shown in Table 3.1.

Table 3.1: MRT performance quantities used for comparison between sequences. E_j is the MRT measurement at time point j, A is the temperature measurement (ground truth), and n is the number of time points. The minimum requirement has been defined previously as being the benchmark for a successful HT treatment; table copied and edited from [134].

Measure	Metric	Definition	Minimum
Bias	Mean error (ME)	$ME = \frac{1}{n}\sum_{j=1}^{n}(E_j - A)$	≤|0.5°C|
Spatial precision	Spatial standard deviation (spatial SD)	$SD^2 = \frac{1}{n}\sum_{j=1}^{n}(E_j - \bar{E})^2$	≤0.5°C
Temporal precision	Temporal standard deviation (temporal SD)	Variability at different time points over 90min	≤0.5°C
Accuracy	Mean absolute error (MAE)	$MAE = \frac{1}{n}\sum_{j=1}^{n}\lvert E_j - A\rvert$	≤1°C

The acquired MRT measurements for the phantom experiment were compared to the “ground truth” obtained from the temperature probes. The slice that was evaluated with MRT corresponded to the depth of the temperature probe. The ROI

had a diameter of about 12 pixels (18.0mm), resulting in 107 voxels selected. This was drawn as large as possible whilst excluding the wall of the vial (Figure 3.4A).

For the MRT performance assessment in volunteers an elliptical ROI was drawn in the brain. The ROI was made as large as possible, while keeping it constant for all volunteers (Figure 3.4B).

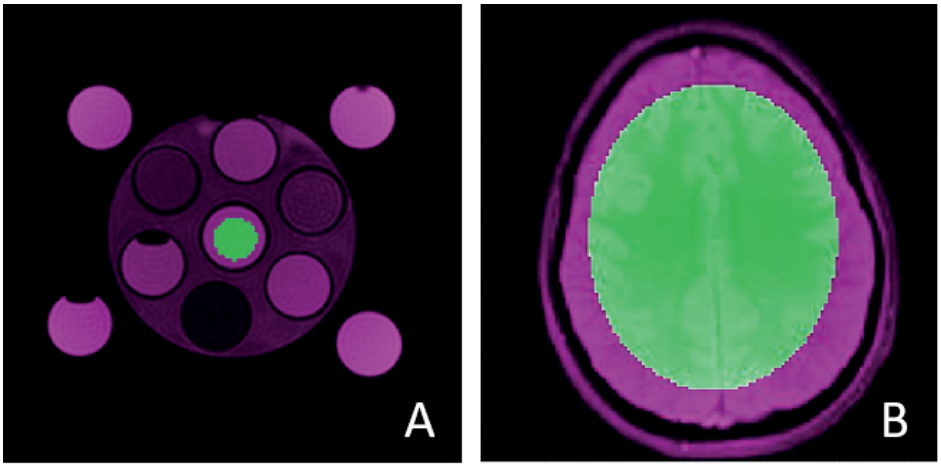

Figure 3.4: ROIs chosen (indicated in green) for MRT evaluations. A) shows the ROI for the phantom: only the vial in the centre containing water mixture was selected; and B) for the volunteers: encompassing an elliptical volume of brain tissue, as large as possible while constant among all volunteers.

Accuracy in volunteers was calculated similarly to the accuracy as described in Table 3.1: the mean deviation from zero of the apparent temperature change in the ROI for each slice. The mean absolute deviation of each slice was then averaged over all slices and all volunteers.

SD in the volunteer data was calculated as the standard deviation of temperatures measured in each ROI evaluated (one for each slice) and then averaged over all slices and volunteers, just as the spatial precision in the volunteer experiments, defined in Table 3.1.

The statistical significance of the differences among the sequences is calculated in SPSS, using a 2-sided t-test ($p<0.05$).

3.3.3 Experiments

All experiments were conducted using a 1.5T MR scanner (GE Healthcare, Waukesha, WI, USA) and a 22-channel GE Head&Neck coil. For comparison between sequences,

we aimed to match them as closely as possible to DE-GRE, with the settings used in the clinic for MRT in the pelvis, regarding the following properties: range of echo times, spatial resolution and the number of echoes for the ME sequences. Additionally, the SNR estimate for each set-up, as indicated by the command window before scanning, was matched as well. The sequences run for both experiments were DE-GRE (TR620), DE-GRE (TR200), ME-FGRE and 3D-ME-FGRE. Scans were run continuously and the FOVs were copied between the sequences so that they covered the same area. All MRT images were acquired with a spatial coverage of 192x192mm^2 and resolution 1.5x1.5x5mm^3.

The SNR of the sequences were measured to be 42 for DE-GRE (both TRs), 47 for MEFGRE, and 64 for 3D-ME-FGRE.

3.3.3.1 Phantom

The water in between the vials with the different mixtures was replaced with hot water (at 70°C) and a temperature probe was inserted into the vial with the water mixture via the catheter. Two experiments were run, both spanning a time of about 205 minutes, where the MR sequences were played out continuously whilst the phantom was slowly cooling down. In the first experiment all sequences were run, but only the DE sequences produced usable results, due to an error in the reconstruction of the ME coil-combined images from the scanner. Hence, for the second experiment, ME-FGRE and 3D-ME-FGRE were run again leading to more measurement points.

The acquisition parameters for different sequences are presented in Table 3.2.

3.3.3.2 Volunteers

All volunteers signed an informed consent (protocol MEC-2014-096, approved by the Erasmus MC review board) and were screened prior to entering the MR room. For imaging, the volunteers were placed in the scanner in supine position with the head coil around the head. In order to investigate the MRT accuracy in-vivo, we acquired brain images from a total of ten volunteers. Detailed acquisition parameters are shown in Table 3.3.

Table 3.2: Acquisition parameters and scan times for different sequences for the phantom experiment. The / shows the differences between the two DE-GRE implementations with 620ms and 200ms.

	DE-GRE	ME-FGRE	3D-ME-FGRE
TR (ms)	620/200	300	48.97
# slices	3	3	4
Slice thickness (cm)	0.5	0.5	0.5
Spacing between slices (cm)	0.7	0.7	0.25
# echoes	2	11	11
TE range (ms)	4.8-19.1	2.2-24.0	1.8-23.3
Echo spacing (ms)	14.3	2.18	2.15
Flip angle (°)	40/30	40	14
NEX	2	1	1
Bandwidth (kHz)	20.83	62.50	83.33
Matrix	128x128	128x128	128x128
Time of acquisition (mm:ss)	02:42/00:54	00:41	00:53

Table 3.3: Parameters of all the sequences as well as their respective scan times for the volunteer experiment using the multi-channel GE head coil (22 channels).

	DE-GRE	ME-FGRE	3D-ME-FGRE
TR (ms)	620/200	300	49.7
# slices	5	5	8
Slice thickness (cm)	0.5	0.5	0.5
Slice spacing (cm)	0.2	0.2	0.2
# echoes	2	11	11
TE range (ms)	4.8-19.1	2.2-24.0	1.8-23.3
Echo spacing (ms)	14.3	2.18	2.15
Flip angle (°)	40/30	40	14
NEX	1	1	1
Bandwidth (kHz)	20.83	62.50	83.33
Matrix	128x128	128x128	128x128
Time of acquisition (mm:ss)	01:23/00:29	00:41	01:18

3.4 RESULTS

3.4.1 Phantom cooling-down experiment

Figure 3.5 shows example MRT maps of the phantom cooling down over time. We excluded low SNR voxels as well as voxels with more than 20% fat, as temperature estimates are unreliable in those voxels with the current method. Note that some temperature errors at the edges of the phantom and the tubes with water-fat mixtures remain.

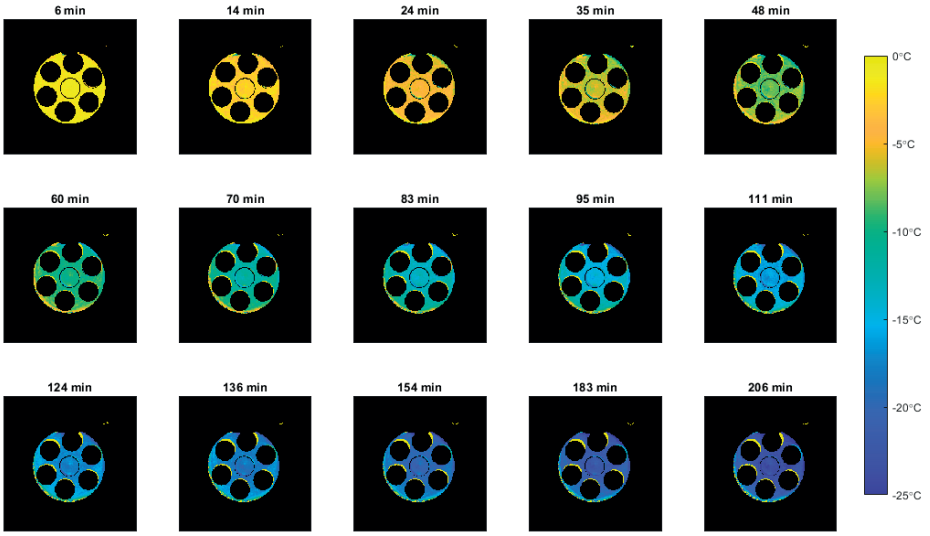

Figure 3.5: Temperature change MRT maps of the phantom cooling down, shown at different time points.

Figure 3.6 displays the temperature changes measured by MRT (as the mean of the ROI evaluated) against the temperature measured by the probe for each time point. The time points in Figure 3.6A are referenced to the first time point acquired during the experiment at the highest temperature, and shows the entire temperature range of the experiment (205 minutes). Figure 3.6B only presents the HT clinical temperature range of 37-43°C, and the MRT measurements are referenced to the time point closest to 37°C, as would be the case during treatment, spanning 65 minutes.

Table 3.4: MRT performances from the multi-coil phantom experiment for the whole temperature range (top) and the clinically HT range 37-43°C (bottom). Values that are within the required standard are printed in bold.

	Bias (ME) (°C)	**spatial SD (°C)**	**temporal SD (°C)**	**Accuracy (MAE) (°C)**
STANDARD VALUES	≤ | 0.5 |	≤0.5	≤0.5	≤1
All temperatures				
DE-GRE TR620	1.92	0.36	0.10	1.92
DE-GRE TR200	1.80	0.50	0.14	1.80
ME-FGRE	-0.08	0.89	0.17	0.46
3D-ME-FGRE	-0.69	0.68	0.16	0.77
37-43°C				
DE-GRE TR620	0.37	0.26	0.15	0.37
DE-GRE TR200	0.31	0.35	0.20	0.31
ME-FGRE	-0.40	0.45	0.11	0.41
3D-ME-FGRE	0.12	0.26	0.07	0.20

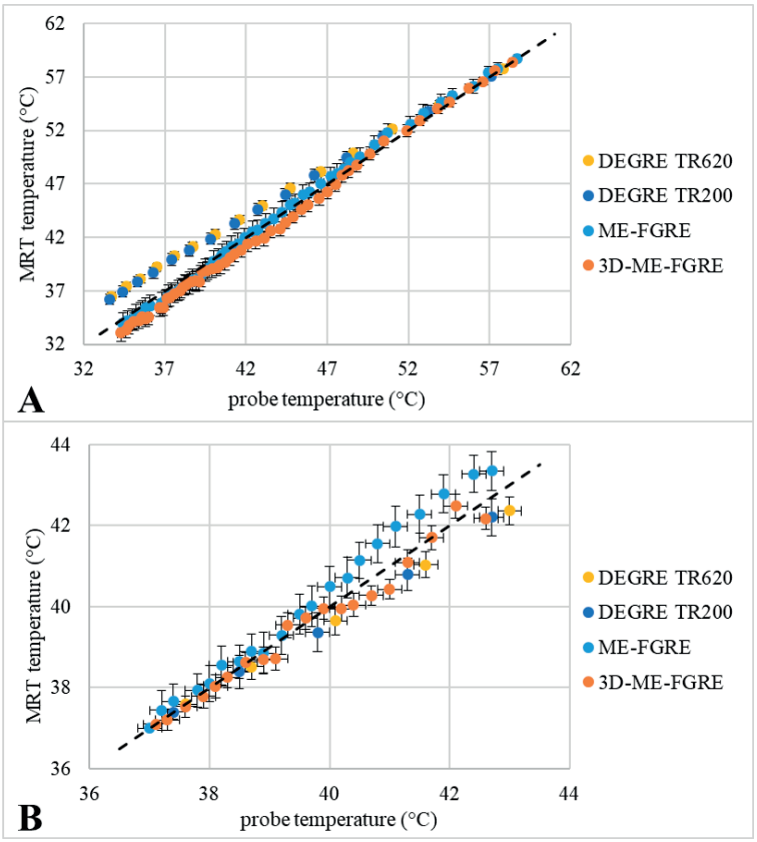

Figure 3.6: Temperature measured by MRT (mean of the ROI evaluated ± SD) vs. the temperature measured by the thermometer probe during the cooling down of the phantom experiment. Each dot represents a temperature reading at a distinct time point for which the acquisition time from the MRI scanner is taken. The dashed line illustrates the perfect scenario, where the temperature of the probe and the temperature measured with the MRI are matching. A shows the entire temperature range, referenced to the first time point acquired during the experiment; and B shows only the clinical temperature range of 37-43°C, referenced to the time point closest to (and above) 37°C. The bias, spatial SD, temporal SD and accuracy are presented in Table 3.4 for both the extended range and the reduced treatment relevant range.

Considering the whole temperature range of the experiment, ME-FGRE had the best accuracy and bias of 0.46°C and -0.08°C. Spatial SD was only sufficient for the DE-GRE sequences and the temporal SD was sufficient in all. Regarding the clinical temperature range of 37-43°C, the 3D-ME-FGRE sequence performed best regarding bias, spatial SD and accuracy.

3.4.2 Volunteer experiment

Figure 3.7 shows example MRT estimations for one volunteer for all sequences. Also here, low SNR voxels as well as voxels with more than 20% fat were excluded, as temperature estimates are unreliable in those voxels with the current method. It

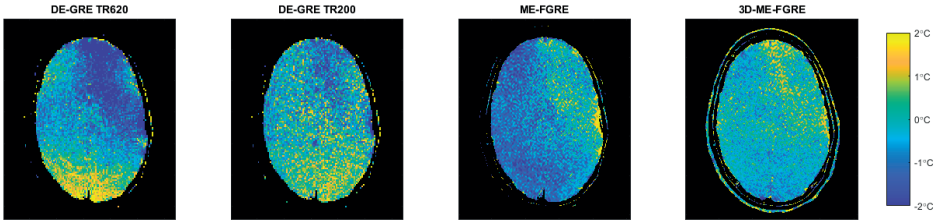

Figure 3.7: MR temperature estimations for all sequences (shown for one slice and one volunteer).

can be seen, that 3D-ME-FGRE estimates the temperature change more homogenous across the slice, as well as closer to 0°C than the other pulse sequences.

The MRT performances for the volunteer experiments in brain are presented in Table 3.5. One volunteer and one ME-FGRE acquisition of another volunteer was excluded because the motion in the slice direction was larger than 20% of the slice thickness. Excluding individual slices due to too little fat voxels being selected for a B0 drift correction was necessary in 2 volunteers and resulted in excluding a total of 6 slices for both DE-GRE sequences, 5 slices for ME-FGRE and 4 slices for 3D-ME-FGRE. The effect of the exclusion criteria is shown in Figure 3.8.

When testing for the statistical significance of the improvements of the accuracy after exclusion, DE-GRE TR200 and ME-FGRE were non-significant ($p=0.415$ and $p=0.088$ respectively). 3D-ME-FGRE however, shows a significant improvement in accuracy compared to the original DE-GRE TR620 sequence, with $p<0.001$. Regarding the SD over the investigated ROI, the multi-echo sequences achieved better values after exclusion, though these improvements were not significant.

An aspect that stood out, was that with 3D-ME-FGRE, only 5% of slices had to be excluded due to selecting too few fat voxels, compared to up to 30% for other sequences.

Table 3.5: MRT performances averages of 10 volunteers in brain over all slices, including all and excluding motion and too little fat voxels. Accuracy is calculated as the mean absolute error (MAE) over all slices from 0°C. Statistically significant improvements when compared to DE-GRE TR620 are marked in bold.

	Including all		Excluding motion + too little fat	
	accuracy (°C)	**SD (°C)**	**accuracy (°C)**	**SD (°C)**
DE-GRE TR620	6.74	3.17	1.96	2.00
DE-GRE TR200	6.95	3.33	1.78	2.00
ME-FGRE	9.72	5.72	1.40	1.56
3D-ME-FGRE	3.09	3.04	0.75	1.82

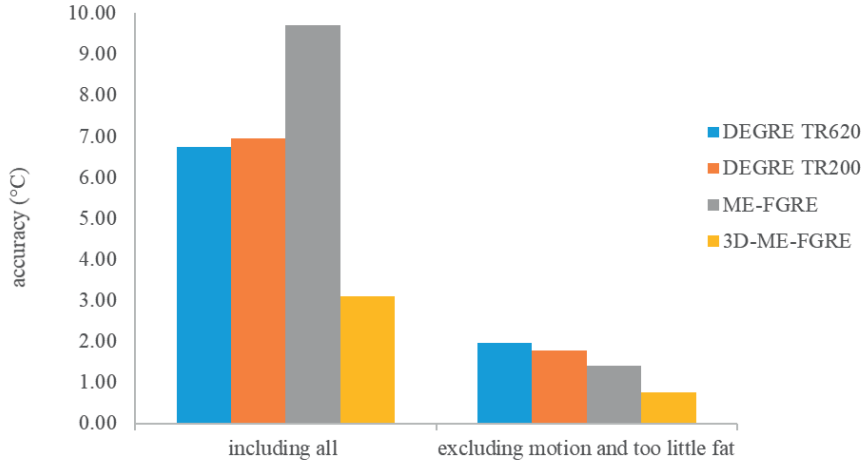

Figure 3.8: Accuracy achieved for all sequences in the volunteer experiments, including all scans and excluding scans with too much motion and too few fat voxels (9/10 volunteers remaining). Accuracy was calculated as mean absolute deviation over all slices of the mean deviation from zero of the apparent temperature change in the ROI for each slice.

3.5 DISCUSSION

In this work the MRT performance of different multi-echo gradient-echo sequences was compared, both in a phantom and in volunteers. This study was aimed to be a first step in improving PRFS-MRT to a more reliable and robust monitoring modality for HT treatments.

The analysis in volunteers presented here was performed only in brain, an ideal testing location due to little motion disturbances, although subject motion had to be compensated, see also the supplementary material for an illustration of this. However, we believe that the results can also be useful when applied to other anatomies. This is because when moving to more challenging areas in the future, we know that any difference in behaviour and the likely increase in temperature errors will be caused by motion and other magnetic field disturbances, and not be due to the sequences and settings themselves. In other words: it is precisely because the effects of the sequences are not being intermixed with big adjustments in the analysis, that they will likely be helpful when considering different anatomical regions.

Accuracy is the most important measure investigated, enabling reliable detection of small temperature increases during the relatively long HT treatment times. ME-FGRE and 3D-ME-FGRE achieve better accuracy and bias than DE-GRE in phantom over the whole temperature range, consequently satisfying the minimum requirement for

successful monitoring during a HT treatment. This improvement in performance was expected, due to the increased number of echoes, which provide more data to estimate the off-resonance frequency. The smaller echo spacing of ME-FGRE also means that we can have a larger bandwidth, which leads to less problems with wrap-around of the phase when dealing with large temperature changes (due to larger ranges being able to unambiguously be identified). This will also affect the B0 compensation positively, especially when fat is sparsely distributed.

Considering the (smaller) clinical temperature range, the errors decrease and all investigated sequences satisfy the minimum requirements. The best accuracy in the clinical temperature range was obtained with 3D-ME-FGRE – representing a clinically relevant and statistically significant improvement of 46% compared to DE-GRE TR620. The trends observed in phantoms is mirrored by the measurements in volunteers. We expected the multi-echo sequences to achieve better (lower) values of SD's compared to the standard DE-GRE, and indeed observe up to a 22% improvement (not statistically significant). Most impressive is the 61.7% statistically significant increase in accuracy shown by 3D-ME-FGRE compared to the standard DE-GRE TR620 sequence. In general, the reduced range is more indicative of the thermometry performance that can be expected in the clinic - also because it spans a shorter cooling time (65 minutes, much closer to the HT treatment time) and comparable effects of B0 drift can be expected.

The possibility to implement automatic fat map selection is an advantage of using multi-echo sequences, making the addition of external fat references superfluous. In current clinical MR-compatible hyperthermia applicators, external fat references are attached to the wall of the applicator. As a result, the fat references are not places close to the subject, but often at the boundary of the imaging FOV. Internal body fat selection provides the opportunity to simplify treatment set-up and reduce the FOV for MRT, therefore shortening treatment time. Additionally it provides a reference as close as possible to the tissue of interest, likely improving accuracy of the field drift correction. Additional benefits include the saving the time of manual delineation of fat, as is common practice when using body fat as a fat reference [49, 95], and which can be a very time consuming task [64].

One of the explanations for the robustness of 3D-ME-FGRE is the sequence's echo spacing, which is optimized for detecting and quantifying fat by the 3-point Dixon method [148], more so than the 2D implementation, making 3D-ME-FGRE superior when selecting the fat mask for reliable B0 drift corrections; something that is of particular importance for the clinic, where the scanner drift can be substantial

during the long treatment times of >60 minutes. This robustness is reflected in the lower amount of slices that had to be excluded (5%) due to selecting too few fat voxels, compared to other sequences (up to 30%). Furthermore, 3D-ME-FGRE is acquiring in 3D, and hence has 3D phase consistency. This gives an advantage for the HT application, because it would enable estimating the field drift only once for the whole volume, rather than for every slice, which is the case for the 2D sequences.

In regards of the results of both phantoms and volunteers, it is noteworthy that DE-GRE TR200 performs as well as the original DE-GRE TR620, whilst the acquisition time is shortened by more than 65%. The accuracy over both temperature changes investigated are similar, and the difference in accuracy in volunteers is not significant. If there is a dependency in clinical scenarios on using a DE-GRE sequence, reducing the TR would provide an easy way to reduce scan time without compromising MRT performance.

Whilst this study presents a comprehensive comparison of different performance metrics, there are some limitations that need to be mentioned. The study only analyses four different sequences with particular acquisition settings, which were matched as closely as possible to the clinically used DE-GRE, but may not be optimized even for imaging the brain, as was done here.

The automatic fat selection method that we constructed is able to select reliable fat voxels for the B0 drift correction. However, sometimes there are not enough fat voxels selected towards the outer edges of the acquisition volume. It may not always be feasible or desirable to acquire a larger volume to avoid these effects, thus improvements in the fat selection method could benefit the HT application. Regarding this aspect, 3D acquisitions could prove beneficial due to the consistency of the off-resonance frequency among slices.

With some volunteers, we observed substantial motion in the z-direction. Since the 2D acquisitions had a slice gap, 3D image registration was not possible and sets of data were excluded where z-motion was exceeding our criteria. We expect that this exclusion of data due to prominent motion is not going to be an issue during HT treatments, as such motion will be restricted by the water bolus of the HT applicator. Of course, for 3D sequences, motion could be compensated in all three dimensions, potentially providing an additional benefit in HT.

Image processing has been performed offline, and is not yet optimised for performing temperature monitoring during HT treatments in real-time. When undertaking HT

treatments with physical probes, the time for transferring the data and analysis takes 1-2 minutes. Thus, the response time for adjusting the heating is in the order of minutes and relying heavily on patient feedback, due to the point-like temperature readings of the probe. With MRT we can achieve a 3D temperature distribution and potentially react to hot spots before the discomfort of the patient, as well as improving temperature coverage.

3.6 CONCLUSION

Different multi-echo gradient-echo sequences were assessed for their MRT performance in a phantom and volunteers. 3D-ME-FGRE offers a statistically significant improvement in accuracy of 62% and 46% in unheated volunteers and temperature varying phantom (in the range of 37.0°C-43.0°C) respectively, compared to the clinical standard DE-GRE sequence. Thus, 3D-ME-FGRE presents a promising improvement to non-invasive MR temperature monitoring that can be implemented promptly. We believe this to be the first essential step towards improved MRT for HT treatments and anticipate to further investigate this 3D multi-echo sequence for MRT by optimising the acquisition settings and corresponding post-processing method.

Chapter 4

Towards quiet and more accurate PRFS MR thermometry with Looping Star

Based on:

Towards quiet and more accurate PRFS MR Thermometry with Looping Star

Theresa V. Feddersen[1,2], Dirk H.J. Poot[2], Ana Beatriz Solana[3], Florian Wiesinger[3], Margarethus M. Paulides[1,4], Gerard C. van Rhoon[1,5], Juan A. Hernandez-Tamames[2,6]

[1] Department of Radiotherapy, Erasmus MC Cancer Institute, University Medical Center Rotterdam, 3015GD Rotterdam, The Netherlands
[2] Department of Radiology and Nuclear Medicine, Erasmus MC Cancer Institute, University Medical Center Rotterdam, 3015GD Rotterdam, The Netherlands
[3] Electromagnetics for Care & Cure Research Lab, Center for Care and Cure Technologies Eindhoven (C3Te), Department of Electrical Engineering, Eindhoven University of Technology, 5600MB Eindhoven, The Netherlands
[4] Department of Applied Radiation and Isotopes, Reactor Institute Delft, Delft University of Technology, 2629JB Delft, The Netherlands
[5] Department of Imaging Physics, Applied Physics Faculty, Delft University of Technology, 2629JB Delft, The Netherlands

Submitted to:

Cancers

4.1 ABSTRACT

The purpose of this research is to evaluate the performance of Looping Star MR sequence for MR thermometry (MRT). When MRT is used during thermal therapy, patients are exposed to loud acoustic noise, contributing to the burden of treatment. In addition, MRT is not always sufficiently accurate. The aim of this study was to test the feasibility, accuracy and sound level of Proton Resonance Frequency Shift (PRFS) based MRT using the Looping Star sequence.

MRT based on Looping Star was applied during a phantom cool-down experiment, and in unheated healthy human subjects. The temperature changes were calculated using the PRFS method for 8-echo (LS8) and 10-echo (LS10) Looping Star acquisitions, as well as the clinical standard double-echo gradient echo sequence (DE-GRE).

Compared to DE-GRE, the mean average error (MAE) of LS10 is significantly lower (up to 74%) in the phantom and (up to 64%) in volunteers. MAE of LS8 also improved: by up to 55% in phantom and 45% in volunteers. Looping Star acoustic noise was reported as more pleasant for the participants compared to DE-GRE, although measured sound pressure levels were not consistently reduced.

We conclude that PRFS thermometry with the Looping Star pulse sequence is not only possible, but may significantly improve MRT accuracy during hyperthermia treatment.

4.2 INTRODUCTION

Hyperthermia is an effective tool to enhance chemo-, radio- and immunotherapy by heating the tumour to 39-43°C [27, 69, 72]. Monitoring the temperature is important, due to the different tissue effects achieved at different temperatures and the narrow target temperature range aimed for [46, 80]. Usually, where possible, catheters with temperature probes are placed invasively in or in close proximity (minimal invasive) to the treatment target volume for real-time feedback and temperature validation [149]. Temperature probes are considered the gold standard as they provide accurate temperature information. However, data is obtained from single location measurements only, and they can be difficult to place [34, 35, 43]. This leads to a clear incentive for MR thermometry (MRT), as MRT can measure tissue temperature during hyperthermia treatments non-invasively and in 3D. MRT thus offers the benefit of avoiding the invasive placement of catheters whilst providing more information about the hyperthermia treatment.

There are an array of different tissue properties that can be exploited to measure the temperature of a region of interest (ROI) with MRT. Proton resonance frequency shift (PRFS) is a popular candidate, as it is independent of tissues with high water content, and varies linearly with temperature [47]. These advantages lead to PRFS being the most frequently used method in the clinic [134].

Hyperthermia treatment times are typically long (>60 minutes) and the sequences for temperature monitoring run approximately every 10 minutes. MR acquisitions can be very loud, with conventional sequences around 85-110dBA [150]. The noise has been shown to be everything from simply annoying, to causing heightened anxiety and temporary hearing loss in patients [151, 152]. Additionally, the noise impedes proper communication between operator and patient, which is a relevant component of the treatment. Hence, having MRI based temperature measurements during hyperthermia treatments currently adds to the patients' overall treatment burden.

For MRI acquisitions/examinations, Sartoretti et al. [153] showed that reducing the acoustic noise created by the MRI scanner significantly increases patient comfort. Different approaches to reducing the acoustic scanner noise have been put forward [154]. One of the solutions for reducing the noise is to use Zero Echo Time (ZTE) pulse sequences [155]. These sequences are nearly silent due to minimal gradient switching, and were first described in Madio et al. [156] (under their original name RUFIS). Ljungberg et al. [157] gives a very good overview of the concept of ZTE, as

well as its different applications. ZTE has already been proposed for silent MRT using T1, to better track the temperature changes in bone and tissue.

Looping Star [158] is a novel ZTE sequence that could be interesting for MRT. It works by exciting many magnetic coherences, which are subsequently gradient-refocused by using a looping k-space trajectory. Looping Star could be a good candidate for MRT, as it provides quiet, fast and robust 3D multi-echo images.

The objective of this study is to investigate the feasibility of quiet PRFS MRT with Looping Star. Whilst MRT is growing more reliable and consequentially more popular, a quiet PRFS implementation is something that has not been explored previously. The Looping Star sequence has the potential to make hyperthermia treatments in the MR not only safer and more information rich compared to invasive temperature probes, but most importantly also more comfortable for the patient and the clinical staff.

To test for the feasibility and quantify the MRT performance with Looping star, temperature mapping was performed in a dedicated phantom and healthy unheated volunteers using 8 (LS8) and 10 (LS10) echoes. In the phantom, the true temperature was measured using a temperature probe during imaging. Mean average error (MAE), mean error (ME), and spatial temperature standard deviation (spatial SD) could thus be quantified. In volunteers, no heating was applied and therefore a true temperature change of 0°C was assumed. All results were compared to the clinically used reference method: double-echo gradient echo sequence (DE-GRE) [95]. Sound measurements were performed to quantify sound pressure levels.

4.3 MATERIALS AND METHODS

4.3.1 Experiments

All data was acquired on a 1.5T MR scanner (Signa MR450, GE Healthcare), using a 22-channel GE Head & Neck coil. The research prototype sequence Coherence Resolved Looping Star [158] was implemented with two different settings, both acquired with 2 spokes per loop and 8192 total spokes per echo:

- LS8: 8 echoes, $TR_{segment}$=45.988ms, BW=±50.0kHz, echo spacing=3.4ms, min TE=0ms, max TE=23.8ms, scan time=03:11
- LS10: 10 echoes, $TR_{segment}$=41.508ms, BW=±62.5kHz, echo spacing=2.2ms, min TE=0ms, max TE=19.8ms, scan time=02:53.

Both acquisitions had a resolution of 1.5x1.5x1.5mm3, flip angle of 3°, and matrix size of 128x128x128. Looping star images are counted FID (1st loop), GRE1 (2nd loop), GRE2 (3rd loop) and so forth. The acquisition parameters were chosen such that they both cover roughly the same echo train length, whilst having sufficiently low echo spacing to separate water and fat with the MMT-fitting tool [159] used in the analysis. The required echo spacing was only possible using the smallest number of spokes per loop and a relatively high bandwidth, as described above. Note that in Looping star field of view and readout bandwidth specify the gradient strength during the RF. As the RF pulse should be non-selective, the pulse duration should be very short, substantially limiting the attainable flip angle in the used configuration.

In addition, images were acquired with DE-GRE. As this is the sequence clinically used at our institution for MRT during hyperthermia treatments in the pelvis, it will serve as the reference method. DE-GRE images were acquired with the following parameters: TE1/TE2/TR=4.8ms/19.1ms/620ms, Flip angle=40°, BW=±20.83kHz, resolution=1.5x1.5x5.0mm^3, matrix size=128x128, scan time=01:23, #slices=4.

4.3.2 Acoustic noise measurements

Acoustic noise was measured as the A-frequency weighted decibels or dBA at inside of the closed door of the 1.5T scanner room with identical gain settings, using a digital sound level meter (Voltcraft, SL-200 SE). Max sound level L_{max} was also measured with A-frequency weighting and a fast measurement interval; it was recorded across the whole duration of the corresponding sequence, excluding any calibration scans.

4.3.3 SNR measurements

SNR was calculated in phantom data using the first gradient echo Looping Star image GRE1 (the second loop data, to avoid the FID image), and the 1st echo for DE-GRE. A small homogeneous ROI was chosen in the water mixture, the signal was taken as the signal intensity of the magnitude image, the standard deviation in the same region was taken as the noise.

4.3.4 Phantom

Figure 4.1 shows a schematic drawing of the home-made phantom that was used for the phantom experiments. The vials were filled with different water and fat percentages, following the recipe introduced by Bush et al. [142]. They were constructed including catheters so that temperature probes (part of the PYREXAR BSD2000-3D-MRI deep hyperthermia system [160]) could be inserted to provide ground truth temperature measurements. The manufacturer states the uncertainty

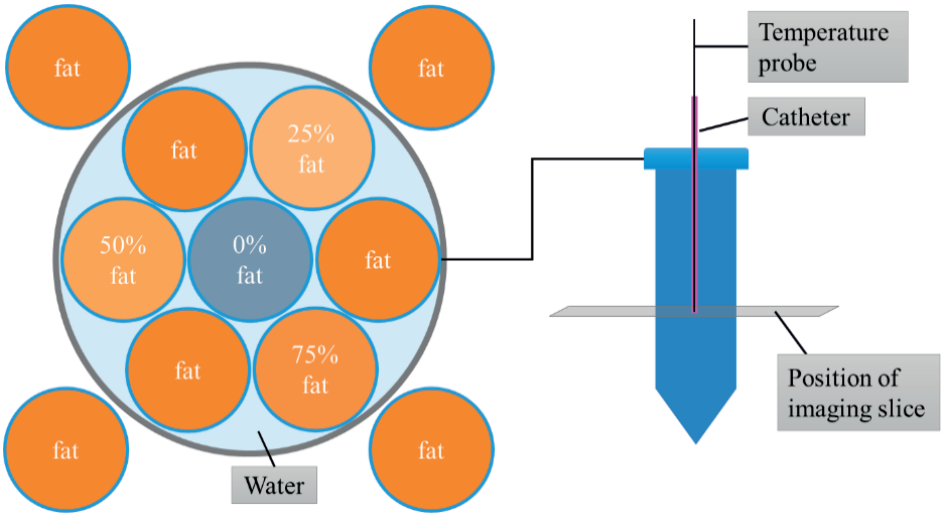

Figure 4.1: Schematic of the home-made phantom used in the experiments. Only the vial in the centre containing the water mixture was evaluated for MRT.

in the temperature measurements of the calibrated temperature sensors to be ±0.2°C.

For the experiment, the phantom was filled with hot water, placed inside the scanner bore and imaged whilst cooling down towards room temperature for approximately 200 minutes.

During the cool-down period, the temperature measured by the probes was recorded continuously. For the MRT measurements, DE-GRE was followed by some sequences not used in the current analysis and then by LS8 and LS10. This entire block was repeated every 13 minutes, to a total of 14 times over the duration of the experiment.

4.3.5 Volunteers

The volunteers gave written consent to the protocol 'MRI technology healthy volunteers' (METC-2014-096, approved by our institutional review board) and were screened prior to entering the MR room.

The brains of 9 healthy volunteers were imaged two times with the same acquisition protocol that was run for the phantom experiment. The body temperature was assumed to stay the same between the two scans - thus, any apparent temperature change measured with MRT was taken to be a measurement error.

4.3.6 Processing of data

All data was processed offline using MATLAB. The detailed post-processing pipeline has been introduced previously [159]. Here we provide an outline of the process:

- **Input data:** For Looping Star, the complex valued individual channel images were obtained. For DE-GRE the raw k-space data was processed using MATLAB. Subsequently for all sequences, coil sensitivity maps were calculated for each time point using all echoes and the images were complex coil-combined. Then, the phase difference between the coil sensitivity maps of different time points was minimised.
- For the volunteer data, **image registration** was used to correct for subject motion between time points. Specifically, a rigid pair-wise image registration of the first echo was performed using Elastix [145][2] , and applied to all echoes. The registration was 3D for Looping star and 2D for DE-GRE due to a slice gap in the acquisition.
- For Looping Star, the **change in off-resonance** frequency as well as the water and fat density maps were calculated at each time point independently, using a MMT-fitting tool [42, 159]. Then, the water and fat model was fitted to the multi-echo images using a maximum likelihood optimization. Initial experiments showed that in the current reconstruction the first echo image (TE=0) did not fit to this model like the rest of the echoes. Hence, the first echo was excluded in the analysis and only echoes 2-8 (for LS8) and 2-10 (for LS10) were used in the fitting. The change in off-resonance was calculated as the difference between the off-resonance at time point i and the reference time point. For DE-GRE, both echoes were used to calculate the off-resonance frequency, as outlined in [146].
- **B0 drift correction**: Fat was selected to correct for the B0 drift as its off-resonance is unaffected by temperature changes, but is modified by all other frequency disturbing effects. For the phantom, the external fat tubes were used. For the volunteers, the density maps of water and fat created by the MMT-fitting tool were used to select a fat mask from the internal body fat. The threshold for fat selection was set for each volunteer individually.

- **MRT**: Finally, the temperature change ΔT was calculated by:

$$\Delta T_{i,j} = \frac{\Delta \omega_{i,j}}{B0 * \gamma * \alpha} \tag{4.1}$$

2 2D parameter file ‘parameters_rigid.txt’ and 3D parameter file ‘parameters_rigid_3D.txt’ at https://github.com/tfeddersen/ElastixModelZoo

where $\Delta\omega_{i,j}$ is the change in off-resonance (rad/s) in voxel i and time point j with respect to the reference time point, B0 is the magnetic field strength of the scanner (=1.5T), γ is the gyromagnetic ratio (=267.513*10^6rad/s/T), and α is the temperature change coefficient for water PRFS (=-0.01ppm/°C).

Since water frequency estimated by our method might be biased in the presence of fat, voxels containing more than 20% of fat were excluded.

For phantom images, the data from the temperature probes was loaded to have a true measurement to assess the MAE and ME of the MRT. A single ROI was chosen close to the tip of the temperature probe to calculate the MRT performance. For volunteers, the centre slice was evaluated. An indication of the size and position evaluated is given in Figure 4.2.

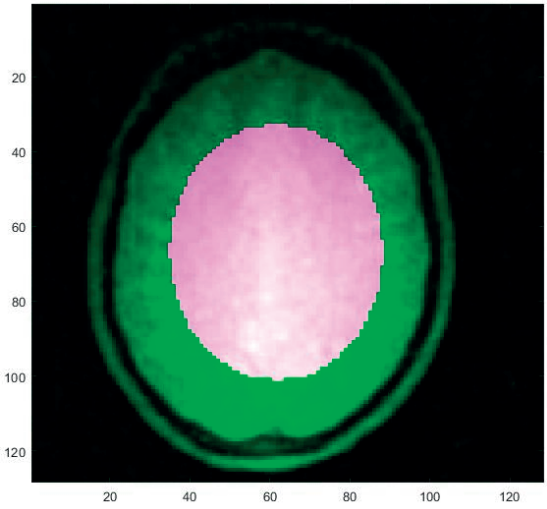

Figure 4.2: Example of the ROI chosen (pink) in the volunteer experiments for the performance evaluation. Here shown overlaid on the corresponding magnitude image (green) of volunteer 10.

Additionally, a post-hoc analysis was performed using only two of the echoes of LS8 and LS10, closest to the DE-GRE echo times (4.8ms, 19.1ms):

- LS8: TE1=3.4ms, TE2=20.4ms
- LS10: TE1=4.4ms, TE2=19.8ms

The off-resonance frequency changes were calculated the same way as DE-GRE, except for 3D image registration.

4.3.7 MRT performance calculations

To evaluate the performance of Looping Star, we followed the metrics introduced in [134]. Accuracy is calculated as the MAE (Equation 4.2); bias is calculated as the ME (Equation 4.3); and spatial precision is calculated as the spatial SD (Equation 4.4).

$$MAE = \frac{1}{n-1}\sum_{j=2}^{n}\left|T_{ROI,j} - A_j\right| \tag{4.2}$$

$$MAE = \frac{1}{n-1}\sum_{j=2}^{n}\left|T_{ROI,j} - A_j\right| \tag{4.3}$$

$$spatial\ SD \quad = \frac{1}{n-1}\sum_{j=2}^{n}\sqrt{\frac{1}{|ROI|}\sum_{i\in ROI}\left|E_{i,j} - T_{ROI,j}\right|^2} \tag{4.4}$$

where $T_{ROI,j} = \frac{1}{N}\sum_{i=1}^{N} E_{i,j}$ is the MRT measurement at time point j calculated as the mean over the ROI with N voxels, $E_{i,j}$ is the MRT measurement of voxel i at time point j, A_j is the ground truth measurement at time point j, and n is the total number of time points where we exclude the first (reference) time point from the evaluation as $E_{i,1}=A_1$ by construction. For the phantom, the ground truth is taken as the reading of the temperature probes. For the volunteers, the ground truth is not measured – instead, we assume that the temperature change in the volunteers within the experiment session is 0°C.

SPSS (IBM Corp. Released 2021. IBM SPSS Statistics for Windows, version 28.0. Armonk, NY: IBM Corp) was used to test for the statistical significance in the differences of results. Equal variances were assumed when the significance of Leven's test for equal variances was >0.05.

4.4 RESULTS

4.4.1 Acoustic noise

L_{max} (A-frequency weighting) measured for all sequences are presented in Table 4.1.

Table 4.1: Sound pressure level measurements for Looping Star, DE-GRE and ambient noise.

	L_{max} (dBA)
LS8	78.0
LS10	89.8
DE-GRE	82.0
Ambient noise	59.0

The results show that with the parameters set in this study, Looping Star is not always quieter than DE-GRE. Perceptually, Looping Star sequences were reported more quiet and pleasant, as can be observed from the audio recordings presented in the supplementary material.

This is probably due to the sound frequency spectrum characteristics, being quite different to DE-GRE.

4.4.2 Phantom experiment

The signal to noise ratio (SNR) of DE-GRE was 43, for LS8 it was 24, and for LS10 it was 26.

The temperature probes showed that temperatures were measured from around 55°C down to 33°C. Figure 4.3 shows an example of the estimated MR temperature change during the cool down towards room temperature. The MRT during the phantom experiment against the readings from the temperature probe is displayed in Figure 4.4. The error bars represent the spatial SD for the MR temperature measurements (see Equation 4.4), and the uncertainty in the temperature probes.

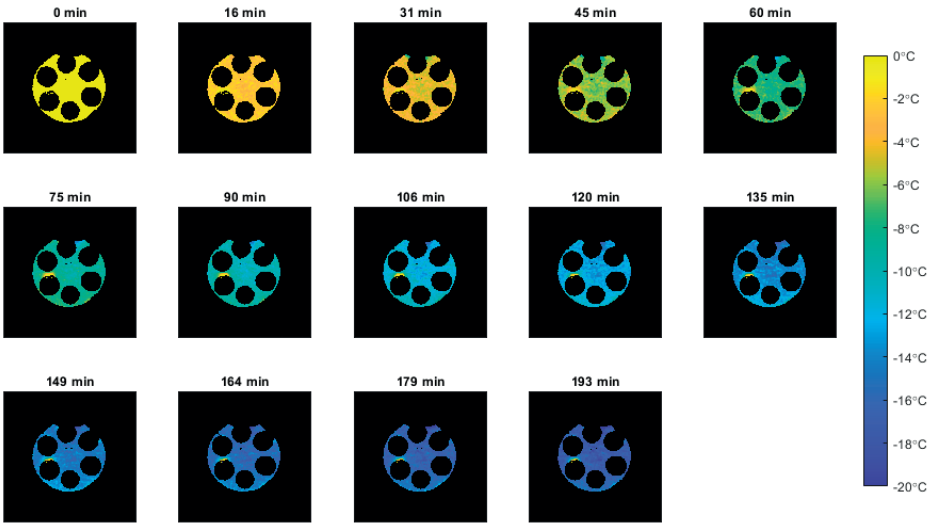

Figure 4.3: Example MRT ΔT images of phantom cooling-down over time, acquired with LS10.

From Figure 4.4 it can be seen, that the MRT obtained with Looping Star is closer to the temperature probe readings than DE-GRE. Table 4.1 quantifies this improvement, by showing the MRT performances from the phantom experiments. LS10 achieved the highest improvement in MAE and ME, although LS8 also improves compared to DE-GRE. Spatial SD was worse for both LS10 and LS8.

The 2-echo Looping Star temperature mapping MAE and ME were better than when using all echoes, spatial SD worsened.

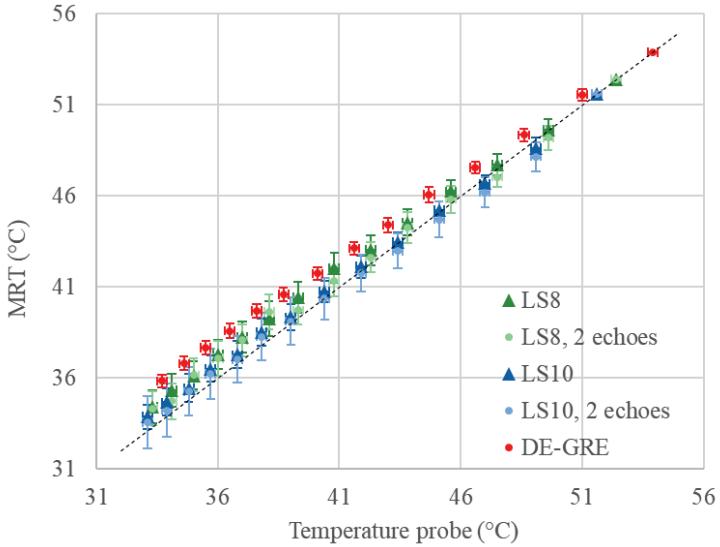

Figure 4.4: MRT vs temperature probe measurements during the phantom cooling down experiment. The error bars represent the spatial SD of the ROI for MRT, and the uncertainty of the temperature probes. The reference time point taken here is the point close to 53°C, which by construction has no error. The dashed black line represents the ideal scenario, when the MRT and the probe temperature measurements would coincide.

MAE and ME of both LS8 and LS10 evaluations were significantly improved compared to DE-GRE; whereas the spatial SD significantly worsened (see Table 4.2).

Table 4.2: MRT performances in phantom for the full temperature range of the experiment (33-53°C) for all echoes evaluated, as well as Looping Star with only 2 echoes. Statistically significant differences compared to DE-GRE are highlighted in bold.

	MAE (°C)	ME (°C)	SD (°C)
LS8	**0.93**	**0.93**	**0.73**
LS8, 2 echoes	**0.72**	**0.59**	**0.84**
LS10	**0.47**	**0.35**	**0.64**
LS10, 2 echoes	**0.41**	**-0.01**	**1.17**
DE-GRE	1.60	1.60	0.36

4.4.3 Volunteer experiment

For volunteers, the MRT maps were calculated in 3D for the whole brain volume. An example of such a map, overlaid on the LS magnitude image is shown in Figure 4.5.

A performance indication from the volunteer experiments, taken from an ROI in the centre slice, is given in Table 4.3. For the DE-GRE data two volunteers had to be excluded. One because of insufficient fat voxel selection and one because of >20% of slice thickness motion in the z-direction that could not be corrected for because the 2D slices were acquired with a slice gap.

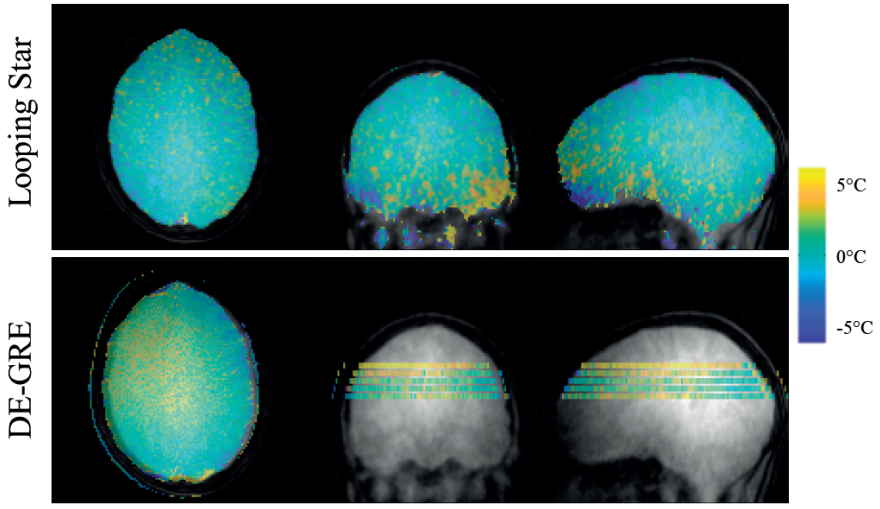

Figure 4.5: Top row: whole-brain Looping Star MRT map (scan time=02:53) overlaid on magnitude image. Bottom row: multi-slice DE-GRE MRT (scan time=01:23) overlaid on Looping Star magnitude image (without registration of images). One can appreciate the advantages of the full 3D acquisition with Looping Star, compared to the few slices with slice gap acquired with DE-GRE.

Table 4.3: MRT performance averages from (unheated) volunteers. The true temperature change was assumed to be 0°C. For the Looping Star acquisition the number of volunteers = 9, for DE-GRE the number of volunteer = 7. Significant differences compared to DE-GRE are highlighted in bold.

	MAE (°C)	ME (°C)	SD (°C)
LS8	1.06	-0.44	**0.79**
LS8, 2 echoes	1.37	**0.32**	0.96
LS10	**0.71**	**-0.45**	**0.84**
LS10, 2 echoes	0.81	**0.24**	1.10
DE-GRE	1.94	-1.94	1.59

The LS10 implementation using all echoes performs significantly better than DE-GRE across all investigated performances. LS8 also improves the performances, but less drastically than LS10.

In our experiment the MRT calculated using all echoes underestimated the temperature, whereas with 2 echoes only, it is overestimated. The ME for all Looping Star implementations

MAE and spatial SD are better (lower) when using all echoes, as opposed to just two. However, the increase in SD is lower than could be expected due to the reduced number of measurements, indicating that the spatial SD is not only caused by acquisition noise.

4.5 DISCUSSION

In this work we compare Looping Star, a multi-gradient echo sequence based on ZTE, to the DE-GRE sequence, which is standard for monitoring hyperthermia, in terms of quality of MRT.

Regarding MRT performance, Looping Star is obtaining significant improvements compared to DE-GRE considering MAE and ME, regardless of whether with two or with all echoes obtained. This improvement leads to the minimum criteria for successful MRT in MAE and ME being met for LS8 and LS10 in phantom, and for LS10 in volunteers. Spatial SD for Looping star worsened in phantom, but improved in volunteers compared to DE-GRE, although the minimum criteria for successful MRT were not reached. The spatial SD in general can be improved by spatial or temporal averaging if needed, e.g. with post processing methods for MRT, such as Kalman filtering [161], which have been successfully applied previously. Hence, spatial SD is less important than ME and MAE.

The sound generated by Looping Star is more pleasant than DE-GRE, and might therefore reduce the burden on the patient. However, contrary to our hypothesis, Looping Star with the parameters used failed to be consistently quieter than DE-GRE, i.e. the sound was more than 25dBA above the ambient acoustic noise at the scanner room. Those acoustic noise levels are higher than previously reported ones [152, 155]. This is most likely due to the requirement of having a small echo spacing for the water-fat separation model used, which made us choose the minimum number of spokes per loop (=2) and a high receiver bandwidth (BW $\geq \pm$50kHz). First, the spokes per loop indicates the number of in-plane lines required to describe a closed trajectory in the excited coherences (a circle) in any arbitrary position in the 3D k-space. The lower the number of spokes per loop, the larger the angle between the spokes in a loop and the stronger the gradient switching. Second, the higher the imaging bandwidth the higher the gradient amplitude required. Combined, they increase the gradient switching in this Looping Star implementation, thereby adding to the acoustic noise. As described in Wiesinger et al. [158], Looping Star is implemented to perform an intermediate gradient update step during each spoke, resulting in bended spokes. However, the number of intermediate steps (gradient smoothing) in this study was set to 14, where the gradient switching for the parameters of our study still resulted in high acoustic noise. We hypothesize that the acoustic noise could be therefore optimized, by increasing the gradient smoothing or using sinusoidal waveforms.

Another way to reduce the noise level is to increase the number of spokes per loop. However, this requires an increase in echo spacing that prevents effective application of the MMP-fitting tool for fat-water separation and off-resonance fitting. One possible solution may be to replace the MMP-fitting by a double-echo phase subtraction, such as for DE-GRE. Based on the results for only 2 of the LS8 or LS10 echoes presented above, this will most likely reduce spatial SD, but worsen MAE and ME, albeit only for volunteer data and not for the phantom experiments. Note, however, that an actual 2-echo acquisition of LS will follow a different acquisition path than the current LS8 and LS10 implementations, and therefore may lead to slightly different results. Further, acquisition with only two echoes prevents semi-automatic fat selection in volunteers based on the density maps of water and fat from the MMT-fitting tool, and also prevents the ≥20% fat exclusion mask that eliminates unreliable regions for PRFS; as was artificially applied for the DE-GRE results in this study.

Considering MAE, LS10 is performing consistently better than LS8. This trend also carries on into the 2-echo analysis, and hence is not likely due to the increased number of echoes. We know that reducing the receiver bandwidth will increase SNR [162]. This thus leads to the conclusion that this is also not a likely caused by a better performance of LS10, as LS10 has a 25% higher bandwidth than LS8. We hypothesize that the most likely reason is the smaller echo spacing of LS10, which leads to a better fat/water separation, which in turn will lead to a better temperature map estimation (but also more acoustic noise). This can still be supported in light of the 2 echo Looping Star results where the echo spacing is not small, as this likely originates from the artificially applied part generated with all echoes (e.g. fat maps), that would have otherwise not been possible.

The results also highlight that SNR is much more related to the spatial SD of the temperature map rather than its accuracy (reflected by MAE). Looping Star has almost half the SNR of DE-GRE, yet the 10-echo implementation performs closer to the truth than DE-GRE, which is reflected by the reduced MAE and ME. On the other hand, using 8 or 10 echoes instead of only two (as is the case for DE-GRE) improves the SNR, as it scales with the square root of the number of measurements, which is reflected by the improvement (reduction) in spatial SD.

4.5.1 Limitations and considerations Looping Star sequence

One of the drawbacks of Looping Star for PRFS MRT is the low flip angle that is inherent to the design of ZTE sequences. The choice of the flip angle of 3° was a compromise between inhomogeneous excitation of the volume, and maximising

the observed signal, as low flip angles lead to lower T1 weighting and lower signal. The choice of flip angle leads to different effects, three of which are discussed below.

Firstly, since the T1 weighting of Looping Star is much lower than with DE-GRE (having a much higher flip angle), the fat signal is relatively lower, due to the reduced saturation of the water compartment. This reduces the number of voxels in which the water signal is less than 10% of the fat signal and it complicates the fat referencing. Hence, the fat mask selection becomes much more difficult, as it relies on the difference in signals between fat and water. One possible solution for this would be to include external fat references in order to correct for the B0 field drift.

Secondly, the low flip angle affects the signal of the imaged tissue, which is highest (and thus most desirable for MRT) when the flip angle is equal to the Ernst angle α_E [163]. As this is related to the T1, by α_E=arccos(e^(-TR/T1)), the low flip angle of Looping Star will obtain sub-optimal signal. This is reflected in the noisy, low-resolution appearance of the Looping Star images, as well as the slightly elevated spatial SD. However, novel approaches to increase flip angle in ZTE have been recently published [164, 165] and could potentially overcome this limitation for MRT.

Thirdly, the chosen flip angle of 3° applied with the readout gradient present, already has a (slightly) in-homogeneous excitation, which is varying for each loop. This causes enhanced image blurring towards the edge of the FOV. Whilst this was not affecting the MRT results directly, it made the selection of internal body fat more difficult, especially in the front of the head.

Looping Star, because of the 3D-looping k-space trajectory, will always have a certain inflexibility in the set-up. The control of the echo spacing is tightly linked with the number of spokes per loop, and may not always be optimal for MRT. Additionally, the acquisition volume will always cover a cubical FOV with isotropic imaging resolution. This inflexibility may be inconsequential for some applications, where extended anatomical monitoring is desirable, such as monitoring possible hot spots for hyperthermia applications – but can present drawbacks for body sites and applications where rapid, non-isotropic acquisition of MRT is desired. The large cubical volume automatically also translates to long processing times, which doesn't pose a problem now that the post processing is conducted offline, but will have to be considered ultimately in context of real-time application during treatments. As a possible solution for faster imaging, low resolution or reduced-FOV approaches can also be explored.

With the method used and presented here, the FID echo is currently not used to estimate the temperature. We hypothesize that the currently observed deviation from the model of this echo to be due to the different k-space filling of the FID echo, consisting of only cantered-out spokes and WASPI-based [166] filling of the centre of k-space. As inclusion of FID might be beneficial and has the potential to improve MRT fitting since it is insensitive to artifacts typical for gradient-echo such as flow, further study on the origin of the current deviation and ways to avoid that seems warranted.

4.5.2 Other limitations

A limitation of the phantom experiment is that the rate of cooling is relatively slow because we let the phantom cool down towards room temperature. This results into the experiment spanning ~200 minutes, approximately three times as long as the expected hyperthermia treatment time. With an increase in time, the images will experience larger external effects, that may not be entirely corrected for as is reflected in the relatively large error found here. In order to address this limitation, it would be best to repeat this experiment with a more appropriate time span, as soon as a suitable hyperthermia device is available for heating.

4.6 CONCLUSIONS

In this work we have compared the MRT performance of Looping Star to DE-GRE. We showed that although Looping Star was not always quieter than the standard DE-GRE measurement, PRFS MRT is feasible and leads to significant improvements. Looping star reduces MAE by up to 74% in phantoms and 64% in volunteers, and likewise lowers the ME by up to 99% in phantoms and 88% in volunteers. Looping Star thus represents an interesting candidate for MRT during hyperthermia treatments, as it provides accurate full volume 3D temperature maps.

Chapter 5

Magnetic resonance thermometry for hyperthermia in the oropharynx region

Based on:

Magnetic resonance thermometry for hyperthermia in the oropharynx region

Theresa V. Feddersen[1,2], Juan A. Hernandez-Tamames[2,3], Margarethus M. Paulides[1,4], Michiel Kroesen[1], Gerard C. van Rhoon[1,5], Dirk H.J. Poot[2]

[1] Department of Radiotherapy, Erasmus MC Cancer Institute, University Medical Center Rotterdam, 3015GD Rotterdam, The Netherlands
[2] Department of Radiology and Nuclear Medicine, Erasmus MC Cancer Institute, University Medical Center Rotterdam, 3015GD Rotterdam, The Netherlands
[3] Electromagnetics for Care & Cure Research Lab, Center for Care and Cure Technologies Eindhoven (C3Te), Department of Electrical Engineering, Eindhoven University of Technology, 5600MB Eindhoven, The Netherlands
[4] Department of Applied Radiation and Isotopes, Reactor Institute Delft, Delft University of Technology, 2629JB Delft, The Netherlands
[5] Department of Imaging Physics, Applied Physics Faculty, Delft University of Technology, 2629JB Delft, The Netherlands

Submitted to:

International Journal of Hyperthermia

5.1 ABSTRACT

Magnetic resonance thermometry (MRT) can measure 3D temperature changes in-vivo in real-time and non-invasively. However, motion potentially introduces large artifacts for the oropharynx region, as well as for the entire head and neck. This study aims to evaluate whether MRT around the oropharynx is realistic for hyperthermia and quantify the effects of breathing and swallowing on MRT performance.

MRT performance was investigated using a 3D-ME-FGRE sequence in a phantom cooling down and around the oropharynx of five volunteers. The imaging protocol consisted of imaging with acceleration=2, number of image averages (NEX)=1,2 and 3. For volunteers the acquisitions also included a breath-hold scan and scans with deliberate swallowing. MRT performance was quantified in neck muscle, spinal cord and masseter muscle, using mean average error (MAE), mean error (ME) and spatial temperature standard deviation (SD).

In phantom, an increase in NEX leads to a significant decrease in SD, whilst the MAE and ME were unchanged. No significant difference was found in volunteers between the normal, breath hold, and swallowing scan. There was a significant difference between the regions evaluated: the neck muscle had the best MAE (=1.96°C) and SD (=0.82°C), followed by the spinal cord (MAE=3.17°C, SD=0.92°C), and the masseter muscle (MAE=4.53°C, SD=1.16°C). Concerning the ME, spinal cord did best, then neck muscle and then masseter muscle, with values of -0.64°C, 1.15°C and -3.05°C, respectively.

Breathing, swallowing, and different ways of imaging (acceleration and NEX) do not significantly influence the MRT performance in the oropharynx region. The ROI selected however, leads to significant differences.

5.2 INTRODUCTION

Patients with head and neck cancer often have a poor prognosis. Common risk factors are tobacco and alcohol use (accounting for 72% of cases when combined [8]), but also human papillomavirus (with a large variation globally, but linked to more than 50% of cases in the UK [167]). Head and neck cancer patients can be difficult to treat, as many important structures are present in a very small region, which limit treatment options and dosage [11].

Hyperthermia therapy is an attractive sensitizer for chemo-, radio- and immunotherapy [28]. This becomes especially relevant for head and neck patients with larger tumours that are inoperable, or in the presence of other limiting factors such as tight dose constraints when re-irradiating or close proximity to critical normal tissues. In order to achieve the maximum effect with the hyperthermia treatment, the temperature of the tumour tissue should lie between 39-43°C for a duration of at least 60 minutes [70].

It is important to validate that the temperature achieved lies in the desired range, because if the temperature is too low, the sensitizing effects of the hyperthermia treatment are limited or not existent; and if the temperature is above the desired range, there is an increased risk in permanent tissue damage in surrounding healthy tissue [168, 169]. The heating behaviour of subjects is highly individual because of the natural variation in tissue properties, such as perfusion, blood flow and energy absorption rate [170], and thus cannot easily be predicted. For these reasons, the temperature needs to be monitored during the treatment, which is usually done using intraluminal or invasive catheters containing temperature probes. However, clinical experience demonstrate that, especially in the head and neck region, it is not without risk or simply impossible to place the probes close to the tumour, especially if the tumour is located in the pharynx or larynx. Moreover, temperature sensors only provide point-like measurements, and thus very limited information, which means that possible hot or cold spots could remain undetected.

Magnetic resonance thermometry (MRT) has as benefit that it can measure three dimensional (3D) temperature changes non-invasively. The most commonly used method is proton resonance frequency shift (PRFS) [53], which has superior accuracy, linearity with temperature and tissue independence (except for fat). PRFS MRT is most commonly acquired with gradient-recalled echo (GRE) acquisitions, although other options have been explored [100, 171, 172]. Clinically, only DE-GRE is currently used. However, 3D-ME-FGRE was shown to significantly improve mean

average error (MAE) and mean error (ME) in the brain [159]. MRT has successfully been demonstrated in sarcomas, pelvis and the brain [46, 64, 159]. Recently, an MR-compatible hyperthermia applicator for the head and neck was developed [44, 45] at our institution: the MRcollar. At time of writing the device is in its final stages of being approved for clinical use and hence creates a need to develop reliable PRFS MRT.

One of the main challenges of PRFS MRT is that the off-resonance frequency changes due to temperature are small, compared to disturbances of the frequency due to motion such as breathing and swallowing [173]. Therefore, temperature feedback during hyperthermia treatments in the head and neck region, currently is very limited [43]. To reduce the effect of intra-scan motion, acceleration of image acquisition is actively researched [109, 174-176], bringing many advantages such as shorter imaging times, less opportunity for anatomy to move during the scan, and the option to increase field of view (FOV) coverage or resolution at the same imaging time.

To compensate inter-scan motion the only in-vivo MRT evaluation done so far, by Pichardo et al.[112], focused on correcting the breathing artifacts in pigs. However, the pigs were immobilised, anesthetised and ventilated, which is not realistic in head and neck patients. A more patient friendly procedure is thus called for, in order to demonstrate the feasibility of MRT in the head and neck in humans.

The objective of this paper is to investigate whether MRT is possible in realistic motion conditions in the region around the oropharynx of healthy unheated volunteers. We aim to identify how MRT performance in the region is affected by swallowing and breathing, as well as pin-point (more) reliable anatomical regions for MRT. Further, we explore possible trends in MRT performance regarding different imaging setting in the form of accelerating the scan and averaging it. All these are important factors to consider in order to advance hyperthermia therapy in the head and neck.

5.3 MATERIALS & METHODS

All acquisitions were made using a 22-channel Head and Neck imaging coil on a 1.5T magnetic resonance imaging (MRI) scanner (GE Healthcare, Waukesha, WI, USA). A 3D-ME-FGRE sequence with settings give below was used for all acquisitions.

5.3.1 Phantom

To evaluate the motion-free baseline performance as well as temperature sensitivity and accuracy of the different acquisitions, we performed an experiment during the cooling down phase of a phantom.

5.3.1.1 Acquisition settings

MRI acquisition parameters for the phantom experiment are listed in Table 5.1.

Table 5.1: MRI acquisition parameters for the phantom experiment.

FOV (cm^3)	19.2×19.2×0.5
voxel size (reconstructed) (mm^3)	0.75×0.75×2.5
acquisition matrix	128×128
acquired voxel size (mm^3)	1.5×1.5×5
TR (ms)	42.3
flip angle (°)	13
ETL	9
BW (kHz)	83.33
Echo spacing (ms)	2.2
TE_{min}- TE_{max} (ms)	1.8-19.0

5.3.1.2 Experimental set-up

In order to investigate the MRT of the phantom it was filled with hot water of about 65°C, positioned in the MRI, and non-perturbing, electromagnetically insensitive temperature sensors with an accuracy of ±0.2°C over a range of 25 to 52°C were placed in the catheters. When the temperature in the centre vial reached a temperature of 49°C, imaging commenced, whilst the phantom was slowly cooling down to 36°C over the course of 140 minutes. The imaging protocol included scans with different settings of accelerations (ARC) and number of image averages (NEX), all of which are presented in Table 5.2.

Table 5.2: Imaging protocol for the phantom experiment, including acceleration settings, number of image averages (NEX) and the resulting acquisition time.

Scan #	Acceleration (ARC)	NEX	Acquisition time
1	2	1	00:27
2	1	1	00:44
3	1	2	01:27
4	1	3	02:11

5.3.1.3 Post processing

The detailed pipeline is described in [159].

5.3.2 In-vivo

5.3.2.1 Subjects

Five volunteers without dental braces or wires were recruited. For the sequence and its settings used here, metal would lead to large artifacts, possibly obscuring the fat and other regions of relevant anatomy for this study. All volunteers signed an informed consent (protocol MEC-2014-096, approved by the Erasmus MC Medical Ethical Committee).

5.3.2.2 Acquisition settings

The acquisition parameters were chosen such that the acquisition time for the fastest scan (acceleration=2) was still feasible for a breath hold scan (assumed maximum of 30 seconds), keeping a resolution >1 mm and as large of a imaging volume as possible in the z-direction, see Table 5.3. For the final volunteer (#5), the anatomy was larger than the original FOV, and hence the FOV was increased as indicated in Table 5.3 causing a different in-plane spatial resolution.

Table 5.3: MRT acquisition parameters for the in-vivo volunteer experiments.

Parameters	Volunteer #1-4	Volunteer #5
FOV (cm)	20.2	21.2
voxel size (reconstructed) (mm^3)	0.79×0.79×2.5	0.83×0.83×2.5
acquisition matrix	128×128	128×128
acquired voxel size (mm^3)	1.58×1.58×5	1.66×1.66×5
TR (ms)	39.8	37.7
flip angle (°)	12	12
ETL	9	9
BW (kHz)	83.33	83.33
Echo spacing	2.1	2.0
TE_{min}- TE_{max} (ms)	1.2-17.9	1.2-17.4

5.3.2.3 Experimental set-up

For the MRT investigation, the volunteers were placed in the MRI in a supine position inside of the head coil. The imaging protocol included nine different scans with different settings (see Table 5.4), that were repeated five times each (for a total duration of ~75 minutes). Table 5.4 also shows the chosen acceleration, resulting acquisition times, as well as the instructions for these respective scans for breath hold and

swallowing. For the breath hold scan, the scanner was automatically instructing the volunteers to hold their breath. The breath hold was only investigated for one scan setting, as we were limited by the physical constraints of the volunteers, assuming a maximum breath hold duration of 30 seconds. For the scans involving swallowing, the volunteers were manually instructed to swallow two times at random.

Table 5.4: Scan protocol for volunteers, including Acquisition times. Acquisition times differed depending on the spatial resolution.

Scan #	Acceleration (ARC)	NEX	Breath hold	Swallowing	Acquisition time
1	2	1	1	0	00:27 / 00:25
2	2	1	0	0	00:27 / 00:25
3	2	1	0	1	00:27 / 00:25
4	1	1	0	0	00:44 / 00:41
5	1	1	0	1	00:44 / 00:41
6	1	2	0	0	01:27 / 01:22
7	1	2	0	1	01:27 / 01:22
8	1	3	0	0	02:11 / 02:00
9	1	3	0	1	02:11 / 02:00

5.3.2.4 Processing

The DICOM images were imported from the scanner into MATLAB (MATLAB and Statistics Toolbox Release 2021b, The MathWorks, Inc., Natick, Massachusetts, United States). The pipeline used for processing the data is as introduced in [159]. The robustness was increased further through multiple starting points in the multi-peak multi-echo thermometry with PRFS (MMT-PRFS, also introduced in [159]) to avoid water/fat swaps due to local minima, and through implementing b-spline image registration.

Initial results showed some water-fat swaps that corrupted the fat mask. This made us add an extra step to exclude individual scans with water-fat swaps from the analysis. The corrupted scans were identified by visual inspection of the change in off-resonance maps and statistics are reported in the results.

For the quantitative evaluation, three different ROIs were chosen: neck muscle, spinal cord and masseter muscle. This selection covers relevant regions across the FOV. The sizes of the ROIs were picked so that they would stay in the type of tissue aimed for, but also at sufficient distance away from fatty tissue. The ROIs size and positioning are indicated in Figure 5.1.

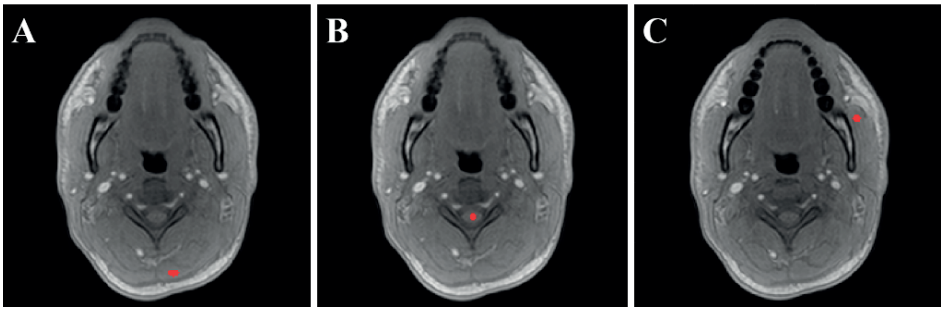

Figure 5.1: Example of position and size of ROIs selected for volunteer MRT performance analysis. From left to right: A) neck muscle, B) spinal cord, and C) masseter muscle.

5.3.3 Performance calculations

Similar to [8], the quantitative MRT performance analysis was performed on the ROIs introduced above using the MAE, ME and SD, defined as:

$$MAE = \frac{1}{n-1}\sum_{j=2}^{n}\left|T_{ROI,j} - A_j\right| \tag{5.1}$$

$$ME = \frac{1}{n-1}\sum_{j=2}^{n}\left(T_{ROI,j} - A_j\right) \tag{5.2}$$

$$SD = \frac{1}{n-1}\sum_{j=2}^{n}\sqrt{\frac{1}{|ROI|}\sum_{i\in ROI}\left|E_{i,j} - T_{ROI,j}\right|^2} \tag{5.3}$$

Statistical significance of the results was calculated with SPSS (IBM Corp. Released 2021. IBM SPSS Statistics for Windows, Version 28.0. Armonk, NY: IBM Corp). A two-sided independent samples t-test was performed and statistical significance was assumed at $p<0.05$. For the phantom the significance of the difference were tested between all of the four different scans. For the volunteers, the significance of the difference was tested between the normal (NEX=1, no breath hold, no swallowing) scans and all other 8 remaining scans for each ROI. Additionally, we also investigated the significance of the difference between scans with the same acquisition settings and different instructions to the volunteers (i.e. no instruction vs. breath hold and vs. swallowing) for all three ROIs.

5.4 RESULTS

5.4.1 Phantom

The results of the phantom experiment are presented in Table 5.5. Results that are significantly different are presented in bold. All values for MAE and ME, satisfied the minimum requirement for successful MRT [23], as did the SD for NEX=2 and NEX=3 scans.

There are no significant differences in MAE and ME when using acceleration, or when increasing the number of NEX. The SD significantly and consistently improves with an increase in NEX. For NEX=2 and NEX=3 the improvement is slightly less than the $1/\sqrt{N}$ improvement expected for uncorrelated noise, indicating that it is not only thermal noise that generated a larger SD.

Table 5.5: Performance of MRT from phantom experiment covering 36-49°C. Significant differences to other results are presented in bold. All values for MAE and ME, satisfied the minimum requirement for successful MRT [134], as did the SD for NEX = 2 and NEX = 3 scans.

	MAE (°C)	ME (°C)	SD (°C)
ACC = 2 (NEX = 1)	0.28	-0.23	0.81
NEX = 1 (ACC = 1)	0.33	-0.32	0.58
NEX = 2 (ACC = 1)	0.28	-0.23	0.48
NEX = 3 (ACC = 1)	0.31	-0.30	0.39

5.4.2 Volunteers

An example of the MRT maps obtained for the different scans is shown in Figure 5.2. It can be seen that there are some susceptibility artifacts present, especially around the teeth. It can also be seen in the swallowing scans 3, 5, 7 and 9 (bottom row of Figure 5.2), that it seems to lead to larger temperature variations from zero than the other scans.

The MRT performance per scan is presented in Figure 5.3, Figure 5.4, and Figure 5.5 for MAE, ME and SD respectively. The outliers originate from the B0 drift correction not always working perfectly, because we have no substantial fat present in the centre of the imaged region (it is mainly located in the back of the neck and the cheeks). Hence, if there is a non-linear change in B0 drift, we cannot correct for that.

Visual inspection for water/fat swaps lead to the exclusion of 1/5 time points for scans 1-8 for one volunteer. Each bin (scan per ROI) thus includes 19 (scan 1-8) or 20 (scan 9) measures from the 4 different time points and 5 volunteers.

There were no significant differences found between the different scans, when comparing them to scan 4 (NEX=1, no swallowing). The difference between motion

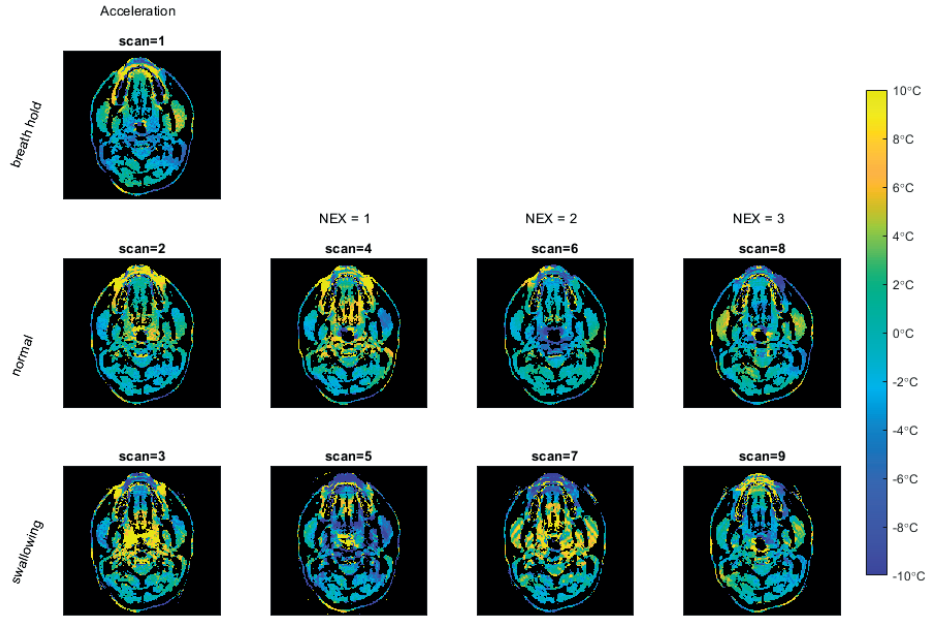

Figure 5.2: MRT maps for the temperature change of one unheated subject (volunteer #3, time point=2) shows the qualitative differences between acquisitions. The rows are (from top to bottom): breath hold, normal free breathing and swallowing. The columns are (from left to right): acceleration, NEX=1, NEX=2, and NEX=3.

(instruction to swallow) and no motion of the same acquisitions (scan 1-3, 4&5, 6&7, and 8&9) were not significant for any ROI, nor on a whole.

However, when comparing the different anatomical ROIs regarding MAE, ME and SD, the differences were significant for all performance metrics (presented in Figure 5.6). The best performance for MAE and SD was observed for ROI 1: neck muscle. For ME ROI 2: spinal cord performed best, as it was closest to zero. None of the ROIs investigated in this study achieved the required performance values for successful MRT in hyperthermia [134].

5.5 DISCUSSION

This presents the first study on MRT in the head and neck region in human subjects, a region which is known to be prone to movement related artifacts in imaging.

5.5.1 Impact of technical measures on MRT

In the volunteer experiments it can be observed that both accelerating the acquisition by parallel imaging as well as increasing scan time by increasing NEX are

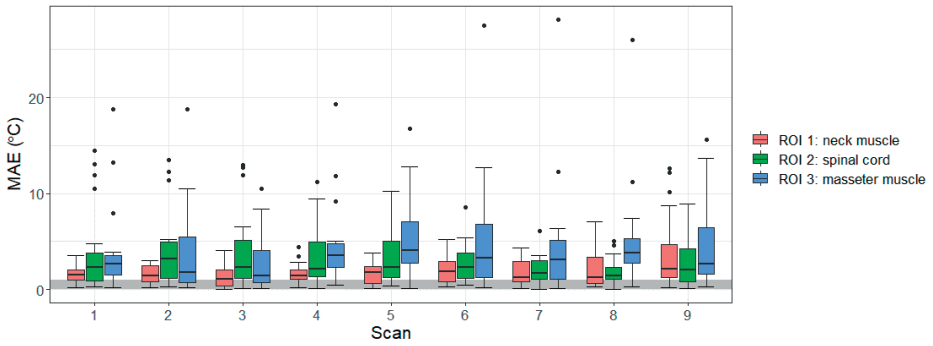

Figure 5.3: MAE across all volunteers, displayed for all ROIs and all different scan. There were no significant differences between the scans (numbered in accordance with Table 5.4). The minimum requirement for successful MRT [134] is indicated by the grey band.

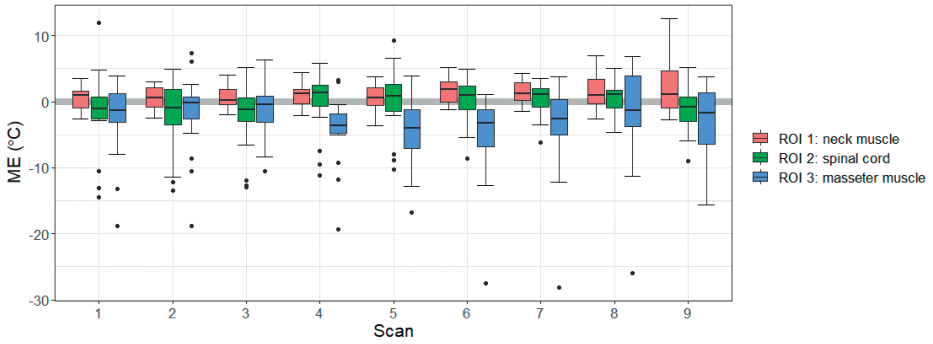

Figure 5.4: ME across all volunteers, displayed for all ROIs and all different scans. There were no significant differences between the scans (numbered in accordance with Table 5.4). The minimum requirement for successful MRT [134] is indicated by the grey band.

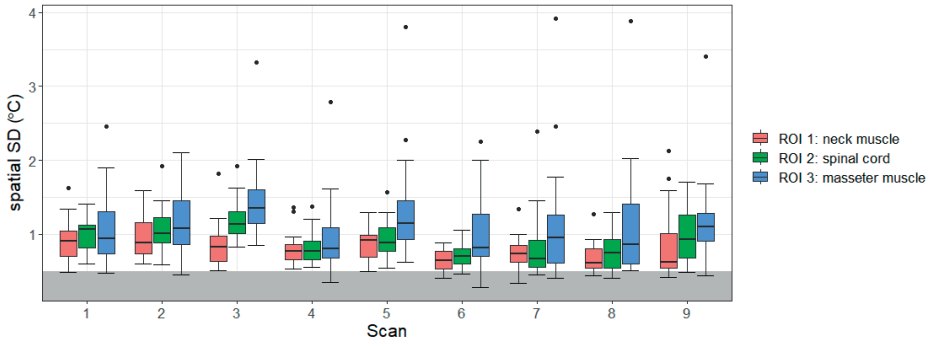

Figure 5.5: SD across all volunteers, displayed for all ROIs and all different scans. There were no significant differences between the scans (numbered in accordance with Table 5.4). The minimum requirement for successful MRT [134] is indicated by the grey band.

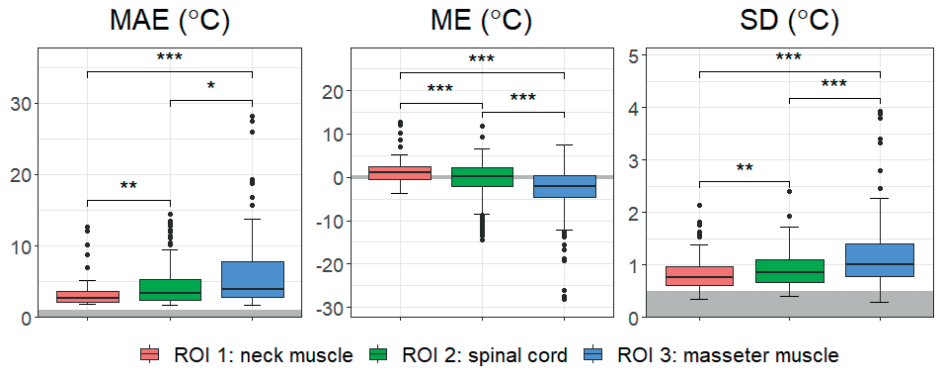

*Figure 5.6: MAE, ME and SD of all scans, shown for the different ROIs. Significant codes are noted as: 0.001=***, 0.01=**, 0.1=*. The minimum requirement for successful MRT [134] is indicated by the grey band.*

not significantly changing the MRT performance in this region. This is an important result, as it shows that scanning faster or slower does not come at the cost of MRT quality. Consequently, we have the freedom to either design a protocol to be as fast as possible, saving imaging time and potentially improving patient comfort; or going towards longer acquisition times with for example increased imaging resolution or a wider FOV. A sufficiently high resolution in the head and neck is desirable, as there are many different small anatomical structures in close proximity to one another that may heat differently, and a more extensive FOV is beneficial to monitor the anatomy surrounding the tumour target region for hot spots, as well as making corrections, for instance for motion, easier and more robust. Past studies have reported that accelerating the acquisition improved the MRT performance [89], which stands in contrast with the present results. A possible explanation for these discrepancies is that there are different motion patterns in different anatomies.

5.5.2 Impact of breathing and swallowing on MRT

Another important result was the insignificance of swallowing and breathing on the quality of MRT. With the settings used, neither breath-hold nor instructions to avoid swallowing seem essential for MRT performance. Not needing to scan under breath hold improves patient comfort, simplifies the scanning protocol and reduces preparation time. The extra time can in turn be used to improve resolution, FOV, or SNR of the acquisition. The fact that swallowing does not significantly impact the quality of MRT might simplify treatments too, as scans where the patient swallowed may not need to be excluded from the analysis. This should be verified for other ROIs and using the treatment set-up in the MRcollar, before generalising this for the whole anatomy of the head and neck. These results are surprising, as one would

have expected swallowing and breathing to be associated with movement-induced artifacts, resulting in greater MRT errors.

5.5.3 Clinical relevance of MRT in different ROIs

Another important outcome of the study is that there are significant differences in MRT performance among the anatomical ROIs chosen. The neck muscle had the best MAE performance with 1.96±1.89°C, as well as the smallest SD of 0.82±0.3°C. However, these measured performance values are still higher than what we aim for and would require to achieve successful MRT [134].

The comparatively better MRT performance of the neck muscle is most likely because of two reasons: firstly, the neck muscle is at the back of the head, which has lower inter-scan motion because of the supine positioning of the volunteer on the scanner bed; secondly, the neck is relatively far away from internal disturbances such as susceptibility artifacts around deforming air cavities and non-rigid repositioning of the tongue. There are methods available, presented in Wu et al. [93] and Nouwens et al. [177], that improve the susceptibility induced temperature error in the pelvis, and might also prove useful in the head and neck.

The ME was best in the spinal cord. This is the only ROI investigated in this study that satisfies the minimum requirements for ME for successful hyperthermia of <0.5°C, albeit only for scans 4-8. This is most likely due to the spinal cord having a central location in the imaged anatomy, which means better magnetic field uniformity as well as only small deformations due to the protecting surrounding structures. Additionally, the B0 drift correction is likely most effective there, as the fat mask used for correction is located in a near-equidistant ring around it.

For this study the masseter muscle was of interest, as trismus (extreme tightness of the jaw muscles making it impossible to (fully) open the mouth) has been observed as a side-effect of hyperthermia in the head and neck region [43], and one of the hypotheses is that the occurrence of trismus may be increased by combining radiotherapy with hyperthermia.

The masseter muscle is located towards the anterior part of the volunteers making it more susceptible to inter-scan motion. The results in this ROI indicate the possible influence of head motion with MAE and SD showing the worst performance of 4.53±5.01°C and 1.16±0.64°C respectively. The spread of the results, shown by the standard deviation of the mean, can be seen as an indication of the reliability of the ROI for MRT. At this moment, regions with large inter-scan motion do not provide

accurate MRT, and unfortunately there are clinically relevant organs at risk in these regions.

It may be an important consideration for monitoring and guiding hyperthermia with MRT, that the tumour can be located in areas where a lot of motion is present, such as the oral cavity. However, before making conclusions in that regard the results of this paper should be expanded by repeating the procedures in the present study in the treatment set-up, once the MRcollar is approved for the use on human subjects. Part of the applicator is a water bolus, which sits snugly between the patient and the antennas used for heating, to cool the skin of the patient and to aid the RF transmission to the tissues. Because of the restricting water bolus around the head of the patient, we expect that head motion will be reduced. During the experiments in this study no confinement was used on the volunteers, and we observed a lot of motion even when asked to be still. Therefore we presume that when imaged in the treatment set-up, MRT performance will likely improve.

For the purpose of improving MRT performance in the future to realize the minimum requirements, one can consider optimizing the acquisition parameters or implementing other technologies that have already been developed. These include advanced filtering techniques [161], explicit modelling of the motion induced susceptibility field changes [99, 136, 178], field monitoring [136], or extrapolating the heating from regions that are reliable.

5.5.4 Limitations

The volunteers included in this study were not heated, so the physiological reaction of in-vivo tissues that arise as response to hyperthermia, such as increase in flow and diffusion, were not present. Repeating the experiments presented in this study using in-vivo heated conditions could thus influence the MRT measurements.

Furthermore, the volunteers used here were healthy subjects and therefore did not have some of the tissues of interest, such as tumour tissue or pathological lymph nodes. Because of their different composition these tissues may behave differently than the regions investigated in this study.

In this study we have covered relevant ROIs across the FOV acquired. In reality it might be interesting to investigate additional areas, depending on the location of the (expected) tumour or potential hot spots during the hyperthermia treatment.

This work is only focused on a small region in the head and neck and the motion that can arise there. It cannot directly be generalised to other areas with different motion e.g. the pelvis.

The FOV of the acquisitions was limited to allow breath-hold scanning. As the results show breath-hold scanning is not essential for MRT performance. Hence, the strong desire of the clinical staff for a larger FOV can probably be accommodated without excessive loss of resolution.

In its current state, the post-processing pipeline takes a substantial amount of time to run (on the order of tens of minutes). For clinical use the processing time needs to be improved to the order of a few minutes to be fast enough for real-time monitoring and enabling MRT guided adaptation of clinical hyperthermia treatment. As the current MATLAB and CPU based post-processing pipeline is not optimized for computation time, we expect sufficient time reduction to be possible with a dedicated optimized implementation.

To isolate the effects of scan duration and inevitable subject motion, we only varied a small amount of acquisition settings and confounders. The current results pave the way for further optimization of MRT by for instance refining the acquisition parameters such as resolution, field of view, bandwidth, number of echoes or repetition time.

5.6 CONCLUSION

We have shown that we can map the temperature in a small region of the head and neck with MRT and in 3D. Acceleration as well as averaging the MRI acquisition does not significantly affect the accuracy of MRT results; nor does performing a scan under breath hold compared to normal breathing or swallowing compared to not swallowing. However, depending on which ROI is selected, the MRT performance is significantly different. Unfortunately, none of the ROIs and scans fulfilled all MRT performance requirements. We indicated relevant research directions to improve MRT, hopefully paving the way towards MRT guided hyperthermia treatment as adjunctive therapy in head and neck cancer patients.

Chapter 6

Discussion

In this thesis we have worked on developing MR thermometry (MRT)-guided hyperthermia in the head and neck.

MRT has been introduced during the 1990s. Promising progress emerged with the swift development of integrated hyperthermia and MRI devices. First was the BSD2000 Sigma-Eye applicator (for pelvic cancer patients), starting in a 0.2T MRI [88] adding exogenous temperature indicators; next in a 1.5T MRI in Berlin [179].

After the development of PRFS MRT, the BSD2000 Sigma-Eye was used in clinical application for hyperthermia in a handful of university hospitals [63, 81, 88, 90, 91, 93, 95]. Since, promising new research was introduced to improve MRT, including accelerating the MR acquisition [180, 181], using treatment modelling [161, 182], or developing novel hyperthermia applicators [183]. However, since 2005 hardly any clinical progress in MRT for hyperthermia treatments was reported. The translation to clinical practice is likely hampered by requiring expensive purchases, or using sequences and post-processing tools that are still under development.

Integrating a heating applicator in the MRI with only the body coil for imaging is sometimes insufficient regarding imaging quality for successful MRT [184], generating the need for improved imaging equipment. Inserting a hyperthermia applicator however can disturb the field homogeneity of the MRI, leading to an increase in susceptibility artifacts – something that PRFS MRT is particularly susceptible to [48]. Different approaches to integrate MRI imaging coils and hyperthermia devices in order to get a higher SNR (signal to noise ratio) are comprehensively presented by Paulides *et al.* [185]. This line of hardware development, integrating hyperthermia transmit and MRI receive coils, has allowed MRT to progress to a higher quality, potentially improving the accuracy and precision of the MRT.

MR-guided hyperthermia of the head and neck region requires a dedicated MR-compatible multi-MR-receive coil integrated hyperthermia applicator. Work on such a device, the MRcollar, has progressed in parallel to the work described in this thesis. The development of the MRcollar involves solving a complex two-fold problem: the device must be able to heat head and neck tumours in patients safely, while at the same time providing accurate and advanced MRT monitoring to demonstrate the safety and effectiveness of head and neck hyperthermia. As both are complex issues, the MRcollar project has two main parts, each contributing to one of these aspects. This thesis is the result of the research on the MRT part.

MRT is working quite successfully in solid and fixed tumours, such as sarcomas in the extremities, which can be considered easy targets with high temperature increases and no motion. Because routine clinical MRT is limited to this tumour type, there is not a large variety of commercially available devices. The ones that are available, are often home build, making comparisons between centres difficult; these applicators are presented in Adibzadeh *et al.* [39]. The lack of commercially available hyperthermia applicators limits the amount of users and therefore also limits research efforts, which in turn lowers the rate at which the field progresses. Sarcoma patients are also a small patient group (800 new patients per year in the Netherlands [186]), divided into many different subgroups and multiple treatment sites. This also hinders progress of the field, as a small number of patients means a smaller study population and therefore less convincing evidence.

As thus far no standardization to report the performances of MRT was defined in literature, previous studies are difficult to compare to each other, largely precluding meta-analysis of and conclusions from the data. In **Chapter 2** we tried to address the unmet need for standardization of MRT metrics, and thus defined a set of minimum performance criteria for successful MRT. This included the accuracy (MAE), bias (ME), as well as the spatial and temporal standard deviation (SD). In order to understand where the greatest need for improving MRT lies, we also conducted a systematic literature review of available clinical MRT in hyperthermia treatment studies. We found that the successes in MRT are limited to areas with no motion, for example sarcomas in the extremities. In contrast, body regions with a lot of movement, especially when air is involved such as in the pelvis or in the head and neck, proved challenging. The available publications also highlight, that each part of the body comes with its own challenges, making a direct translation of methods from one region to another nearly impossible.

The development of the MRcollar described above has created the need to re-address a number of issues in MRT. In relation to MRT of the head and neck area, we found that literature was thus far lacking data on which MRI sequences could be used to achieve MRT to the standard defined in **Chapter 2**. As numerous sequences can be used, a number of considerations of a technical nature, but also issues related to patient comfort have to be taken account. Furthermore, as already alluded to, the head and neck region has considerable challenges with regard to acquiring stable imaging signals due to frequent motion taking place in this part of the body. As research has thus far largely focused on stationary targets, novel acquisition and post-processing strategies might be needed.

In order to also advance clinical MRT, we are presented with the explicit need for practical solutions that are easy to implement on most MR scanners. Thus, in the studies conducted in **Chapter 3** and **Chapter 5**, we present practical solutions, focussing on using tools that are widely available and do not require expensive additional purchases beyond the MR machine or complicated procedures. Beyond accessibility, we also thought it important to focus on commercially available components in order to accelerate progress in this field of research. Therefore, in **Chapter 3,** we compared several multi-echo gradient echo sequences that are already commercially available. We found that 3D-ME-FGRE, compared to DE-GRE, offers a statistically significant improvement in accuracy of 62% in the brain of unheated volunteers, and 46% in phantom (37°C-43°C). As the 3D-ME-FGRE is readily available, the use of this multi-echo sequence for MRT is an improvement of these important performance characteristics which is easily and swiftly implemented. In this chapter we thus demonstrated that MRT can be improved by using tools that are already widely available.

The issue of motion related artefacts in the head and neck area, specifically swallowing and breathing, were investigated in **Chapter 5**. Surprisingly, we found that, with the settings used, there were no significant differences in the quality of MRT in the regions investigated when performing the scan under breath hold or with deliberate swallowing. This is an important insight for making a clinical protocol in the future, as this affects a number of decisions. Firstly, one is not bound to adjusting the acquisition times to the physiological limitations of breath holds. Performing a scan under normal breathing also reduces the burden on patients. Secondly, scans where the subject swallows don't need to be discarded.

As stated previously, not only technical issues, but also patient comfort are of importance in the treatment of head and neck cancer patients. The main source of patient discomfort due to MRT is acoustic noise. In **Chapter 4** we therefore investigated a novel quiet MRI sequence called Looping Star, in order to reduce subject stress through acoustic noise. In this study, it was indeed reported that subjects experienced a subjective reduction of acoustic stress, while at the same time yielding more accurate MRT results.

The MRcollar is not yet approved for the use on human subjects. The MRT techniques and approaches that have been developed and presented in this thesis, especially in **Chapter 3** (identifying the most promising sequence as 3D-ME-FGRE) and **Chapter 5** (confirming that breath hold and swallowing as well as acceleration and averaging holds no benefit for MRT), will need to be partially reinvestigated using the novel

applicator. A small reduction in MRT performance can be expected due to the MRcollar having fewer receiver coils than the Head and Neck coil used for the experiments in this thesis. On the flip side, the MRT performance will likely improve, as the subjects' rigid inter-scan motion will be strongly restricted by the water bolus of the MRcollar. It remains to be seen what, if any, differences will be found especially regarding the MRT accuracy. Should the minimum requirements for successful MRT in hyperthermia treatments defined in **Chapter 2** not be achieved, additional post-processing measures extensively discussed in **Chapter 5** can be considered.

In order to be clinically viable, i.e. still offering real-time feedback during the hyperthermia treatment, MRT processing time needs to be shortened to a time in the order of minutes (<5mins). This is because the rate of temperature change during hyperthermia treatment is approximately 1-2°C every five minutes. Several modifications were already added that made the pipeline more efficient, even if that was not always the primary aim. Still there is a considerable amount of room for improvement, as the MRT quality was the main focus in these studies. Additionally, to enable easy accessibility during treatment, the method should be integrated (or at least displayed) on a computer in the scanner room.

At the time of writing, MRT-guided hyperthermia treatments are unfortunately still a research modality. Naturally it is desired to move towards clinical application in the future. In order to do so, several important steps are needed, which build on this thesis and will be highlighted in the following sub-section.

6.1 TOWARDS CLINICAL APPLICATION OF MRT-GUIDED HYPERTHERMIA IN HEAD AND NECK CANCER

Building on the work described in this thesis, the field of MRT-guided hyperthermia in the head and neck can be progressed by

1. technical testing of the MRcollar (when available), and subsequently
2. clinical validation to advance MRT to be the clinical standard for hyperthermia treatments in head and neck cancer

A prerequisite for treating head and neck cancer patients in the MRcollar is the testing of the imaging and heating capabilities using the treatment set-up. This requires both a phantom study, conducting the heating with the hyperthermia device, and a subsequent in-vivo study using volunteers to assess the imaging performance of the receive coils. Then, in a next step, initial patient studies can be

performed using both MRT and the invasive probes, starting with a low power (with no treatment intent) to understand the efficiency of the heating of the MRcollar and extending to a heat-dose-escalation toxicity study.

After the technical testing of the MRcollar is complete, clinical studies on the reliability, involving among others correlative studies between invasive temperature measurements and MRT need to be performed. And additionally, the clinical advantages of MRT over non-MRT-guided hyperthermia treatment need to be shown.

Demonstrating successful MRT during hyperthermia will facilitate proving the relation between the treatment temperature achieved and the clinical outcome; thus potentially enabling hyperthermia to gain acceptance as a treatment modality for head and neck cancer. Measuring the temperature in the head and neck during hyperthermia treatments will provide much needed data to bring hyperthermia treatment forward in clinical practice through better understanding, and potentially predicting, clinical outcome.

Lastly, accurate, dependable and clinically feasible MRT may potentially aid in guiding the decisions about what techniques are to be used and also to identify further lines of research. Currently, hyperthermia treatment is guided either by real-time, invasive temperature measurement probes, subjective patient feedback or by pre-treatment modelling. Each of these methods have their own drawbacks, due to the need for invasive measures, subjectivity and inter-patient variation of heat tolerability or lack of sufficient precise, real-life data of variance of heat distribution on which planning models are based. Certainly, MRT will be able to improve on each option, either by obviating invasive measurements or subjective reporting, or by providing a wealth of real-life data with which pre-treatment simulations can be improved.

As described in the previous paragraphs, improvement of MRT is influenced by both patient specific parameters that cannot be controlled and technical limitations. A direct benefit of successful MRT is of course knowing the treatment temperature. However, for widespread clinical use that alone is not sufficient. Other benefits, such as toxicity, quality of life, disease control and patient satisfaction should also be proven. Collecting these parameters is key to obtain indications to support writing a clinical study proposal in the future. In order to provide reliable data, large study populations are required to achieve sufficient statistical reliability. At the time of writing, population studies are neither available nor do they seem attainable in the near future. Therefore, a careful and considered design of a structured research

plan is necessary which can achieve the maximum results with the limited study population that are available at the current juncture.

In summary, the work described in this thesis presents a significant step towards clinical MRT-guided hyperthermia for head and neck cancer patients. We have introduced standardization of MRT performance reporting as well as defined minimum criteria for these performances. Additionally, we have demonstrated MRT in the head and neck region, addressing motion challenges and other concerns. Using this work as a guide, it will be possible to further develop MRT towards a clinical standard method for real-time, non-invasive temperature monitoring for use during thermal therapy. For the patient the benefit will be a slight reduction of the burden in an otherwise already intensive, stressful multi-modality cancer treatment process.

Summary

Hyperthermia is a cancer treatment which consists of heating the tumour to 39-43°C. When clinically possible, the temperature during the treatment is measured by placing temperature probes intraluminal or invasively. The only possibility to measure the 3D temperature distribution non-invasively in and around deep seated tumours is by magnetic resonance thermometry (MRT). However, in order to be able to fully replace conventional temperature probes, MRT needs to become clinically viable.

Current applications of MRT in hyperthermia mainly include anatomical regions that are not influenced by motion, such as sarcomas in extremities, or as adjuvant to invasive probe-based approaches. Motion-rich anatomy is difficult to image with MRI and also non-local organ motion due to, e.g., respiration can lead to large artifacts for MRT. One of the things that can improve on the quality of MRT is the signal to noise ratio (SNR) of the MRI images. SNR can be improved by adding receive coils close to the anatomy that is being imaged, the closest location they can be placed is within the hyperthermia applicator itself.

Recently, we have started the development of an MR-compatible hyperthermia applicator, that includes integrated MR-receive coils, for the head and neck: the MRcollar. Because the MRcollar is the first of its kind, there is very little experience on MRT in the head and neck in humans. In this thesis we sought to investigate how we can improve and adapt MRT to the difficult anatomy in the head and neck.

In **Chapter 2** we report our systematic literature review, which showed that there is a lack of standardization and reporting of MRT performances during hyperthermia, which makes comparing results hard and hinders progress. Subsequently, we defined standardized minimum performance thresholds for successful MRT for hyperthermia treatments: ≤1°C for the accuracy, ≤|0.5°C| for the bias/trueness, and ≤0.5°C for the spatial and temporal temperature precision. When reviewing the literature, we found that 10% of the clinical studies reported no metric, 50% of studies reported one, 30% reported two, 10% reported three, and none reported all four. 67% of the clinical studies that reported metrics met the minimum requirements we defined. Common problems that hinder the realization of the defined minimum criteria were found to be motion, as well as B0 changes, especially in challenging anatomical regions such as the pelvis. Additionally, we reviewed pre-clinical results to identify where the biggest potential lies to improve these problems. Methods to improve these issues included novel reconstruction methods to accelerate the imaging, imaging under breath hold, the use of navigator echoes, as well as correction and stabilisation strategies.

MRT was developed between 1990 to 2000 using technology of that decade or older. During the last two decades, despite technological developments, MRT during hyperthermia treatments largely remained the same. Clinical MRT usually consists of a double echo gradient echo (DE-GRE) sequence with basic phase subtraction as post processing, using external fat references to correct for the B0 scanner drift. Therefore, we saw a lot of room for improvement using MRI sequences already available such as multi-echo and 3D multi-echo gradient sequences, as well as post-processing tools such as image registration and a multi-peak fitting tool, which have already been developed and appeared promising to improve MRT. In **Chapter 3** we identified 3D-ME-FGRE as the most promising imaging sequence by comparing the MRT performance of different multi-echo gradient-echo sequences in phantom and volunteers. In the volunteer experiments we scanned the brain, an ideal anatomical region for testing, because it is far away from motion disturbances and (regarding MRT) quite homogeneous. 3D-ME-FGRE had the most improvement in accuracy of 62% in volunteers and 46% in phantom (temperature varying from 37°C-43°C), compared to the clinical standard sequence (DE-GRE). Additionally, we developed a post processing method to suit the need for the current research. The in-vivo post-processing pipeline included rigid body image registration to correct for inter-scan motion, a novel multi-peak fitting tool that improves the estimation of parameters by using all of the available echoes, and automatic body fat selection developed specifically for this study using water/fat density maps (originating from the multi-peak fitting tool) that makes the addition of external fat references for B0 scanner drift correction superfluous.

In order to also include the benefits of the latest developments in modern technology, such as quiet MRI sequences, we tested a novel 3D-radial gradient echo sequence called Looping Star in **Chapter 4**. A lower noise level is considered to increase the comfort of patients and staff substantially during the 60-90 minutes of the hyperthermia treatment. We compared the MRT performance of Looping Star to DE-GRE in phantom and volunteers, and found that the accuracy is significantly improved: up to 74% in the phantom and up to 64% in volunteers. Although, the measured sound pressure levels were not consistently reduced with the parameters used in this study, the participants reported the Looping Star acoustic noise as more pleasant compared to DE-GRE. Hence, while further research into the optimum sequence parameters is still required, the sequence holds promise as an accurate and more comfortable approach.

In **Chapter 5** we used the 3D-ME-FGRE sequence, which was identified as best performing in **Chapter 3**, and conducted an investigation into MRT in the head

and neck region of volunteers. We showed that MRT is possible in that region and that different sources of motion (specifically breathing and swallowing), have no significant effect on the quality of MRT. Additionally, we demonstrated that changing the acquisition strategy either towards acceleration or towards increasing the amount of image averaging (NEX) does not significantly affect the quality of the measured results. However, the MRT performance is significantly different depending on the region of interest that is selected, with regions less affected by inter-scan motion performing better. The neck muscle had the best MAE (=1.96°C) and SD (=0.82°C), followed by the spinal cord (MAE=3.17°C, SD=0.92°C), and the masseter muscle (MAE=4.53°C, SD=1.16°C). Concerning the ME, the spinal cord did best, then the neck muscle and then the masseter muscle, with values of -0.64°C, 1.15°C and -3.05°C respectively. As none of the regions managed to satisfy our minimum requirements for successful MRT defined in **Chapter 2**, more work is required to improve the MRT performance. The most logical next step is to repeat the experiment in the treatment set-up, as the rigid inter-scan motion of volunteers will be severely restricted by the water bolus, possibly already providing enough upgrade in MRT quality. If needed, additional correction or acquisition strategies, such as advanced filtering techniques, can be considered.

This thesis presents a definition of minimum performance characteristics for successful MRT; the identification of 3D-ME-FGRE as a viable and promising sequence for MRT; identification of Looping Star as an alternative more pleasant MRT sequence; and a demonstration that 3D-ME-FGRE used in head and neck is impervious to movement artifacts. This work is thus a significant step towards clinical application of MRT-guided hyperthermia for head and neck cancer patients. Guided by the results presented here, it is possible to design new research strategies to further develop MRT towards a clinical standard method facilitating real-time, non-invasive, 3D temperature monitoring for use during thermal therapy.

Samenvatting

Hyperthermie is een kankerbehandeling waarbij de tumor wordt verhit tot 39-43°C. Indien klinisch mogelijk wordt de temperatuur tijdens de behandeling gemeten door temperatuursondes intraluminaal of invasief te plaatsen. De enige mogelijkheid om de driedimensionale temperatuurverdeling in en om diepgelegen tumoren niet-invasief te meten is magnetic resonance thermometrie (MRT). Echter, om conventionele temperatuursondes volledig te kunnen vervangen, moet MRT klinisch haalbaar worden.

Huidige toepassingen van MRT in hyperthermie omvatten voornamelijk anatomische gebieden die niet beïnvloed worden door beweging, zoals sarcomen in extremiteiten, of als aanvulling op benaderingen gebaseerd op metingen met een invasieve sonde. Anatomie met veel beweging is moeilijk in beeld te brengen met MRI en niet-lokale orgaanbewegingen zoals ademhaling kunnen leiden tot grote artefacten bij MRT. Een factor die de kwaliteit van MRT kan verbeteren, is de signal-to-noise ratio (SNR) van de MRI-beelden. SNR kan verbeterd worden door ontvangstspoelen dicht bij de anatomie die in beeld wordt gebracht te plaatsen, waarbij de dichtstbijzijnde locatie binnen de hyperthermie-applicator zelf is.

Onlangs zijn we begonnen met de ontwikkeling van een MR-compatibele hyperthermie-applicator, inclusief geïntegreerde MR-ontvangstspoelen, voor het hoofd-hals gebied: de MRcollar. Omdat de MRcollar de eerste in zijn soort is, is er weinig ervaring met MRT in het hoofd-hals gebied bij mensen. In dit proefschrift onderzochten we hoe we MRT kunnen verbeteren en aanpassen aan de complexe anatomie in het hoofd-hals gebied.

In **Hoofdstuk 2** rapporteren we onze systematische literatuurstudie, die liet zien dat er een gebrek is aan standaardisatie en rapportage van MRT-prestaties tijdens hyperthermie, wat het vergelijken van resultaten bemoeilijkt en de vooruitgang belemmert. Vervolgens hebben we gestandaardiseerde minimumeisen voor de prestatie gedefinieerd voor succesvolle MRT bij hyperthermiebehandelingen: ≤1°C voor nauwkeurigheid, ≤|0.5°C| voor de vertekening/waarheidsgetrouwheid en ≤0.5°C voor de ruimtelijke en temporele temperatuurprecisie. Bij het beoordelen van de literatuur bleek dat 10% van de klinische studies geen enkele metriek rapporteerde, 50% één metriek rapporteerde, 30% twee metrieken rapporteerde, 10% drie metrieken rapporteerde en geen enkele studie alle vier de metrieken rapporteerde. 67% van de klinische studies die metrieken rapporteerden, voldeed aan de door ons gedefinieerde minimumeisen. Veel voorkomende problemen, die de verwezenlijking van de gedefinieerde minimale criteria belemmeren, waren beweging en ook B0-veranderingen, vooral in uitdagende anatomische regio's zoals

het bekkengebied. Bovendien hebben we preklinische resultaten beoordeeld om te identificeren waar het grootste potentieel ligt om deze problemen te verbeteren. Methoden om deze kwesties te verbeteren omvatten nieuwe reconstructiemethoden om de beeldvorming te versnellen, beeldvorming tijdens adem inhouden, het gebruik van navigator-echo's, evenals correctie- en stabilisatiestrategieën.

MRT werd ontwikkeld tussen 1990 en 2000 met technologie van dat decennium of ouder. Gedurende de afgelopen twee decennia is MRT tijdens hyperthermiebehandelingen ondanks de technologische ontwikkelingen grotendeels hetzelfde gebleven. Klinische MRT bestaat meestal uit een dubbel-echo gradient echo (DE-GRE) sequentie met basis fasesubtractie als post-processing, waarbij externe vet referenties worden gebruikt om te corrigeren voor de B0-scannerdrift. Daarom zagen we veel ruimte voor verbetering door het gebruik van MRI-sequenties die al beschikbaar zijn, zoals multi-echo en 3D-multi-echo-gradient-echo sequenties, evenals door het gebruik van post-processing tools zoals beeldregistratie en een multi-peak fitting tool, die al zijn ontwikkeld en veelbelovend lijken om MRT te verbeteren. In **Hoofdstuk 3** hebben we 3D-ME-FGRE geïdentificeerd als de meest veelbelovende beeldvormingssequentie door de MRT-prestaties van verschillende multi-echo gradient-echo sequenties te vergelijken in een fantoom en bij vrijwilligers. In de experimenten met vrijwilligers hebben we de hersenen gescand, een ideaal anatomisch gebied voor testen, omdat het ver weg is van bewegingsverstoringen en (met betrekking tot MRT) redelijk homogeen is. 3D-ME-FGRE liet de grootste verbetering zien in nauwkeurigheid, namelijk 62% bij vrijwilligers en 46% bij het fantoom (37°C-43°C), vergeleken met de klinische standaardsequentie (DE-GRE). Bovendien hebben we een post-processing methode ontwikkeld die past bij de behoeften van dit onderzoek. De in-vivo post-processing pijplijn omvatte rigide beeldregistratie om beweging tussen scans te corrigeren, een nieuwe multi-peak fitting tool die de schatting van parameters verbetert door gebruik te maken van alle beschikbare echo's en automatische selectie van lichaamsvet, specifiek ontwikkeld voor deze studie met behulp van water/vet dichtheidskaarten (afkomstig van de multi-peak fitting tool), waardoor de toevoeging van externe vetreferenties voor B0-scannerdriftcorrectie overbodig wordt.

Om ook te profiteren van de voordelen van de nieuwste ontwikkelingen in moderne technologie, zoals stille MRI-sequenties, hebben we in **Hoofdstuk 4** een nieuwe 3D-radiale gradient-echo sequentie genaamd Looping Star getest. Een lager geluidsniveau wordt beschouwd als aanzienlijk comfortabeler voor patiënten en personeel tijdens de 60-90 minuten durende hyperthermiebehandeling. We vergeleken de MRT-prestaties van Looping Star met DE-GRE in een fantoom en bij

vrijwilligers, en ontdekten dat de nauwkeurigheid bij gebruik van Looping Star aanzienlijk verbeterde: tot 74% in het fantoom en tot 64% bij vrijwilligers. Hoewel de gemeten niveaus van de geluidsdruk niet consistent werden verminderd met de parameters die in deze studie werden gebruikt, meldden de deelnemers dat het akoestische geluid van Looping Star aangenamer was dan dat van DE-GRE. Dus hoewel verder onderzoek naar de optimale sequentieparameters nog vereist is, lijkt de sequentie veelbelovend als een nauwkeurige en comfortabelere benadering.

In **Hoofdstuk 5** hebben we de 3D-ME-FGRE sequentie, die in **Hoofdstuk 3** als best presterend werd geïdentificeerd, gebruikt om bij vrijwilligers een onderzoek uit te voeren naar MRT in het hoofd- en halsgebied. We toonden aan dat MRT mogelijk is in dit gebied en dat verschillende bronnen van beweging (met name ademhaling en slikken) geen significante invloed hebben op de kwaliteit van MRT. Bovendien toonden we aan dat het veranderen van de opnamemethode ofwel door versnelling, ofwel door een toename van het aantal beeldgemiddelden (NEX) de kwaliteit van de gemeten resultaten niet significant beïnvloedt. De MRT-prestaties verschillen echter aanzienlijk tussen de verschillende gebieden die we hebben geanalyseerd, waarbij gebieden die minder worden beïnvloed door beweging tussen scans beter presteren. De nekspier had de beste MAE (=1,96°C) en SD (=0,82°C), gevolgd door het ruggenmerg (MAE=3,17°C, SD=0,92°C) en de masseter-spier (MAE=4,53°C, SD=1,16°C). Wat betreft de ME presteerde het ruggenmerg het beste, gevolgd door de nekspier en vervolgens de masseter-spier, met waarden van respectievelijk -0,64°C, 1,15°C en -3,05°C. Aangezien in geen van de gebieden onze minimumeisen voor succesvolle MRT zoals gedefinieerd in Hoofdstuk 2 werden bereikt, is meer werk nodig om de MRT-prestaties te verbeteren. De meest logische volgende stap is om het experiment met gebruik van de MRcollar te herhalen zodra deze goedgekeurd is voor in-vivo gebuik, omdat de beweging van vrijwilligers tussen scans sterk wordt beperkt door de waterbolus, wat mogelijk al voldoende verbetering van de MRT-kwaliteit biedt. Indien nodig, kunnen aanvullende correctie- of verwervingsstrategieën, zoals filtertechnieken, worden overwogen.

Dit proefschrift presenteert een definitie van minimale prestatiekenmerken voor succesvolle MRT; de identificatie van 3D-ME-FGRE als een levensvatbare en veelbelovende sequentie voor MRT; de identificatie van Looping Star als een alternatieve, prettigere sequentie voor MRT; en een demonstratie dat 3D-ME-FGRE gebruikt in hoofd- en halsgebied ongevoelig is voor bewegingsartefacten. Dit werk is daarom een belangrijke stap richting klinische toepassing van MRT-geleide hyperthermie voor patiënten met kanker in het hoofd-hals gebied. Op basis van de hier gepresenteerde resultaten is het mogelijk om nieuwe onderzoeksstrategieën te

ontwerpen om MRT verder te ontwikkelen naar een klinische standaardmethode die real-time, niet-invasieve, driedimensionale temperatuurmonitoring mogelijk maakt tijdens behandeling met hyperthermie.

Zusammenfassung

Hyperthermie ist eine Behandlungsmethode zur Therapie bei Tumorerkrankungen. Dabei wird gezielt der Bereich des veränderten Gewebes auf 39-43°C erhitzt. Die Temperaturveränderung des Gewebes während der Behandlung kann mit Sensoren gemessen werden, die interluminal oder invasiv platziert werden müssen. Die einzige nicht invasive Methode, die Temperaturverteilung in 3D in tiefsitzenden Geweben darzustellen, ist die Magnetresonanz Thermometrie (MRTh). Dabei werden Temperaturänderung im Magnetresonanztomographen sichtbar gemacht. Um konventionelle Sensoren ersetzen zu können, muss MRTh jedoch klinisch zuverlässig angewandt werden können.

Klinische Anwendungen von MRTh in der Hyperthermie beschränken sich momentan entweder auf anatomische Regionen in denen keine Bewegung die Darstellung beeinflusst, oder als Ergänzung von invasiven Sonden. Temperaturänderung in Gewebe mit viel Bewegung im MRTh darzustellen ist schwierig, so kann z.B. die Atmung zu großen Fehldarstellungen führen. Eine Möglichkeit die Darstellung der MRTh Aufnahmen zu verbessern, ist die MR-Empfangsspulen so nah wie möglich an dem zu behandelndem Gewebe zu platzieren, was in diesem Fall in dem Hyperthermieapplikator selbst ist.

Deswegen haben wir mit der Entwicklung eines Applikators für den Kopf- und Halsbereich mit integrierten MR-Empfangsspulen begonnen: dem MRcollar. Damit kann das Gewebe gezielt erhitzt und gleichzeitig die MRTh Bildgebung verbessert werden. Da der MRcollar der erste Applikator seiner Art ist, gibt es keine Erfahrung mit MRT im Kopf- und Halsbereich. Somit haben wir in dieser Arbeit MRTh für die schwierigen Anatomie im Kopf- und Halsbereich entwickelt und verbessert.

Kapitel 2 handelt von unser systematischen Literaturrecherche, die gezeigt hat, dass es einen Mangel an Standardisierung und Berichterstattung über die Leistungsfähigkeit von MRTh während der Hyperthermie-Behandlung gibt, was den Vergleich von Ergebnissen erschwert. Daraufhin haben wir Mindestleistungsschwellen für erfolgreiche MRTh bei Hyperthermie-Behandlungen definiert: ≤1°C für den mittleren absolute Fehler (MAE), ≤|0,5°C| für den mittleren Fehler (ME) und ≤0,5°C für die räumliche und zeitliche Temperaturstandardabweichung (SD). 67% der klinischen Studien erfüllten die von uns definierten Mindestanforderungen. Häufige Probleme, die die Umsetzung behindern, waren Bewegung, sowie B0-Scanner-Drift, insbesondere in anspruchsvollen anatomischen Regionen. Außerdem haben wir präklinische Ergebnisse überprüft, um zu identifizieren, wo das größte Potenzial zur Verbesserung dieser Probleme liegt. Diese umfassten neuartige Rekonstruktionsmethoden zur Beschleunigung der Bildgebung, Bildgebung

unter Atemanhalten, die Verwendung von Navigator-Echos sowie Korrektur- und Stabilisierungsstrategien.

MRTh wurde zwischen 1990 und 2000 mit Technologien der damaligen Zeit entwickelt, und ist seitdem trotz technologischen Fortschritts weitgehend unverändert geblieben. MRTh besteht normalerweise aus einer Doppel-Echo-Gradienten-Echo (DE-GRE)-Sequenz mit einfacher Phasen-Subtraktion. Zur Korrektur des B0-Scanner-Drifts werden meistens externer Fettreferenzen verwendet. So haben wir viel Verbesserungspotential durch bereits verfügbaren MR-Sequenzen wie Multi-Echo und 3D-Multi-Echo-Gradient-Sequenzen vermutet, sowie auch durch Nachverarbeitungsmethoden wie Bildregistrierung und einem Multi-Peak-Fitting-Tool. Im **Kapitel 3** haben wir die MRTh-Performance verschiedener Multi-Echo-Gradienten-Echo-Sequenzen im Phantom und Freiwilligen verglichen. 3D-ME-FGRE war die vielversprechendste Sequenz. In den Freiwilligen haben wir das Gehirn gescannt, eine ideale anatomische Region für Tests, da es weit von Bewegungen entfernt und (bezogen auf die MRTh) ziemlich homogen ist. Im Vergleich zur klinischen Standardsequenz (DE-GRE) zeigte 3D-ME-FGRE die größte Verbesserung in der MAE: bis zu 62% bei Freiwilligen und 46% im Phantom (Temperatur 37°C-43°C). Darüber hinaus haben wir eine Nachverarbeitungsmethode entwickelt; diese umfasst rigide Bildregistrierung zur Korrektur der inter-scan Bewegung; ein Multi-Peak-Fitting-Tool, das die Berechnung der Parameter verbessert indem es alle verfügbaren Echos verwendet; und die speziell für diese Studie entwickelte automatische Körperfettselektion, die externe Fettreferenzen für die B0-Scanner-Drift Korrektur überflüssig macht.

Um auch neue technologische Entwicklungen zu nutzen, wie z.B. leise MRI-Sequenzen, haben wir im **Kapitel 4** eine neue 3D-Radial-GRE-Sequenz namens Looping Star getestet. Ein niedrigerer Geräuschpegel während der 60-90-minütigen Hyperthermie-Behandlung wäre für Patienten und Personal deutlich komfortabler als traditionelle Sequenzen. Wir verglichen die MRTh-Performance von Looping Star mit DE-GRE in einem Phantom und bei Freiwilligen und stellten fest, dass der MAE signifikant besser ist: bis zu 74% im Phantom und bis zu 64% bei Freiwilligen. Obwohl der Schalldruckpegel mit diesen Parametern nicht immer reduziert wurde, berichteten die Teilnehmer, dass das Geräusch von Looping Star im Vergleich zu DE-GRE angenehmer war. Die Sequenz scheint daher vielversprechend als genaue und angenehmere Methode im Vergleich zu DE-GRE, jedoch ist die Ermittlung nach den optimalen Sequenzparameter noch erforderlich.

Im **Kapitel 5** haben wir die 3D-ME-FGRE-Sequenz verwendet, die in **Kapitel 3** am besten abgeschnitten hat, und MRTh im Kopf- und Halsbereich bei Freiwilligen untersucht. Wir haben gezeigt, dass MRTh in dieser anatomischen Region möglich ist und dass Atmen und Schlucken keinen signifikanten Einfluss auf die Qualität haben. Außerdem haben wir gezeigt, dass das Beschleunigen, sowie die Erhöhung der Anzahl der Bilder (NEX), MRTh nicht signifikant beeinflusst. Die MRTh-Performance unterscheidet sich jedoch stark zwischen den von uns analysierten Bereichen, wobei Regionen, die weniger von inter-scan Bewegung betroffen sind, besser abschneiden. Der Nackenmuskel hatte den besten MAE (=1,96°C) und SD (=0,82°C), gefolgt vom Rückenmark (MAE=3,17°C, SD=0,92°C) und dem Massetermuskel (MAE=4,53°C, SD=1,16°C). In Bezug auf den ME schnitt das Rückenmark am besten ab, gefolgt vom Nackenmuskel und dem Massetermuskel, mit Werten von -0,64°C, 1,15°C bzw. -3,05°C. Da keine der Regionen unsere Mindestanforderungen für erfolgreiche MRTh aus **Kapitel 2** erfüllen konnte, ist mehr Forschung erforderlich. Ein wichtiger nächster Schritt ist die Wiederholung des Experiments im Behandlungs-Setup mit dem MRcollar, da die inter-scan Bewegung von Freiwilligen durch den Wasserbolus stark eingeschränkt werden wird. Diese Einschränkung könnte bereits eine ausreichende Verbesserung der MRTh-Qualität liefern. Wenn nötig, können zusätzliche Korrektur- oder Erfassungsstrategien, wie z.B. Filtertechniken, in Betracht gezogen werden.

In dieser Arbeit definieren wir die minimalen Anforderung für erfolgreiche MRTh; identifizieren 3D-ME-FGRE als praktikable und vielversprechende Sequenz für MRTh; identifizieren Looping Star als eine alternative, angenehmere MRTh-Sequenz; und zeigen, dass die in Kopf- und Halsbereich verwendete 3D-ME-FGRE unempfindlich gegenüber Bewegungsartefakten ist. Diese Arbeit ist somit eine wichtige Stufe zur klinischen Anwendung von MRTh-gesteuerten Hyperthermie bei Patienten mit Kopf- und Halskrebs. Aufgrund unserer Ergebnisse ist es möglich, neue Forschungsstrategien hervorzubringen, um MRTh zu einer klinischen Standardmethode für die Temperaturmessung während Hyperthermiebehandlungen zu entwickeln.

List of Abbreviations

3D	Three dimensional
CT	Computerised tomography
DE-GRE	Double echo gradient recalled echo
FOV	Field of view
GRE	Gradient recalled echo
MAE	Mean absolute error
ME	Mean error
ME-FGRE	Multi echo fast gradient recalled echo
MR-HIFU	MR-high intensity focused ultrasound
MRI	Magnetic resonance imaging
MRT	Magnetic resonance thermometry
MSE	Mean squared error
NEX	Number of excitations
PRFS	Proton resonance frequency shift
RF	Radiofrequency
RMSE	Root mean squared error
ROI	Region of interest
SD	Standard deviation
SE	Spin echo
SNR	Signal to noise ratio
TE	Time to echo
TR	Time to repetition

References

1. Ferlay, J.E., M.; Lam, F.; Colombet, M.; Mery, L.; Piñeros, M.; Znaor, A.; Soerjomataram, I.; Bray, F. *Global Cancer Observatory: Cancer Today*. 2020 December 2020 [cited 2022 18 October 2022]; Available from: https://gco.iarc.fr/today.
2. Sung, H., et al., *Global Cancer Statistics 2020: GLOBOCAN Estimates of Incidence and Mortality Worldwide for 36 Cancers in 185 Countries.* CA Cancer J Clin, 2021. **71**(3): p. 209-249.
3. Miller, K.D., et al., *Cancer treatment and survivorship statistics, 2022.* CA Cancer J Clin, 2022. **72**(5): p. 409-436.
4. Finck, A., S.I. Gill, and C.H. June, *Cancer immunotherapy comes of age and looks for maturity.* Nat Commun, 2020. **11**(1): p. 3325.
5. Zitvogel, L. and G. Kroemer, *Anticancer immunochemotherapy using adjuvants with direct cytotoxic effects.* J Clin Invest, 2009. **119**(8): p. 2127-30.
6. Seiwert, T.Y., J.K. Salama, and E.E. Vokes, *The concurrent chemoradiation paradigm--general principles.* Nat Clin Pract Oncol, 2007. **4**(2): p. 86-100.
7. Patel, S.A. and A.J. Minn, *Combination Cancer Therapy with Immune Checkpoint Blockade: Mechanisms and Strategies.* Immunity, 2018. **48**(3): p. 417-433.
8. Gormley, M., et al., *Reviewing the epidemiology of head and neck cancer: definitions, trends and risk factors.* Br Dent J, 2022. **233**(9): p. 780-786.
9. Chow, L.Q.M., *Head and neck cancer.* New England Journal of Medicine, 2020. **382**(1): p. 60-72.
10. Bosetti, C., et al., *Global trends in oral and pharyngeal cancer incidence and mortality.* Int J Cancer, 2020. **147**(4): p. 1040-1049.
11. Corry, J., et al., *The 'QUAD SHOT'—a phase II study of palliative radiotherapy for incurable head and neck cancer.* Radiotherapy and oncology, 2005. **77**(2): p. 137-142.
12. Agarwal, P., R. Upadhyay, and A. Agarwal, *Radiotherapy complications and their possible management in the head and neck region.* Indian Journal of Dental Research, 2012. **23**(6): p. 843.
13. Supportive, P.D.Q. and P.C.E. Board. *Oral Complications of Chemotherapy and Head/Neck Radiation (PDQ®): Health Professional Version*. PDQ Cancer Information Summaries 2002 21/10/2022 [cited 2023 21/04/2023]; Available from: https://www.cancer.gov/about-cancer/treatment/side-effects/mouth-throat/oral-complications-hp-pdq
14. Oksuz, D.C., et al., *Recurrence patterns of locally advanced head and neck squamous cell carcinoma after 3D conformal (chemo)-radiotherapy.* Radiat Oncol, 2011. **6**(1): p. 54.
15. Ang, K.K., et al., *Randomized phase III trial of concurrent accelerated radiation plus cisplatin with or without cetuximab for stage III to IV head and neck carcinoma: RTOG 0522.* Journal of clinical oncology, 2014. **32**(27): p. 2940.
16. Forastiere, A.A., et al., *Long-term results of RTOG 91-11: a comparison of three nonsurgical treatment strategies to preserve the larynx in patients with locally advanced larynx cancer.* J Clin Oncol, 2013. **31**(7): p. 845-52.
17. Beitler, J.J., et al., *Final results of local-regional control and late toxicity of RTOG 9003: a randomized trial of altered fractionation radiation for locally advanced head and neck cancer.* Int J Radiat Oncol Biol Phys, 2014. **89**(1): p. 13-20.
18. Morris, L.G., et al., *Second primary cancers after an index head and neck cancer: subsite-specific trends in the era of human papillomavirus-associated oropharyngeal cancer.* J Clin Oncol, 2011. **29**(6): p. 739-46.
19. Cramer, J.D., et al., *The changing therapeutic landscape of head and neck cancer.* Nat Rev Clin Oncol, 2019. **16**(11): p. 669-683.

20. Machiels, J.P., et al., *Zalutumumab plus best supportive care versus best supportive care alone in patients with recurrent or metastatic squamous-cell carcinoma of the head and neck after failure of platinum-based chemotherapy: an open-label, randomised phase 3 trial.* Lancet Oncol, 2011. **12**(4): p. 333-43.
21. Forastiere, A.A., et al., *Randomized comparison of cisplatin plus fluorouracil and carboplatin plus fluorouracil versus methotrexate in advanced squamous-cell carcinoma of the head and neck: a Southwest Oncology Group study.* J Clin Oncol, 1992. **10**(8): p. 1245-51.
22. Gibson, M.K., et al., *Randomized phase III evaluation of cisplatin plus fluorouracil versus cisplatin plus paclitaxel in advanced head and neck cancer (E1395): an intergroup trial of the Eastern Cooperative Oncology Group.* J Clin Oncol, 2005. **23**(15): p. 3562-7.
23. Cohen, E.E.W., et al., *Pembrolizumab versus methotrexate, docetaxel, or cetuximab for recurrent or metastatic head-and-neck squamous cell carcinoma (KEYNOTE-040): a randomised, open-label, phase 3 study.* Lancet, 2019. **393**(10167): p. 156-167.
24. Vermorken, J.B., et al., *Open-label, uncontrolled, multicenter phase II study to evaluate the efficacy and toxicity of cetuximab as a single agent in patients with recurrent and/or metastatic squamous cell carcinoma of the.* Journal of clinical oncology, 2007. **25**(16): p. 2171-2177.
25. Datta, N.R., et al., *Hyperthermia and radiotherapy in the management of head and neck cancers: A systematic review and meta-analysis.* Int J Hyperthermia, 2016. **32**(1): p. 31-40.
26. Repasky, E.A., S.S. Evans, and M.W. Dewhirst, *Temperature matters! And why it should matter to tumor immunologists.* Cancer immunology research, 2013. **1**(4): p. 210-216.
27. van den Tempel, N., M.R. Horsman, and R. Kanaar, *Improving efficacy of hyperthermia in oncology by exploiting biological mechanisms.* Int J Hyperthermia, 2016. **32**(4): p. 446-54.
28. Yang, X., et al., *Hyperthermia combined with immune checkpoint inhibitor therapy in the treatment of primary and metastatic tumors.* Front Immunol, 2022. **13**: p. 969447.
29. Overgaard, J., et al., *Randomised trial of hyperthermia as adjuvant to radiotherapy for recurrent or metastatic malignant melanoma.* The Lancet, 1995. **345**(8949): p. 540-543.
30. Peeken, J.C., P. Vaupel, and S.E. Combs, *Integrating hyperthermia into modern radiation oncology: what evidence is necessary?* Frontiers in oncology, 2017. **7**: p. 132.
31. Kok, H.P., et al., *Heating technology for malignant tumors: a review.* Int J Hyperthermia, 2020. **37**(1): p. 711-741.
32. Kroesen, M., et al., *Confirmation of thermal dose as a predictor of local control in cervical carcinoma patients treated with state-of-the-art radiation therapy and hyperthermia.* Radiother Oncol, 2019. **140**: p. 150-158.
33. Wust, P., et al., *Thermal monitoring: invasive, minimal-invasive and non-invasive approaches.* Int J Hyperthermia, 2006. **22**(3): p. 255-62.
34. van der Zee, J., et al., *Practical limitations of interstitial thermometry during deep hyperthermia.* Int J Radiat Oncol Biol Phys, 1998. **40**(5): p. 1205-12.
35. Sneed, P.K., et al., *Should interstitial thermometry be used for deep hyperthermia?* Int J Radiat Oncol Biol Phys, 1998. **40**: p. 1015–17.
36. van Rhoon, G.C. and P. Wust, *Introduction: non-invasive thermometry for thermotherapy.* Int J Hyperthermia, 2005. **21**(6): p. 489-95.
37. Gellermann, J., et al., *Methods and potentials of magnetic resonance imaging for monitoring radiofrequency hyperthermia in a hybrid system.* Int J Hyperthermia, 2005. **21**(6): p. 497-513.
38. Gellermann, J., et al., *Image artifacts during MRT hybrid hyperthermia--causes and elimination.* Int J Hyperthermia, 2008. **24**(4): p. 327-35.

39. Adibzadeh, F., et al., *Systematic review of pre-clinical and clinical devices for magnetic resonance-guided radiofrequency hyperthermia.* Int J Hyperthermia, 2020. **37**(1): p. 15-27.
40. Paulides, M.M., et al., *Winner of the "New Investigator Award" at the European Society of Hyperthermia Oncology Meeting 2007. The HYPERcollar: a novel applicator for hyperthermia in the head and neck.* Int J Hyperthermia, 2007. **23**(7): p. 567-76.
41. Verduijn, G.M., et al., *Deep hyperthermia with the HYPERcollar system combined with irradiation for advanced head and neck carcinoma - a feasibility study.* Int J Hyperthermia, 2018. **34**(7): p. 994-1001.
42. Salim, G., et al. *Multipeak multiecho modeling for improved PRF-based thermometry*. in *32nd Annual Scientific Meeting of the ESMRMB*. 2015. Edinburgh, UK.
43. Kroesen, M., et al., *Feasibility, SAR distribution, and clinical outcome upon reirradiation and deep hyperthermia using the hypercollar3D in head and neck cancer patients.* Cancers, 2021. **13**(23): p. 6149.
44. Drizdal, T., et al., *Simulation guided design of the MRcollar: a MR compatible applicator for deep heating in the head and neck region.* Int J Hyperthermia, 2021. **38**(1): p. 382-392.
45. Sumser, K., et al., *Experimental Validation of the MRcollar: An MR Compatible Applicator for Deep Heating in the Head and Neck Region.* Cancers (Basel), 2021. **13**(22): p. 5617.
46. VilasBoas-Ribeiro, I., et al., *MR Thermometry Accuracy and Prospective Imaging-Based Patient Selection in MR-Guided Hyperthermia Treatment for Locally Advanced Cervical Cancer.* Cancers (Basel), 2021. **13**(14): p. 3503.
47. Rieke, V. and K. Butts Pauly, *MR thermometry.* J Magn Reson Imaging, 2008. **27**(2): p. 376-90.
48. Ludemann, L., et al., *Non-invasive magnetic resonance thermography during regional hyperthermia.* Int J Hyperthermia, 2010. **26**(3): p. 273-82.
49. Winter, L., et al., *Magnetic resonance thermometry: Methodology, pitfalls and practical solutions.* Int J Hyperthermia, 2016. **32**(1): p. 63-75.
50. Hindman, J.C., *Proton resonance shift of water in the gas and liquid states.* The Journal of Chemical Physics, 1966. **44**(12): p. 4582-4592.
51. Quesson, B., J.A. de Zwart, and C.T. Moonen, *Magnetic resonance temperature imaging for guidance of thermotherapy.* J Magn Reson Imaging, 2000. **12**(4): p. 525-33.
52. Wlodarczyk, W., et al., *Comparison of four magnetic resonance methods for mapping small temperature changes.* Phys Med Biol, 1999. **44**(2): p. 607-24.
53. Ishihara, Y., et al., *A precise and fast temperature mapping using water proton chemical shift.* Magn Reson Med, 1995. **34**(6): p. 814-23.
54. Elster, A.D., *Gradient-echo MR imaging: techniques and acronyms.* Radiology, 1993. **186**(1): p. 1-8.
55. Outwater, E.K., et al., *Detection of lipid in abdominal tissues with opposed-phase gradient-echo images at 1.5 T: techniques and diagnostic importance.* Radiographics, 1998. **18**(6): p. 1465-1480.
56. Markl, M. and J. Leupold, *Gradient echo imaging.* J Magn Reson Imaging, 2012. **35**(6): p. 1274-89.
57. Cline, H.E., et al., *Simultaneous magnetic resonance phase and magnitude temperature maps in muscle.* Magn Reson Med, 1996. **35**(3): p. 309-15.
58. Bley, T.A., et al., *Fat and water magnetic resonance imaging.* J Magn Reson Imaging, 2010. **31**(1): p. 4-18.

59. Slipsager, J.M., et al., *Quantifying the Financial Savings of Motion Correction in Brain MRI: A Model-Based Estimate of the Costs Arising From Patient Head Motion and Potential Savings From Implementation of Motion Correction.* J Magn Reson Imaging, 2020. **52**(3): p. 731-738.
60. Salomir, R., B.D. De Senneville, and C.T.W. Moonen, *A fast calculation method for magnetic field inhomogeneity due to an arbitrary distribution of bulk susceptibility.* Concepts in Magnetic Resonance Part B: Magnetic Resonance Engineering: An Educational Journal, 2003. **19**(1): p. 26-34.
61. Kuroda, K., et al., *Temperature mapping using the water proton chemical shift: self-referenced method with echo-planar spectroscopic imaging.* Magnetic Resonance in Medicine: An Official Journal of the International Society for Magnetic Resonance in Medicine, 2000. **43**(2): p. 220-225.
62. Walter, E.J. and M. Carraretto, *The neurological and cognitive consequences of hyperthermia.* Crit Care, 2016. **20**(1): p. 199.
63. Craciunescu, O.I., et al., *Accuracy of real time noninvasive temperature measurements using magnetic resonance thermal imaging in patients treated for high grade extremity soft tissue sarcomas.* Med Phys, 2009. **36**(11): p. 4848-58.
64. Gellermann, J., et al., *Noninvasive magnetic resonance thermography of soft tissue sarcomas during regional hyperthermia: correlation with response and direct thermometry.* Cancer, 2006. **107**(6): p. 1373-82.
65. Parker, D.L., *Applications of NMR imaging in hyperthermia: an evaluation of the potential for localized tissue heating and noninvasive temperature monitoring.* IEEE Trans Biomed Eng, 1984. **31**(1): p. 161-7.
66. Baron, P., et al., *T1 and T2 temperature dependence of female human breast adipose tissue at 1.5 T: groundwork for monitoring thermal therapies in the breast.* NMR Biomed, 2015. **28**(11): p. 1463-70.
67. Zhang, L., et al., *A variable flip angle golden-angle-ordered 3D stack-of-radial MRI technique for simultaneous proton resonant frequency shift and T(1) -based thermometry.* Magn Reson Med, 2019. **82**(6): p. 2062-2076.
68. Todd, N., et al., *In vivo evaluation of multi-echo hybrid PRF/T1 approach for temperature monitoring during breast MR-guided focused ultrasound surgery treatments.* Magn Reson Med, 2014. **72**(3): p. 793-9.
69. Datta, N.R., et al., *Integrating Loco-Regional Hyperthermia Into the Current Oncology Practice: SWOT and TOWS Analyses.* Front Oncol, 2020. **10**: p. 819.
70. Issels, R., et al., *Hallmarks of hyperthermia in driving the future of clinical hyperthermia as targeted therapy: translation into clinical application.* Int J Hyperthermia, 2016. **32**(1): p. 89-95.
71. Datta, N.R., et al., *Local hyperthermia combined with radiotherapy and-/or chemotherapy: recent advances and promises for the future.* Cancer Treat Rev, 2015. **41**(9): p. 742-53.
72. Wust, P., et al., *Hyperthermia in combined treatment of cancer.* Lancet Oncol, 2002. **3**(8): p. 487-97.
73. van der Zee, J., et al., *Comparison of radiotherapy alone with radiotherapy plus hyperthermia in locally advanced pelvic tumours: a prospective, randomised, multicentre trial. Dutch Deep Hyperthermia Group.* Lancet, 2000. **355**(9210): p. 1119-25.
74. Issels, R.D., *Hyperthermia adds to chemotherapy.* Eur J Cancer, 2008. **44**(17): p. 2546-54.
75. Jones, E.L., et al., *Randomized trial of hyperthermia and radiation for superficial tumors.* J Clin Oncol, 2005. **23**(13): p. 3079-85.

76. Franckena, M., et al., *Hyperthermia dose-effect relationship in 420 patients with cervical cancer treated with combined radiotherapy and hyperthermia.* Eur J Cancer, 2009. **45**(11): p. 1969-78.
77. Fotopoulou, C., et al., *Regional abdominal hyperthermia combined with systemic chemotherapy for the treatment of patients with ovarian cancer relapse: Results of a pilot study.* Int J Hyperthermia, 2010. **26**(2): p. 118-26.
78. Rau, B., et al., *Preoperative radio-chemotherapy in locally advanced recurrent rectal cancer: regional radiofrequency hyperthermia correlates with clinical parameters.* Int J Radiat Oncol Biol Phys 2000. **48**: p. 381–91.
79. Kapp, D.S. and R.S. Cox, *Thermal treatment parameters are most predictive of outcome in patients with single tumor nodules per treatment field in recurrent adenocarcinoma of the breast.* Int J Radiat Oncol Biol Phys, 1995. **33**: p. 887–99.
80. Oleson, J.R., et al., *Sensitivity of hyperthermia trial outcomes to temperature and time: implications for thermal goals of treatment.* Int J Radiat Oncol Biol Phys, 1993. **25**(2): p. 289-97.
81. Unsoeld, M., et al., *MR Thermometry Data Correlate with Pathological Response for Soft Tissue Sarcoma of the Lower Extremity in a Single Center Analysis of Prospectively Registered Patients.* Cancers (Basel), 2020. **12**(4).
82. Sherar, M., et al., *Relationship between thermal dose and outcome in thermoradiotherapy treatments for superficial recurrences of breast cancer: data from a phase III trial.* Int J Radiat Oncol Biol Phys 1997. **39**: p. 371–80.
83. Canters, R.A., et al., *Implementation of treatment planning in the routine clinical procedure of regional hyperthermia treatment of cervical cancer: an overview and the Rotterdam experience.* Int J Hyperthermia, 2012. **28**(6): p. 570-81.
84. Kok, H.P., et al., *Current state of the art of regional hyperthermia treatment planning: a review.* Radiat Oncol, 2015. **10**(1): p. 196.
85. Walther, B.A.M., J.L., *The concepts of bias, precision and accuracy, and their use in testing the performance of species richness estimators, with a literature review of estimator performance.* Ecography, 2005. **28**: p. 815-829.
86. Curto, S., et al., *Quantitative, Multi-institutional Evaluation of MR Thermometry Accuracy for Deep-Pelvic MR-Hyperthermia Systems Operating in Multi-vendor MR-systems Using a New Anthropomorphic Phantom.* Cancers (Basel), 2019. **11**(11).
87. Bramer, W.M., J. Milic, and F. Mast, *Reviewing retrieved references for inclusion in systematic reviews using EndNote.* J Med Libr Assoc, 2017. **105**(1): p. 84-87.
88. Peller, M., et al., *T1 relaxation time at 0.2 Tesla for monitoring regional hyperthermia: feasibility study in muscle and adipose tissue.* Magn Reson Med, 2002. **47**(6): p. 1194-201.
89. Yuan, J., et al., *Towards fast and accurate temperature mapping with proton resonance frequency-based MR thermometry.* Quant Imaging Med Surg, 2012. **2**(1): p. 21-32.
90. Stauffer, P., et al., *Clinical Utility of Magnetic Resonance Thermal Imaging (MRTI) For Realtime Guidance of Deep Hyperthermia.* Proc SPIE Int Soc Opt Eng, 2009. **7181**: p. 71810I.
91. Dadakova, T., et al., *Fast PRF-based MR thermometry using double-echo EPI: in vivo comparison in a clinical hyperthermia setting.* MAGMA, 2015. **28**(4): p. 305-14.
92. Craciunescu, O.I., et al., *3D numerical reconstruction of the hyperthermia induced temperature distribution in human sarcomas using DE-MRI measured tissue perfusion: validation against non-invasive MR temperature measurements.* Int J Hyperthermia, 2001. **17**(3): p. 221-39.
93. Wu, M., et al., *Correction of motion-induced susceptibility artifacts and B(0) drift during proton resonance frequency shift-based MR thermometry in the pelvis with background field removal methods.* Magn Reson Med, 2020. **84**(5): p. 2495-2511.

94. Carter, D.L., et al., *Magnetic resonance thermometry during hyperthermia for human high-grade sarcoma.* Int J Radiat Oncol Biol Phys, 1998. **40**(4): p. 815-22.
95. Gellermann, J., et al., *Noninvasive magnetic resonance thermography of recurrent rectal carcinoma in a 1.5 Tesla hybrid system.* Cancer Res, 2005. **65**(13): p. 5872-80.
96. Ferrer, C.J., et al., *Field drift correction of proton resonance frequency shift temperature mapping with multichannel fast alternating nonselective free induction decay readouts.* Magn Reson Med, 2020. **83**(3): p. 962-973.
97. Bing, C., et al., *Breath-hold MR-HIFU hyperthermia: phantom and in vivo feasibility.* Int J Hyperthermia, 2019. **36**(1): p. 1084-1097.
98. Odeen, H. and D.L. Parker, *Magnetic resonance thermometry and its biological applications - Physical principles and practical considerations.* Prog Nucl Magn Reson Spectrosc, 2019. **110**: p. 34-61.
99. Tan, J., et al., *Motion compensation using principal component analysis and projection onto dipole fields for abdominal magnetic resonance thermometry.* Magn Reson Med, 2019. **81**(1): p. 195-207.
100. Wu, M., et al., *A phase-cycled temperature-sensitive fast spin echo sequence with conductivity bias correction for monitoring of mild RF hyperthermia with PRFS.* MAGMA, 2019. **32**(3): p. 369-380.
101. Zhu, L., et al., *Feasibility and safety assessment of magnetic resonance-guided high-intensity focused ultrasound (MRgHIFU)-mediated mild hyperthermia in pelvic targets evaluated using an in vivo porcine model.* Int J Hyperthermia, 2019. **36**(1): p. 1147-1159.
102. Jonathan, S.V. and W.A. Grissom, *Volumetric MRI thermometry using a three-dimensional stack-of-stars echo-planar imaging pulse sequence.* Magn Reson Med, 2018. **79**(4): p. 2003-2013.
103. S, V.V.N.K., et al., *Evaluation and selection of anatomic sites for magnetic resonance imaging-guided mild hyperthermia therapy: a healthy volunteer study.* Int J Hyperthermia, 2018. **34**(8): p. 1381-1389.
104. Chu, W., et al., *Magnetic Resonance-Guided High-Intensity Focused Ultrasound Hyperthermia for Recurrent Rectal Cancer: MR Thermometry Evaluation and Preclinical Validation.* Int J Radiat Oncol Biol Phys, 2016. **95**(4): p. 1259-67.
105. Svedin, B.T., A. Payne, and D.L. Parker, *Respiration artifact correction in three-dimensional proton resonance frequency MR thermometry using phase navigators.* Magn Reson Med, 2016. **76**(1): p. 206-13.
106. Tillander, M., et al., *High intensity focused ultrasound induced in vivo large volume hyperthermia under 3D MRI temperature control.* Med Phys, 2016. **43**(3): p. 1539-49.
107. Boulant, N., et al., *FID navigator-based MR thermometry method to monitor small temperature changes in the brain of ventilated animals.* NMR Biomed, 2015. **28**(1): p. 101-7.
108. Denis de Senneville, B., A. El Hamidi, and C. Moonen, *A direct PCA-based approach for real-time description of physiological organ deformations.* IEEE Trans Med Imaging, 2015. **34**(4): p. 974-82.
109. Gaur, P. and W.A. Grissom, *Accelerated MRI thermometry by direct estimation of temperature from undersampled k-space data.* Magn Reson Med, 2015. **73**(5): p. 1914-25.
110. Marx, M., J. Plata, and K.B. Pauly, *Toward volumetric MR thermometry with the MASTER sequence.* IEEE Trans Med Imaging, 2015. **34**(1): p. 148-55.
111. Mei, C.S., et al., *Accurate field mapping in the presence of B0 inhomogeneities, applied to MR thermometry.* Magn Reson Med, 2015. **73**(6): p. 2142-51.

112. Pichardo, S., et al., *In vivo optimisation study for multi-baseline MR-based thermometry in the context of hyperthermia using MR-guided high intensity focused ultrasound for head and neck applications.* Int J Hyperthermia, 2014. **30**(8): p. 579-92.
113. Shi, C.Y., et al., *Referenceless PRFS MR Thermometry Using Partial Separability Model.* Appl. Magn. Reson., 2014. **45**(1): p. 93-108.
114. Minalga, E., et al., *An 11-channel radio frequency phased array coil for magnetic resonance guided high-intensity focused ultrasound of the breast.* Magn Reson Med, 2013. **69**(1): p. 295-302.
115. Ramsay, E., et al., *MR thermometry in the human prostate gland at 3.0T for transurethral ultrasound therapy.* J Magn Reson Imaging, 2013. **38**(6): p. 1564-71.
116. Kickhefel, A., et al., *Accuracy of real-time MR temperature mapping in the brain: a comparison of fast sequences.* Phys Med, 2010. **26**(4): p. 192-201.
117. Wyatt, C.R., B.J. Soher, and J.R. MacFall, *Correction of breathing-induced errors in magnetic resonance thermometry of hyperthermia using multiecho field fitting techniques.* Med Phys, 2010. **37**(12): p. 6300-9.
118. Roujol, S., et al., *Online real-time reconstruction of adaptive TSENSE with commodity CPU/GPU hardware.* Magn Reson Med, 2009. **62**(6): p. 1658-64.
119. Wyatt, C., et al., *Hyperthermia MRI temperature measurement: evaluation of measurement stabilisation strategies for extremity and breast tumours.* Int J Hyperthermia, 2009. **25**(6): p. 422-33.
120. Silcox, C.E., et al., *MRI-guided ultrasonic heating allows spatial control of exogenous luciferase in canine prostate.* Ultrasound Med Biol, 2005. **31**(7): p. 965-70.
121. Sun, L., et al., *Adaptive Real-Time Closed-Loop Temperature Control for Ultrasound Hyperthermia Using Magnetic Resonance Thermometry.* Concepts Magn Reson Part B Magn Reson Eng, 2005. **27B**(1): p. 51-63.
122. Il'yasov, K.A. and J. Hennig, *Single-shot diffusion-weighted RARE sequence: application for temperature monitoring during hyperthermia session.* J Magn Reson Imaging, 1998. **8**(6): p. 1296-305.
123. Corbett, R., A. Laptook, and P. Weatherall, *Noninvasive measurements of human brain temperature using volume-localized proton magnetic resonance spectroscopy.* J Cereb Blood Flow Metab, 1997. **17**(4): p. 363-9.
124. MacFall, J.R., et al., *1H MRI phase thermometry in vivo in canine brain, muscle, and tumor tissue.* Med Phys, 1996. **23**(10): p. 1775-82.
125. De Poorter, J., et al., *Noninvasive MRI thermometry with the proton resonance frequency (PRF) method: in vivo results in human muscle.* Magn Reson Med, 1995. **33**(1): p. 74-81.
126. MacFall, J., et al., *Temperature dependence of canine brain tissue diffusion coefficient measured in vivo with magnetic resonance echo-planar imaging.* Int J Hyperthermia, 1995. **11**(1): p. 73-86.
127. Young, I.R., et al., *Modeling and observation of temperature changes in vivo using MRI.* Magn Reson Med, 1994. **32**(3): p. 358-69.
128. Hall, A.S., et al., *Observation by MR imaging of in vivo temperature changes induced by radio frequency hyperthermia.* J Comput Assist Tomogr, 1990. **14**(3): p. 430-6.
129. Odeen, H. and D.L. Parker, *Improved MR thermometry for laser interstitial thermotherapy.* Lasers Surg Med, 2019. **51**(3): p. 286-300.
130. Kothapalli, S., et al., *A convenient, reliable, and fast acoustic pressure field measurement method for magnetic resonance-guided high-intensity focused ultrasound systems with phased array transducers.* J Ther Ultrasound, 2018. **6**(1): p. 5.

131. Paulides, M.M., et al., *Novel applicator design for MR guided RF hyperthermia in head and neck cancers: heating performance and RF coupling.* Paris(France): International Society for Magnetic Resonance in Medicine (ISMRM), 2018.
132. Nakagawa, Y., et al., *Image reconstruction method with compressed sensing for high-speed MR temperature measurement of abdominal organs().* Annu Int Conf IEEE Eng Med Biol Soc, 2019. **2019**: p. 2731-2735.
133. Bing, C., et al., *Drift correction for accurate PRF-shift MR thermometry during mild hyperthermia treatments with MR-HIFU.* Int J Hyperthermia, 2016. **32**(6): p. 673-87.
134. Feddersen, T.V., et al., *Clinical Performance and Future Potential of Magnetic Resonance Thermometry in Hyperthermia.* Cancers (Basel), 2020. **13**(1).
135. Le Ster, C., et al., *RF heating measurement using MR thermometry and field monitoring: Methodological considerations and first in vivo results.* Magn Reson Med, 2021. **85**(3): p. 1282-1293.
136. Le Ster, C., et al., *Measuring radiofrequency field-induced temperature variations in brain MRI exams with motion compensated MR thermometry and field monitoring.* Magn Reson Med, 2022. **87**(3): p. 1390-1400.
137. Poorman, M.E., et al., *Multi-echo MR thermometry using iterative separation of baseline water and fat images.* Magn Reson Med, 2019. **81**(4): p. 2385-2398.
138. Cheng, C., et al., *Dual-step iterative temperature estimation method for accurate and precise fat-referenced PRFS temperature imaging.* Magn Reson Med, 2019. **81**(2): p. 1322-1334.
139. Hofstetter, L.W., et al., *Fat-referenced MR thermometry in the breast and prostate using IDEAL.* J Magn Reson Imaging, 2012. **36**(3): p. 722-32.
140. Reeder, S.B., et al., *Iterative decomposition of water and fat with echo asymmetry and least-squares estimation (IDEAL): application with fast spin-echo imaging.* Magn Reson Med, 2005. **54**(3): p. 636-44.
141. Ikemoto, Y., et al., *Development of a human-tissue-like phantom for 3.0-T MRI.* Med Phys, 2011. **38**(11): p. 6336-42.
142. Bush, E.C., et al., *Fat-Water Phantoms for Magnetic Resonance Imaging Validation: A Flexible and Scalable Protocol.* J Vis Exp, 2018(139).
143. *Products & Services - An overview of Pyrexar's line of Hyperthermia Medical Devices for the Treatment of Cancer*. 2015-2023 [cited 2021 07-Dec]; Available from: https://www.pyrexar.com/hyperthermia/product-overview.
144. Uecker, M., et al., *ESPIRiT--an eigenvalue approach to autocalibrating parallel MRI: where SENSE meets GRAPPA.* Magn Reson Med, 2014. **71**(3): p. 990-1001.
145. Klein, S., et al., *elastix: a toolbox for intensity-based medical image registration.* IEEE Trans Med Imaging, 2010. **29**(1): p. 196-205.
146. Peters, R.D. and R.M. Henkelman, *Proton-resonance frequency shift MR thermometry is affected by changes in the electrical conductivity of tissue.* Magn Reson Med, 2000. **43**(1): p. 62-71.
147. Kuroda, K., et al., *Optimization of chemical shift selective suppression of fat.* Magn Reson Med, 1998. **40**(4): p. 505-10.
148. Glover, G.H., *Multipoint Dixon technique for water and fat proton and susceptibility imaging.* J Magn Reson Imaging, 1991. **1**(5): p. 521-30.
149. Dewhirst, M.W., et al., *RTOG quality assurance guidelines for clinical trials using hyperthermia.* Int J Radiat Oncol Biol Phys, 1990. **18**(5): p. 1249-59.
150. McJury, M.J., *Acoustic noise levels generated during high field MR imaging.* Clin Radiol, 1995. **50**(5): p. 331-4.

151. McJury PhD, M. and F.G. Shellock PhD, *Auditory noise associated with MR procedures: a review.* Journal of Magnetic Resonance Imaging, 2000. **12**(1): p. 37-45.
152. Quirk, M.E., et al., *Anxiety in patients undergoing MR imaging.* Radiology, 1989. **170**(2): p. 463-6.
153. Sartoretti, E., et al., *Impact of Acoustic Noise Reduction on Patient Experience in Routine Clinical Magnetic Resonance Imaging.* Acad Radiol, 2022. **29**(2): p. 269-276.
154. Amaro, E., Jr., et al., *Acoustic noise and functional magnetic resonance imaging: current strategies and future prospects.* J Magn Reson Imaging, 2002. **16**(5): p. 497-510.
155. Weiger, M., et al., *ZTE imaging in humans.* Magn Reson Med, 2013. **70**(2): p. 328-32.
156. Madio, D.P. and I.J. Lowe, *Ultra-fast imaging using low flip angles and FIDs.* Magn Reson Med, 1995. **34**(4): p. 525-9.
157. Ljungberg, E., et al., *Silent zero TE MR neuroimaging: Current state-of-the-art and future directions.* Prog Nucl Magn Reson Spectrosc, 2021. **123**: p. 73-93.
158. Wiesinger, F., A. Menini, and A.B. Solana, *Looping Star.* Magn Reson Med, 2019. **81**(1): p. 57-68.
159. Feddersen, T.V., et al., *Multi-echo gradient echo pulse sequences: which is best for PRFS MR thermometry guided hyperthermia?* Int J Hyperthermia, 2023. **40**(1): p. 2184399.
160. Mulder, H.T., et al., *Systematic quality assurance of the BSD2000-3D MR-compatible hyperthermia applicator performance using MR temperature imaging.* Int J Hyperthermia, 2018. **35**(1): p. 305-313.
161. VilasBoas-Ribeiro, I., et al., *POD-Kalman filtering for improving noninvasive 3D temperature monitoring in MR-guided hyperthermia.* Med Phys, 2022. **49**(8): p. 4955-4970.
162. Graessner, J., *Bandwidth in MRI.* Magnetom Flash, 2013. **2**: p. 3-8.
163. Pelc, N.J., *Optimization of flip angle for T1dependent contrast in MRI.* Magnetic resonance in medicine, 1993. **29**(5): p. 695-699.
164. Schieban, K., et al., *ZTE imaging with enhanced flip angle using modulated excitation.* Magn Reson Med, 2015. **74**(3): p. 684-93.
165. Froidevaux, R., M. Weiger, and K.P. Pruessmann, *Pulse encoding for ZTE imaging: RF excitation without dead-time penalty.* Magnetic Resonance in Medicine, 2022. **87**(3): p. 1360-1374.
166. Wu, Y., et al., *Density of organic matrix of native mineralized bone measured by water- and fat-suppressed proton projection MRI.* Magn Reson Med, 2003. **50**(1): p. 59-68.
167. Schache, A.G., et al., *HPV-Related Oropharynx Cancer in the United Kingdom: An Evolution in the Understanding of Disease EtiologyHPV OPSCC in the UK.* Cancer research, 2016. **76**(22): p. 6598-6606.
168. Ong, B.B., *INJURY, FATAL AND NONFATAL | Burns and Scalds*, in *Encyclopedia of Forensic and Legal Medicine*, J. Payne-James, Editor. 2005, Elsevier: Philadelphia, USA. p. 90-98.
169. Behrouzkia, Z., et al., *Hyperthermia: how can it be used?* Oman medical journal, 2016. **31**(2): p. 89.
170. Billard, B.E., K. Hynynen, and R.B. Roemer, *Effects of physical parameters on high temperature ultrasound hyperthermia.* Ultrasound Med Biol, 1990. **16**(4): p. 409-20.
171. Lechner-Greite, S.M., et al., *Proton Density and T1 weighted Zero TE MR Thermometry*, in *U.S. Patent No. 10,076,249*. 2018: Washington, DC: U.S. Patent and Trademark Office.
172. Paliwal, V., et al., *SSFP-based MR thermometry.* Magn Reson Med, 2004. **52**(4): p. 704-8.
173. Kern, A.L., et al., *Absolute thermometry using hyperpolarized 129Xe free-induction decay and spin-echo chemical-shift imaging in rats.* Magnetic Resonance in Medicine, 2023. **89**(1): p. 54-63.

174. Mei, C.S., et al., *Combining two-dimensional spatially selective RF excitation, parallel imaging, and UNFOLD for accelerated MR thermometry imaging.* Magn Reson Med, 2011. **66**(1): p. 112-22.
175. Leonard, P., R. Chopra, and A. Nachman, *Compressed sensing for accelerated MR thermometry in MRI-controlled transurethral ultrasound therapy.* Proc. 20th Sci. Meet. ISMRM, Melb. Melbourne, 2012. **2918**.
176. Fielden, S., et al., *Accelerating 3D spiral MR thermometry with Kalman filter.* Int. Soc. Magn. Reson. Med. Milan, 2014. **22**: p. 2346.
177. Nouwens, S.A.N., et al., *Integrated thermal and magnetic susceptibility modeling for air-motion artifact correction in proton resonance frequency shift thermometry.* Int J Hyperthermia, 2022. **39**(1): p. 967-976.
178. Boehm, C., et al., *Susceptibility artifact correction in MR thermometry for monitoring of mild radiofrequency hyperthermia using total field inversion.* Magn Reson Med, 2022. **88**(1): p. 120-132.
179. Wust, P., et al., *Teilkorperhyperthermie mit einem Radiofrequenz-Multiantennen-Applikator unter online Kontrolle in einem 1.5 T MR-Tomographen [Part-body hyperthermia with a radiofrequency multiantenna applicator under online control in a 1.5 T MR-tomograph].* Rofo, 2004. **176**(3): p. 363-74.
180. Marx, M., P. Ghanouni, and K. Butts Pauly, *Specialized volumetric thermometry for improved guidance of mr g fus in brain.* Magnetic resonance in medicine, 2017. **78**(2): p. 508-517.
181. Svedin, B.T., et al., *Multiecho pseudo-golden angle stack of stars thermometry with high spatial and temporal resolution using k-space weighted image contrast.* Magn Reson Med, 2018. **79**(3): p. 1407-1419.
182. Hendrikx, R.W.M., et al. *POD-based recursive temperature estimation for MR-guided RF hyperthermia cancer treatment: a pilot study*. in *2018 IEEE Conference on Decision and Control (CDC)*. 2018. IEEE.
183. Saha, N., et al., *Advanced Radio Frequency Applicators for Thermal Magnetic Resonance Theranostics of Brain Tumors.* Cancers (Basel), 2023. **15**(8): p. 2303.
184. Adibzadeh, F., M.M. Paulides, and G.C. van Rhoon, *SAR thresholds for electromagnetic exposure using functional thermal dose limits.* Int J Hyperthermia, 2018. **34**(8): p. 1248-1254.
185. Paulides, M.M., et al., *Recent technological advancements in radiofrequency- andmicrowave-mediated hyperthermia for enhancing drug delivery.* Adv Drug Deliv Rev, 2020. **163-164**: p. 3-18.
186. *Cijfers over wekedelentumoren*. February 2022 August 2023]; Available from: https://www.kanker.nl/kankersoorten/wekedelentumoren-wekedelensarcomen/algemeen/cijfers-over-wekedelentumoren.

List of Publications

Feddersen, T. V., Hernandez-Tamames, J. A., Franckena, M., van Rhoon, G. C., & Paulides, M. M. (2020). Clinical performance and future potential of magnetic resonance thermometry in hyperthermia. *Cancers*, *13*(1), 31.

Feddersen, T. V., Poot, D. H., Paulides, M. M., Salim, G., van Rhoon, G. C., & Hernandez-Tamames, J. A. (2023). Multi-echo gradient echo pulse sequences: which is best for PRFS MR thermometry guided hyperthermia?. *International Journal of Hyperthermia*, *40*(1), 2184399.

Feddersen, T. V., Poot, D. H., Solana A. B., Wiesinger F., Paulides, M. M., van Rhoon, G. C., & Hernandez-Tamames, J. A.. Towards quiet and more accurate PRFS MR Thermometry with Looping Star. *Cancers*. (submitted)

Feddersen, T. V., Hernandez-Tamames, J. A., Paulides, M. M., Kroesen M., & van Rhoon, G. C.. Magnetic resonance thermometry for hyperthermia in the oropharynx region. *International Journal of Hyperthermia*. (submitted)

VilasBoas-Ribeiro, I., Sumser, K., Nouwens, S., Feddersen, T.V., Heemels, W.P.M.H., van Rhoon, G.C., & Paulides, M. M., Adapting temperature predictions to MR imaging in treatment position to improve simulation-guided hyperthermia for cervical cancer. *IEEE Open Journal of Engineering in Medicine and Biology,* doi: 10.1109/OJEMB.2023.3321990.

PhD portfolio

Name of PhD student	Theresa V. Feddersen
Erasmus MC departments	Radiotherapy Radiology & Nuclear Medicine
Promotors	Prof. dr. Gerard C. van Rhoon Prof. dr. Juan A. Hernandez Tamames Prof. dr. ir. Margarethus M. Paulides
Co-promotor	Dr. ir. Dirk H.J. Poot

Description	Organizer	EC
Hyperthermia Symposium (2018)	Amsterdam UMC	0.50
Course - Basic Life Support (BLS) (2018)	European Resuscitation Council (ERC)	0.20
Course - MRI safety (2018)	Erasmus MC	0.20
Course - Advanced MR for physicists 1 (2019)	Utrecht University	5.00
Course - Scientific Integrity (2019)	Erasmus MC Graduate School	0.30
23rd MolMed day 2019 (2019)	Molecular Medicine Post Graduate School	0.20
Course - Advanced MR for physicists 2 (2019)	Utrecht University	5.00
Course - CPO-course: Patient Oriented Research (2019)	Erasmus MC	0.30
Course - BROK® (Basic course Rules and Organisation for Clinical researchers) (2019)	Erasmus MC	1.50
Radiotherapy Research Day (2019)	Erasmus MC	0.30
ISMRM Benelux Chapter 2020 (Poster) (2020)	ISMRM Benelux	0.50
Stakeholder Workshop RacHy (2020)	VSL - Dutch Metrology Institute	0.30
Career support workshop (2020)	Erasmus MC	0.15
24th MolMed day 2020 (Poster) (2020)	Molecular Medicine Post Graduate School	0.30
Course - PowerPoint Tricks you didn't know (2021)	Erasmus MC	0.30
Course - Word Advanced: Create (large) documents the right way (2021)	Erasmus MC	0.30
Promeras workshop - Time management (2021)	Promeras	0.10
PhD day 2021 (2021)	Erasmus MC	0.20
Workshop for early researchers: Scientists reaching out (2021)	KNAW (Royal Netherlands Academy of Arts and Science)	0.10
Career Development, CV and LinkedIn workshop (2021)	Molecular Medicine Post Graduate School	0.15
Course - Biomedical English Writing Course for MSc and PhD students (2021)	Erasmus MC	2.50
Course - Personal Leadership & Communication (2021)	Erasmus MC	1.00
ICHO 2021 conference (Presentation) (2021)	ICHO	1.00

Presenting Skills for junior researchers (2021)	Erasmus MC	1.00
ISMRM Benelux Chapter 2022 (Poster) (2022)	ISMRM Benelux	0.80
ISMRM Annual Meeting (2022)	ISMRM	1.80
Biomedical Science PhD day (2022)	Erasmus MC	0.30
MedTech day TUe (2022)	TUe	0.15
Career Development Workshop (2022)	Promeras	0.30
Radiotherapy Research Day (2022)	Erasmus MC	0.30
ESHO conference 2022 (Presentation) (2022)	ESHO	2.20
Journal club hyperthermia (2018-2023)	Erasmus MC	3.40
R&D meetings Radiotherapy (2018-2023)	Erasmus MC	1.00
MR physics seminars (2018-2023)	Erasmus MC	2.80
IMET MRI Stakeholder Workshop (Presentation) (2023)	IMET	0.80
Erasmus MC Cancer Retreat (Poster) (2023)	Erasmus MC	0.80
ISMRM Benelux Organising Committee 2023 (2022-2023)	ISMRM Benelux	3.85
Refereermiddag Radiotherapy (2018-2023)	Erasmus MC	1.00
Working Group: PhD well-being (2021-2023)	Erasmus MC	1.00
Total EC		41.90

Acknowledgements

I could have not undertaken this journey without my promotors and supervisors. To start with Prof. Gerard van Rhoon, you are my first promotor and have offered deep knowledge and experiences in hyperthermia; although what I will remember the most will be your unfaltering optimism and not shying away from discussions with people that do not share your view.

Prof. Juan Hernandez Tamames, you started as my supervisor and were appointed professor during our time together. I remember your advice at the very beginning of my PhD to “keep your threshold of frustration high”, and I tried, even though I did not always succeed. You were the one I went to for advice about all things outside of my research, and even in the busiest times I feel that you always had my back, thank you.

Prof. Maarten Paulides, also you started as my supervisor and likewise were appointed professor at the TUe during my PhD. Throughout the years, I saw that you have a way of turning things around for the better. No matter how bleak some results seemed to me at times, you have a talent of spinning perspectives so that things are not only fine, but even great.

Dr. ir. Dirk Poot, je bent pas na een jaar van mijn promotie als mijn nieuwe supervisor erbij gekomen, omdat Juan en Maarten allebei tot hoogleraar waren gepromoveerd. Maar zelfs voordat je er officieel bij was, was je altijd beschikbaar voor al mijn vragen (en frustraties) over Matlab. En ik ben overtuigd ervan dat je de geduldigste mens ter wereld bent. Ik was ook altijd onder de indruk van je inzet boven het noodzakelijke uit, zoals het beoordelen van abstracts voor de IRMSM Benelux of het organiseren van onze MR fysica seminars.

Additionally, I would like to acknowledge the Dutch Cancer Society (KWF), project number 11368. Without your funding this project would not have been possible.

I’m also grateful to my colleagues from both my research groups. The hyperthermia group in the department of Radiotherapy: Sergio, Kemal, Iva, Jannis, Rogier, Loes, Carolina, Ellen, Ali, Anderson, Anton, Robin and Michiel. And the MR physics group in the department of Radiology & Nuclear medicine: Piotr, Stefan, Gyula, Esther, Samy, Riwaj, Emanoel, Nienke, Krishna, Yulun, Fatemeh and Joost. You have always provided valuable discussions and plenty of opportunities for cake.

In het bijzonder wil ik hier mijn geadopteerde werkgroep op de 25e verdieping van de Na-toren noemen. Jullie namen mij steeds om stipt 11 uur en stipt 3 uur mee om

koffie te halen, hoewel ik het nog steeds niet drink. De Kamerplanten Koffiepauze gaf niet alleen structuur aan mijn dag, maar bezorgde mij ook de nodige beweging, sociale interactie en oefening in de Nederlandse taal. Dank jullie daarvoor: Sophie, Swaay, Esther, Celine (of was het Cecile?), Ilanah, Patrick en Joep.

A special mention also needs to go to the ISMRM Benelux organising committee: Maša, Dani, Daniëlle, Donnie, Emma, Natalia, Sam and Sarah. Apart from the fact that I had an incredibly good time with you all and feel very fortunate to have been in such a great team, it gave me a much-needed balance to the usual PhD life. Thank you.

I would have not even started this PhD, without plenty of inspirations at earlier stages in my life.

Henry Higgins, you didn't just get me admitted to Royal Holloway without which I may have never been able to pursue my path in physics, but also gave me some valuable life lessons back at school. One of the most memorable ones being: "Theresa, be good. And if you can't be good, be careful. ". In every sense, this is something I still try and live by!

Prof. Dr. Karl-Heinz Altendorf, du hast mir immer den Rücken gestärkt, obwohl du mich „leider" an die Physik verloren hast. Wir haben Ideen ausgetauscht und Perspektiven zwischen Ländern und Fächern und Sitten gewechselt. Deine akademische Verstärkung aus engen Kreisen hat mir viel geholfen.

Dr. Pejman Rowshan Farzad, you sparked a love for medical physics that is still going strong and for all I can say will never diminish. Not only did you excel in teaching us all ranging from medical imaging to radiotherapy (I think I can still draw a linear accelerator on the fly), but you gave me the options to explore also the clinical applications. I visited the cyclotron, surgeries, and nuclear medicine treatments. Thank you for helping me explore!

Dr. Martin Ebert, even though research has not always been easy for me (and somehow, I now even did my PhD…) we made it in the end. Not only that, but then you facilitated a contact to the IAEA, which I subsequently successfully applied to. This set me on my path back to Europe and to where I am now, thank you.

On this note I also want to thank the people at the Dosimetry and Medical Radiation Physics section at the IAEA, especially Dr. Gian Luca Poli, who encouraged me to be brave and gave key advice, one of which was to pursue this PhD.

Special thanks should also go to my friends, near and far outside the academic world.

Ten eerste mij Skadi ploeg MGD 2020: Eve, Pau, Maaike, Yas, Marit, Vienna en Carlijn. Jullie waren mijn speed-introductie in taal en studentenleven in Nederland.

Next, my beach volleyball friends and coaches, who I always had enormous amounts of fun with, but who also had to put up with a lot of my ups and downs.

Iva and Jannis, thank you both for regularly checking in on me, also outside of work. I'm thrilled that you are also planning on staying in Rotterdam, and I cannot wait to discover the next exciting food places with you!

Laura, as soon as I moved my workplace to the tower you took me under your wing. Whenever there was another moment of utter exasperation, you gave me the comforting words – as well as the real-life example – that really, in the end everything will work out.

Lukas, mit dir gibt es eine Garantie jedes (aber wirklich jedes) vermeintliches Dilemma in null Komma nichts aufzulösen. Oft ist es genau dieser radikale Perspektivenwechsel, der den Unterschied macht, und der mich in den letzten Jahren immer wieder motiviert hat weiter zu machen, danke.

Felix, schon während der Schulzeit hast du mich immer wieder zurück in die Realität geholt. Wir kennen uns jetzt schon über 20 Jahre, und ich freue mich auf alle die, die noch kommen werden! Du wolltest immer mal genau wissen, was ich denn jetzt genau mache in meinem PhD- ich hoffe, dass diese Thesis etwas Aufklärung geben kann!

Jasmin, Jassi, JJ, ab meiner ersten Volleyballstrunde hast du vielen mit mir erlebt und hast mich in allen erdenklichen Ecken dieser Welt schon besucht und getroffen. Unsere schon fast rituellen Spaziergänge will ich auch in Zukunft nicht missen. Danke, dass du immer an mich gelaubt hast!

Berna, obwohl du in der Woche in der ich nach Rotterdam kam wieder nach Delft gezogen bist, ist es immer noch der Rekord von nah-aneinander-wohnen. Wir haben

auch schon so ziemlich alles Erdenkliche zusammen erlebt, und es ist durch dich, dass ich mich hier in Holland so schnell zu Hause gefühlt habe. Danke dafür!

Nicole, durch Jane Russell, viel Käse und jede Menge Bubble Tea haben wir uns Länderübergreifend nie aus den Augen verloren. Von Eggnog im Ritz bis zur Fondue Party in deiner Küche, von Ibiza bis Balaguer, vom Ski-Rennanzug bis zu Bikinis, dein Optimismus und deine Lebensfreude sind ansteckend. Und meine einzige Beschwerde ist, dass du viel zu weit weg wohnst… bottoms up!

Sarah and Rachael, my Aussie friends, I'm extremely grateful to have you, even though you live rudely far away. Countless letters, flowers and parcels contained not only endless supply of Papaw, but most importantly words of encouragement and future plans are brightening my days. I can't wait for the next time I get to see you in person.

Anna, obwohl wir nur ein einziges Jahr in derselben Stadt gelebt haben schaffen wir es doch immer noch uns regelmäßig zu sehen. Orientierung außerhalb des strikt akademischen Feldes hast du immer unterstützt, sowie auch alles andere.

Robin, despite being more on the road than at home lately, you always manage to energise and inspire me to follow my heart (and your balcony has a pretty good view too). Whenever I needed a quick escape, I knew where to go. Also our shared love for beaches probably helped. Thank you!

Jeremy and Lieke, whether it's at work or on the sand, I can't thank you enough for the games, the teas and the outside perspectives for when I needed it the most. If not for you, I would have most likely not persevered in this journey.

Anne, ik denk dat zeker de helft van mijn Nederlands aan jou te danken is. Je bleef bij me in één boot ondanks botsingen, hooikoorts, zonneallergie, bloed, zweet en tranen. Dank je wel dat je mij vandaag als paranymph bij wilt staan.

Jasmijn, ik denk dat ik zonder jou de lockdown niet had overleefd. Met jou heb ik wandelend, hardlopend en fietsend de nieuwe omgeving leren kennen. Ups-and-downs hebben we samen wandelend doorgesproken. Ik ben heel blij dat ik je op deze dag achter mij heb staan.

Diese Reise wäre nicht möglich gewesen ohne meine Familie, besonders ohne dich Mama (Dr. Regina Feddersen). Du hast strukturell versucht den Druck etwas

herauszunehmen mit einem „nicht zu viel arbeiten!“. Auch dir Papa (Fritz Homann) will ich danken, für viele unvergessliche Reisen und Abenteuer, nach denen ich wieder einen frischen Blick auf die Arbeit werfen konnte. Und auch dir Oma Wally, du bist Inspiration pur. Ich möchte mit 88 genauso im Leben stehen wie du jetzt.

Erik, ich kann mit Überzeugung sagen, dass ich unsere Unterhaltungen, Entdeckungen und den Austausch mit dir nicht mehr missen möchte. Unsere Geschichte, die mit Douglas Adams, Kwartjes und vielen Earl Greys anfing (wage ich es WOG/SOG zu schreiben?), ist über Motoradfahren, Strand, Musik, Sport, Reisen, Essen und generelle Neugier immer mehr gewachsen, und anscheinend immer noch nicht ansatzweise fertig. Deine Begeisterung und Leidenschaft für dein Fach und das Leben sind ansteckend, und machen Lust auf alles was noch kommt.

Curriculum Vitae

Theresa Feddersen was born in Georgsmarienhütte, Germany on January 21st 1993. After completing her high school education with an International Baccalaureate in 2011 at Institut Le Rosey in Switzerland, she went on to study civil engineering at the Technische Universität München (TUM) in Munich, Germany.

She changed university, subject and country in 2012, when she commenced her BSc degree in Physics at Royal Holloway University of London (RHUL), Egham, UK. In her 3rd year she obtained an international exchange scholarship to go study at the University of Western Australia (UWA), Perth, Australia for a year. In light of the choice of master specialisations offered she subsequently didn't return to the UK but transferred to UWA, where she obtained her BSc Physics degree in 2015. After that, she also completed her MSc in Medical Physics at the same university.

An internship with the International Atomic Energy Agency (IAEA), at the Dosimetry and Medical Radiation Physics Section, Division of Human Health, saw her return to Europe in 2017.

From 2018-2023 she has been working on her PhD at the Erasmus MC in Rotterdam, the Netherlands. Her project involved the improvement of MR thermometry for hyperthermia treatments in the head and neck.